# Expression and characterization of plant produced AHSV nanoparticles encapsulating EGFP

Angelo Martins

Dissertation presented for the degree of

**Master of Science**

Supervisor: Dr A. E. Meyers




Molecular and Cell Biology Department

Faculty of Science

University of Cape Town

July 2023

# Plagiarism declaration

| | |
|---|---|
| ***Name:*** | ***Angelo Martins*** |
| **Student Number:** | **MRTANG009** |
| **Course:** | **MCB5005W** |

**Plagiarism Declaration**

I know that plagiarism is wrong. Plagiarism is to use another's work and pretend that it is one's own.

I have used the **Harvard** convention for citation and referencing. Each contribution to, and quotation in this **Dissertation** from the work(s) of other people has been attributed and has been cited and referenced.

This Dissertation, presented for the degree of Master of Science in the Department of Molecular and Cell Biology, is my own work. I have not allowed and will not allow anyone to copy my work with the intention of passing it off as their own work.

**Signature** Signed by candidate

**Date _____ 22nd July 2023_____**

# Acknowledgments

I would like to take this opportunity to thank everyone who has been a part of my MSc journey from beginning to end. There were ups and downs, struggles, and triumphs, but at the end of the day, conducting this MSc research provided me with a great opportunity to grow as a person, interact with others and acquire new skills and for that I am forever grateful.

I would like to extend my sincerest thanks to my supervisor, Dr Ann Meyers. Thank you for always being a friendly, welcoming person who was always open to talk about an experimental result and offer me advice and encouragement, especially during the hard times where I struggled to see the light at the end of the tunnel and needed some reassurance to get back on the right path.

To all my fellow lab members from the Biopharming research unit, thank you for helping me get settled with life in the lab and always being around to help me whenever I needed a favour or some advice on a lab protocol.

Thank you to Mr. Mohammed Jaffer for all your help with transmission electron microscope imaging and for always trying your best to fit me into your busy schedule, even on very short notice.

I would also like to thank Liselo for the bursary they provided me for the duration of my MSc studies, and I am deeply grateful for all their financial assistance, without which my MSc studies may not have been possible.

Finally, I would like to thank all my family members from the bottom of my heart. Thank you for always supporting and believing in me. I would like to thank my parents for raising me and instilling the value of hard work from a young age and teaching me to be strong in the face of adversity, without all your support I would have never reached this point in my life, and for that I am eternally grateful.

# List of Abbreviations

| | |
|---|---|
| **AA(s)** | **amino acid(s)** |
| **A555** | **alexa fluor 555** |
| **AGQ** | **alanine-glycine-glutamine** |
| **AHSV** | **African horse sickness virus** |
| **AP** | **alkaline phosphatase** |
| **BTV** | **bluetongue virus** |
| **BMV** | **brome mosaic virus** |
| **BeYDV** | **bean yellow dwarf virus** |
| **BRU** | **biopharming research unit** |
| **Bp(s)** | **base pair(s)** |
| **BSA** | **bovine serum albumin** |
| **BCIP** | **5-bromo-4-chlor-3-indolyl phosphate** |
| **CCMV** | **cowpea chlorotic mottle virus** |
| **CP(s)** | **coat protein(s)** |
| **CPMV** | **cowpea mosaic virus** |
| **CLP(s)** | **core-like particle(s)** |
| **cm** | **centimetre** |
| **cPCR** | **colony PCR** |
| **$cm^2$** | **square centimetre(s)** |
| **DNA** | **deoxyribonucleic acid** |
| **DOX** | **doxorubicin** |
| **dsRNA** | **double-stranded RNA** |
| **$ddH_20$** | **double-distilled water** |
| **DPI** | **day(s) post-infiltration** |
| **DTT** | **dithiothreitol** |
| **EPR** | **enhanced permeability and retention** |
| **EGFP** | **enhanced green fluorescent protein** |
| **EtBr** | **ethidium bromide** |
| **FP** | **forward primer** |

| | |
|---|---|
| **F** | **fraction** |
| **GGS** | **glycine-glycine-serine** |
| **GFP** | **green fluorescent protein** |
| **g** | **grams** |
| ***g*** | **gravitational force** |
| ***HT*** | **hyper-translational** |
| **hr(s)** | **hour(s)** |
| **kV** | **kilovolt** |
| **kPa** | **kilopascal** |
| **LB** | **Luria Bertani** |
| **mg** | **milligram** |
| **mL** | **millilitre** |
| **min** | **minute** |
| **NP(s)** | **nanoparticle(s)** |
| **NHS** | **N-hydroxysuccinimidyl** |
| **nm** | **nanometre** |
| **NBT** | **nitroblue tetrazolium chloride** |
| **NLS** | **N-lauroyl sarcosine** |
| **O/N** | **overnight** |
| **$OD_{600}$** | **optical density at 600 nm** |
| **PEG** | **polyethylene glycol** |
| **PBS** | **phosphate buffered saline** |
| **PTM(s)** | **post-translational modification(s)** |
| **PMF** | **plant molecular farming** |
| **PVX** | **potato virus X** |
| **PCR** | **polymerase chain reaction** |
| **PI** | **protease inhibitor** |
| **PAGE** | **polyacrylamide gel electrophoresis** |
| **RNA** | **ribonucleic acid** |
| **RV** | **rotavirus** |

| | |
|---|---|
| **RP** | **reverse primer** |
| **Re** | **restriction** |
| **RGD** | **arginine-glycine-aspartate** |
| **rpm** | **revolutions per minute** |
| **ROI** | **region of interest** |
| **sHsp(s)** | **small heat shock protein(s)** |
| **SA** | **serum albumin** |
| **SAB** | **sample application buffer** |
| **SDS** | **sodium dodecyl sulfate** |
| **TMV** | **tobacco mosaic virus** |
| **Ti** | **tumour-inducing** |
| **T-DNA** | **transfer-DNA** |
| **TBE** | **tris-borate EDTA** |
| **TSP** | **total soluble protein** |
| **TEM** | **transmission electron microscopy** |
| **uAA(s)** | **unnatural amino acid(s)** |
| **UTR(s)** | **untranslated region(s)** |
| **UV** | **ultraviolet** |
| **UA** | **uranyl acetate** |
| **µg** | **microgram** |
| **µg/mL** | **microgram per millilitre** |
| **w/v** | **weight per volume** |

# Table of Contents

# Abstract

Virus-like particles (VLPs) are virus-based nanoparticles that resemble the native virion but do not contain the viral genome. Heterologous expression of the viral structural proteins results in the spontaneous self-assembly of VLPs that have an empty inner cavity. These particles have an organized, repetitive structure that is very amenable to modification. One can take advantage of this property and fuse a foreign molecule to one of the viral structural proteins and upon VLP self-assembly this foreign molecule may be encapsulated within the empty inner cavity of the VLP. One can also take advantage of the high tailorability of VLPs and functionalize the external surface with targeting ligands for delivery purposes. Alternatively, the structural proteins that form VLPs can have inherent amino acid motifs with a natural targeting affinity for receptors that may be overexpressed on the surface of certain types of cells, for example cancer cells. These properties impart VLPs with great potential as delivery vehicles of diagnostic and/or therapeutic molecules. Core-like particles (CLPs) are a derivative of VLPs that share all the same properties and modification potential, however unlike VLPs, CLPs are comprised of only the viral structural proteins that form the inner capsid layer or 'core' of the native virion. Herein, two cloning techniques have been used to successfully fuse a fluorescent protein, enhanced green fluorescent protein (EGFP), to the VP3 structural protein of African horse sickness virus (AHSV). Plant-based transient expression of the AHSV EGFP-VP3 and AHSV VP7 structural proteins has been used to generate CLPs from *N. benthamiana* leaves that successfully encapsulate the EGFP protein. However, interaction of this particle with the human integrin receptor, αvβ3, a receptor that is commonly found overexpressed on the surface of cancer cells could not be confirmed. These results highlight the potential of AHSV CLPs as a cargo carrier, but more research is required to elucidate its potential as a delivery vehicle.

# Chapter 1: Literature review

## 1.1 Introduction

The ever-expanding field of nanotechnology encompasses the manufacturing of nanoscale assemblies with potential applications in cosmetic, industrial and therapeutic industries (Mejía-Méndez et al., 2022). These nanoscale assemblies, commonly referred to as nanoparticles (NPs), typically fall between 1 and 100 nm in size and can be produced from polymeric, inorganic, or biological building blocks. 'Bionanoparticles' refer to NPs constructed using biological building blocks such as lipids, nucleic acids, and proteins (Doll et al., 2013). In contrast to synthetic nanoparticles, bionanoparticles include a massive variety of well-organized, highly sophisticated architectures, are monodisperse and can be produced on a large scale economically (Lee and Wang, 2006). Commonly investigated bionanoparticles include the lipid-based NPs such as liposomes and micelles (Ojha et al., 2022) and the protein-based NPs such as ferritins, small heat shock proteins (sHsps), vault proteins and viral nanoparticles (VNPs)(Lee et al., 2016).

### 1.1.1 Protein cage nanoparticles

The protein-based NPs are commonly classified as protein cages (Zangabad et al., 2017). Protein cages can be divided into two categories: non-viral protein cages and VNPs (Ludwig and Wagner, 2007, Zeltins, 2013, Mateu, 2013). Protein cages are constructed from protein sub-units that self-assemble into a protein shell with a hollow interior cavity (Rother et al., 2016). The protein sub-units can be comprised of a single or multiple proteins (Molino and Wang, 2014), however many copies of each individual protein sub-unit are required to form the complete protein cage (Rother et al., 2016). The resulting protein cage will possess a highly uniform, symmetrical structure and exhibit a narrow size distribution (Estrada and Champion, 2015). Protein cages can be broken down into the interior, exterior and inter sub-unit interfaces (Figure 1) (Zhang et al., 2016) .The interior interface projects towards the hollow protein cage interior and is separated from the exterior by pores/openings in the protein shell found between the protein sub-units (Rother et al., 2016, Zhang et al., 2016). The most unique property of protein cages, not present in synthetic and lipid-based NPs, is their amenability to both genetic (Brown et al., 2009) and chemical functionalization strategies (Ma et al., 2012, Schoonen and van Hest, 2014, Lee et al., 2009). Therefore, there are theoretically limitless opportunities for the precise sub-molecular alteration of protein cages (Lee and Wang, 2006). Additionally, since

protein cages possess a highly repetitive structure, a single modification will be represented across the entire particle in a consistent manner (Lee et al., 2016). These advantageous properties greatly increase the versatility of the protein cage interfaces and enable the utilization of protein cages as delivery vehicles for various applications (Sharma et al., 2017, Douglas and Young, 2006, Uchida et al., 2010). The hollow interior cavity can be loaded with diagnostic/ therapeutic agents and the exterior surface can be functionalized with targeting ligands. Furthermore, the interactions between the protein sub-units can be manipulated to open/close pores or prompt the disassembly and subsequent reassembly of the protein cage after encapsulation of a drug molecule (Choi et al., 2018, Lee et al., 2016).

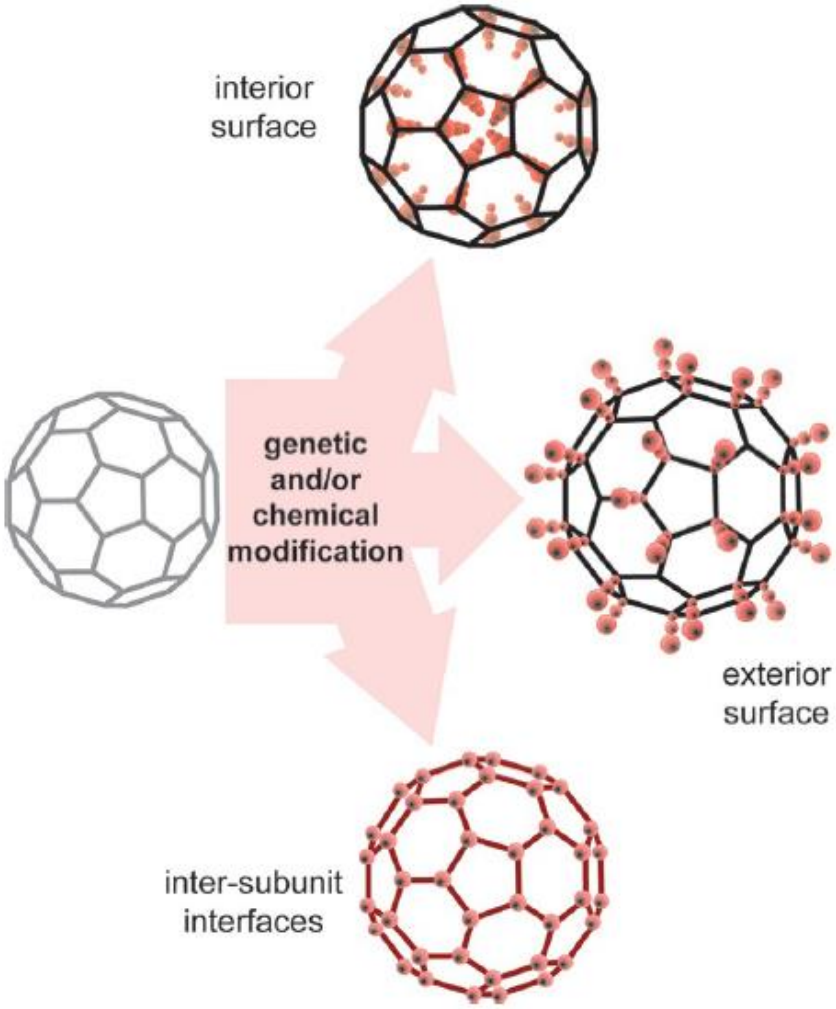


Figure 1: Schematic representation of the protein cage (interior, exterior and inter-subunit) interfaces amenable to genetic and/or chemical modification (Zhang et al., 2016).

## 1.2 Viral nanoparticles: Virus derived protein nanocages

Viruses have naturally evolved to efficiently infect specific host cells (Yildiz et al., 2011). In general, either DNA or RNA genetic material and a symmetrical protein coat known as a capsid are the major constituents of a virus (Villarreal, 2004). Delivery of genetic material into a host cell is the primary function of the infectious virion (Cohrs et al., 2003) and is made possible due to the intrinsic ability of viruses to assemble and disassemble (Brown and Bhella, 2016). Consequently, the ability to successfully infiltrate, target and deliver genetic cargo into a host are considered inherent negative viral traits. These traits, however, have proven to be extremely beneficial for nanomedical applications. The same traits that enable viruses to succeed as effective pathogens can be engineered to create tools for biological delivery (Schwarz and Douglas, 2015). Viruses are thus an excellent platform for developing vehicles for targeted delivery of drugs or imaging reagents and can be classified into two distinct groups: viral nanoparticles (VNPs) and virus-like particles (VLPs).

### 1.2.1 Structural organization of VNPs and VLPs

VLPs are comprised of one or more viral structural proteins (capsomers) which spontaneously self-assemble into a particular spatial conformation (Yan et al., 2015, Zdanowicz and Chroboczek, 2016). VLPs possess a highly organized repetitive structure presenting viral/antigenic epitopes, thereby mimicking the morphological structure of the native virion (Marsian and Lomonossoff, 2016, Hill et al., 2018). However, unlike VNPs, they are devoid of viral genetic material and can be considered a subclass of VNPs (Rohovie et al., 2017, Yildiz et al., 2011). Thus, VLPs are able to preserve the majority of viral traits without risk of infectivity (Benjamin et al., 2020). A VLP can therefore be viewed as an ‘empty shell’ (Shirbaghaee and Bolhassani, 2016) comprised of many repeated viral protein sub-units organized in a precise manner (Steinmetz et al., 2020).

## 1.3 Cargo loading

The aforementioned structural characteristics impart VLPs with great potential for functionalization (Hill et al., 2018). Consequently, VLPs are considered attractive nanoparticle candidates for a plethora of applications beyond the presentation of viral/antigenic epitopes (Hill et al., 2018). One of the most important capabilities of VLPs owing to their structural properties is the ability to act as cargo-bearing carriers for delivery applications (Zangabad et al., 2017). Cargo can either be encapsulated within the empty cavity of the capsid structure

(Chung et al., 2020, Steinmetz, 2010) or attached to the VLP surface (Zdanowicz and Chroboczek, 2016, Ramqvist et al., 2007). Cargo loading strategies based on non-specific encapsulation, genetic engineering and bioconjugation are discussed in detail below.

## 1.3.1 Non-specific interactions

When cargo proteins are present in high concentrations during VLP assembly, non-specific interactions may result in cargo encapsulation. Under these conditions, in-vitro assembly using purified products is required to ensure specific cargo loading (McNeale et al., 2022).

### 1.3.1.1 Statistical encapsulation

Mixture of free protein cargo at high concentrations with VLP capsid proteins may result in encapsulation of cargo during in-vitro VLP assembly (Figure 2) (McNeale et al., 2022). This strategy was notably used to encapsulate the first protein cargo inside a capsid-based VLP, namely the cowpea chlorotic mottle virus (CCMV) VLP. Researchers accomplished this by taking advantage of the unique pH dependent gating behaviour of CCMV. The in-vitro disassembly of CCMV virions was facilitated by a change in pH. Once the viral RNA was removed, a further pH change resulted in the reassembly of the capsid protein sub-units around the enzyme horse radish peroxidase (HRP) , thus 'caging' this foreign cargo within the CCMV VLP interior cavity (Comellas-Aragonès et al., 2007). Since statistical encapsulation requires VLPs to be amenable to in-vitro assembly, it is easier to chemically control VLP assembly and increase cargo loading specificity. However, to successfully encapsulate cargo using this loading strategy requires a very high cargo concentration which acts as a limiting factor for the cargo loading density (McNeale et al., 2022).

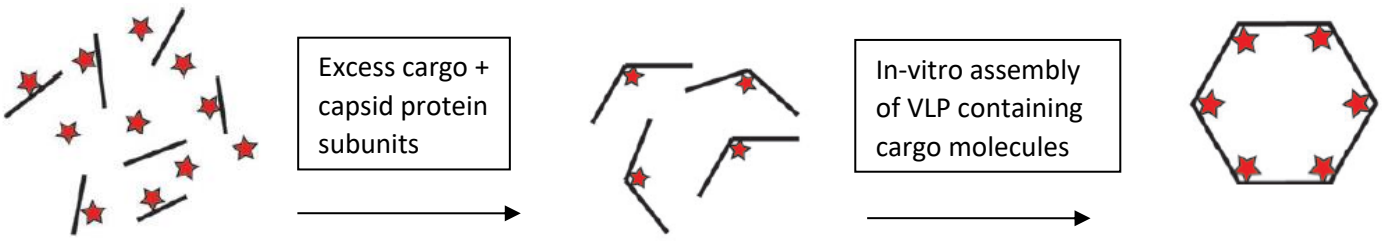


Figure 2: Statistical encapsulation of a foreign protein cargo. During in-vitro VLP assembly, cargo present at high concentrations, non-specifically interact with capsid proteins and are encapsulated within VLPs (Steele et al., 2017).

### 1.3.1.2 Electrostatic interactions

Electrostatic interactions between viral coat proteins (CPs) and nucleic acids are responsible for initiating capsid formation and encapsulation of genomic cargo inside viruses. To initiate encapsulation via electrostatic interactions, there must be charge complementarity between the cargo molecule and the particle interior (Figure 3) (Chakraborti et al., 2020). This requirement is met by many capsid-based viruses which possess a positively charged interior and can encapsulate viral genetic material carrying a negative charge. Therefore, it is possible to take advantage of charge complementarity to encapsulate negatively charged foreign cargo inside VLPs with a positively charged interior surface (McNeale et al., 2022). However, the intended cargo may not always carry an inherent negative charge. Fortunately, a negative charge can be imparted to cargo following nucleic acid conjugation to facilitate charge-mediated encapsulation (Brasch et al., 2017, Glasgow et al., 2012, Wu et al., 1995) . In one such example, nucleic acid adapters were chemically linked to the exterior of chosen enzyme cargoes. In doing so, interaction with an arginine-enriched N-terminal region of CCMV was able to successfully trigger capsid assembly and charge-mediated encapsulation of the modified enzyme cargo (Brasch et al., 2017). In summary, this method of cargo encapsulation is simple and has proven especially useful in cases where VLP assembly requires a charged cargo. However, as one would expect cargo loading density is lower than encapsulation techniques involving specific interactions. Despite this, one can tune the cargo loading density by varying the length of nucleic acid adapters or ionic strength which makes charge-mediated encapsulation a relatively flexible loading technique (McNeale et al., 2022).

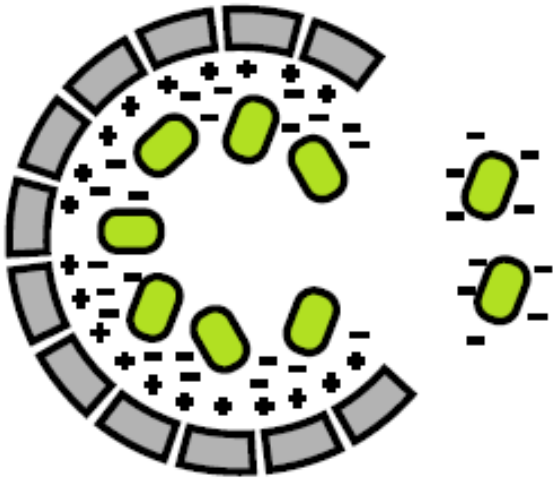

Figure 3: Electrostatic interaction-mediated encapsulation of a foreign cargo. Charge complementarity between negatively charged cargo and positively charged VLP interior facilitates cargo encapsulation (McNeale et al., 2022).

## 1.3.2 Genetic engineering

A foreign protein cargo can be encapsulated by direct genetic fusion to the the viral CP sub-units. This loading technique can be described as encapsulation by translational fusion and to date has been used to encapsulate foreign protein cargo within several capsid-based VLPs (McNeale et al., 2022). This technique has been utilized to encapsulate a fluorescent protein cargo inside bluetongue virus (BTV) and rotavirus (RV) VLPs. BTV and RV VLPs are comprised of 4 different proteins arranged into three layers. However, core-like particles (CLPs) containing two different proteins in a double layer and subcore particles containing only one protein in a single layer can also be produced. It was found that an N-terminal fusion of a green fluorescent protein (GFP) to a scaffolding protein comprising the subcore particle resulted in successful encapsulation of GFP cargo in both BTV and RV (Brillault et al., 2017, Charpilienne et al., 2001). Besides encapsulation, genetic engineering can be used to load cargo to the VLP exterior surface (Yildiz et al., 2011). By doing so, useful cargo such as purification tags and specific cell targeting sequences can be incorporated into the VLP coat (Yildiz et al., 2011, Plummer and Manchester, 2011). Thus, genetic based cargo loading can extend VLP functionality beyond simple cargo encapsulation. Genetic-based cargo loading to the interior/exterior of VLPs is often achieved after in-vivo capsid assembly during a process referred to as expression loading (Figure 4) (Shahgolzari et al., 2020). Complete protein and/or peptide sequences can be inserted, removed from, or substituted into the nucleic acid sequence of the viral CP (Juarez et al., 2012, Kaczmarczyk et al., 2011), and this can be done at the termini or within the CP sequence (Balke and Zeltins, 2019, Bendahmane et al., 1999). The final result is the heterologous expression of a chimera CP, followed by spontaneous self-assembly of chimeric VLPs loaded with cargo molecules (Shahgolzari et al., 2020). Genetic-based cargo loading is advantageous as it enables efficient cargo encapsulation at high concentrations (McNeale et al., 2022) , and allows precise loading of cargo to the VLP surface (Shahgolzari et al., 2020). Thus, genetic engineering is able to facilitate spatial control over cargo incorporation and direct production of complex, modified VLPs (Sharma et al., 2017, Patterson et al., 2012, Patterson et al., 2014). Furthermore, genetic engineering can be used as a precursor to other cargo loading strategies such as bio-conjugation by controlling the number of sites available for the covalent attachment of cargo. Additionally, by changing the structural configuration of the VLP, genetic engineering can alter the physicochemical properties of the VLP such as its electrostatic potential (Badri Narayanan and Soo Han, 2017). However, one must be careful when using genetic-based cargo loading as insertion of larger cargo molecules

may impair the capsid assembly process and/or reduce capsid stability (Shahgolzari et al., 2020).

A

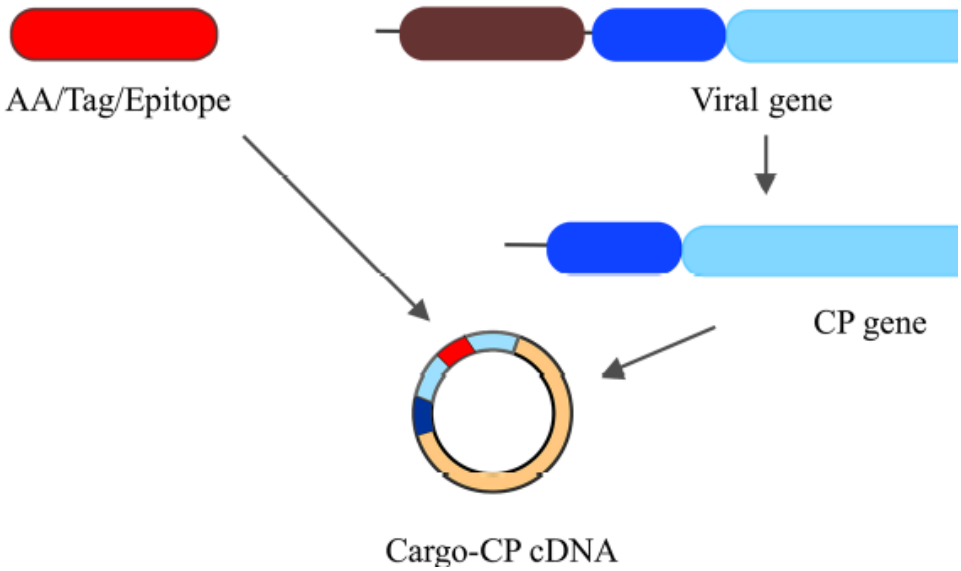


B

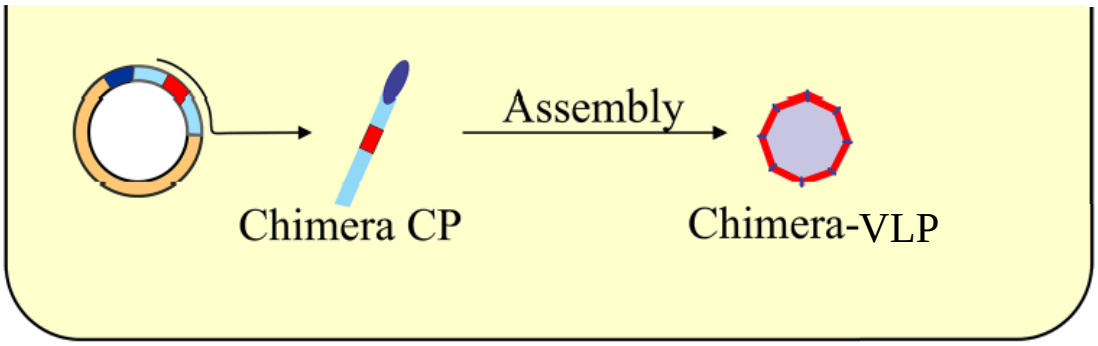


Figure 4: Expression loading of a foreign cargo during in-vivo capsid assembly. (A) the foreign cargo (AA/Tag/Eptitope) and the CP gene are cloned into a plasmid where they are fused to each other. (B) Heterologous expression of the chimeric CP from a recombinant plasmid and subsequent in-vivo assembly of chimeric VLPs containing a foreign cargo. Reprinted (adapted) with permission from (Shahgolzari et al., 2020). Copyright 2020 Wiley Periodicals, *Inc*.

## 1.3.3 Bioconjugation

Bioconjugation involves the chemical conjugation of cargo to the VLP CPs (Wu et al., 2013). The interior and exterior VLP surfaces are amenable to bioconjugation, therefore cargo encapsulation and VLP surface functionalization can be achieved with this loading method (Hill et al., 2018). Loading is mediated by covalent interactions between the cargo molecule and functional groups of chemically reactive amino acid side chains on the VLP CPs (Chung et al., 2020, Pokorski and Steinmetz, 2011). The functional groups of the natural amino acids, particularly cysteine and lysine are the most common bioconjugation targets (Hill et al., 2018).

Lysine

The primary amine group of lysine ($R\text{-}NH_2$) reacts with N-hydroxysuccinimidyl-esters (NHS-esters) to generate an amide bond (Figure 5a, left)(Smith et al., 2013, Sun and Cui, 2020). This reaction has successfully enabled conjugation of ligands such as PEG, polymers and small organic molecules to VLPs. Lysine is particularly useful for surface bioconjugation as it is one of the most prevalent amino acids in any given protein and often exposed on the surface of VLPs due to its hydrophylicity. As a result, lysine residues provide ideal targets for high density VLP surface loading (Smith et al., 2013). However, excessive loading may shield other VLP traits and should be avoided (Carrico et al., 2012). An alternative lysine-related bioconjugation strategy involves a reaction between amine and thioimidates (Figure 5A, right), but due to high commercial availability and a simple reaction proccess, conjugation with NHS-esters are utilized more readily (Running et al., 2012).

Cysteine

A free sulfhydryl group on cysteine (R-SH) is able to form an irreversible thioether bond to compounds with maleimide chemistry (Figure 5b) (Rohovie et al., 2017, Sun and Cui, 2020). This is referred to as a ‘maleimide-thiol reaction’ and has been used to conjugate a variety of ligands including fluorescent probes, cancer drugs and peptides to the surface of VLPs. The simplicity of this reaction makes it an especially attractive option for bioconjugation of cargo to VLPs (Smith et al., 2013). However, one must take care to avoid unwanted spontaneous disulfide bond formation between the free sulfhydryl group of cysteine and other sulfhydryl-containing compounds. To circumvent this issue, one may be required to remove potentially reactable cysteine residues (Jegerlehner et al., 2002).

Unnatural amino acids (uAAs)

Although natural amino acids are commonly used for bioconjugation, unnatural amino acids (uAAs) provide new opportunities for covalent modification of VLPs (Smith et al., 2013). The incorporation of uAAs into VLP CPs introduces unique functional groups that are bio-orthogonal to the functional groups of natural amino acids. Furthermore, conjugation to uAAs is generally more efficient than conjugation to natural AAs, and results in greater VLP homogeneity (Kim et al., 2013). uAA incorporation strategies and their bioconjugation chemistries have been described in detail elsewhere (Smith et al., 2013, Rohovie et al., 2017, Pokorski and Steinmetz, 2011).

Although bioconjugation is an extremely versatile cargo loading strategy, it does have several downsides. Since this strategy is often carried out in-vitro after VLP assembly, it generally involves long reaction steps (Schlick et al., 2005) and several purification stages (Destito et al., 2007) which increases the potential of losing VLPs (Aljabali et al., 2013). However, problems relating to VLP assembly, stability and unwanted VLP structural changes as a result of genetic engineering are easily avoided by using bioconjugation strategies (Nassal et al., 2005, Carreira et al., 2004).

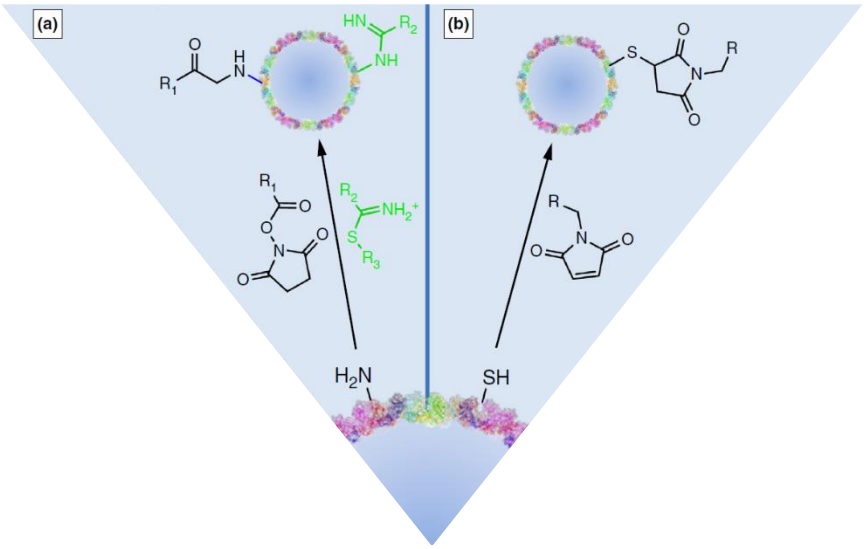


Figure 5: Bioconjugation strategies based on chemistires possessed by the natural amino acids, lysine and cysteine. (a) Conjugation of ligand to VLP, whereby the primary amine of lysine ($R\text{-}NH_2$) reacts with either an NHS-ester (left) or an imidoester (right). (b) Conjugation of ligand to VLP, whereby the sulfhydryl group of cysteine (R-SH) reacts with a maleimide-based compound. Reprinted (adapted) with permission from (Smith et al., 2013). Copyright 2013 Elsevier Ltd. All rights reserved.

# 1.4 Targeting

The overall goal of targeting is to maximize the uptake efficiency of a chosen diagnostic/therapeutic agent in a specific region such as a tumour (Petros and DeSimone, 2010). Targeting is advantageous as it helps to minimize side effects and enhances the efficiency of therapeutic/diagnostic agents. Therefore, targeting is of great importance towards ensuring successful treatment of many diseases (Doll et al., 2013). Passive and active targeting comprise the two major targeting approaches (Benjamin et al., 2020). A schematic representation of the passive and active targeting mechanisms are represented in Figure 6.

## 1.4.1 Passive targeting

This targeting strategy does not utilize ligands for specific targeting of tissues/organs (Attia et al., 2019). It is instead dependent on physical characteristics of the nanocarrier such as particle size and shape and physiological characteristics of bodily tissues such as its pathological state (Zangabad et al., 2017). Particle size (diameter) influences the circulation half-life of the carrier. A reduction in particle size has been shown to increase its circulation half-life and subsequent accumulation in targeted tissues. Particle shape influences cellular uptake of NPs, with spherical and rod-shaped NPs displaying the greatest cellular uptake (Albanese et al., 2012). However, passive tumour targeting primarily relies on the enhanced permeability and retention (EPR) effect (Figure 6A) to facilitate targeted accumulation of a cargo molecule in tumour tissues (Zangabad et al., 2017, Brigger et al., 2012). The EPR effect is caused by a combination of leaky blood vessels and reduced/absent lymphatic drainage which are commonly found within a tumor microenvironment (Farokhzad and Langer, 2009). As a result of the enhanced permeability of the tumour vasculature, the EPR effect facilitates selective accumulation of VLPs in tumour tissue, but not healthy tissue (Fang et al., 2011). Furthermore, poor lymphatic drainage under EPR conditions reduces the potential escape of VLPs from the tumour microenvironment, thereby limiting potential damage to healthy tissues (Molino and Wang, 2014).

## 1.4.2 Active targeting

This targeting strategy involves the decoration of a NP with targeting ligands to facilitate specific targeting of a desired tissue/cell (Figure 6B) (Zangabad et al., 2017, Attia et al., 2019). These targeting ligands can either be introduced using a genetic engineering approach **(section 1.3.2)** or via bioconjugation strategies **(section 1.3.3)** (Schwarz and Douglas, 2015).

Commonly used targeting ligands include peptides, aptamers and receptor-specific ligands. Peptides are a popular targeting ligand as they can be produced on a large-scale and enable targeted localized delivery while generating few side-effects. Aptamers are single-stranded DNA/RNA oligonucleotides and are useful for active targeting as they possess a high binding affinity and offer good tissue penetration (Zangabad et al., 2017). Finally, receptor-specific ligands are typically used to bind specific receptors that are over-expressed on the surface of tumour cells compared to normal, healthy cells (Attia et al., 2019, Clemons et al., 2018). Overall, active targeting is advantageous as it limits off-target cargo release (Clemons et al., 2018), and facilitates greater cellular uptake compared to a passive targeting approach (Zangabad et al., 2017).

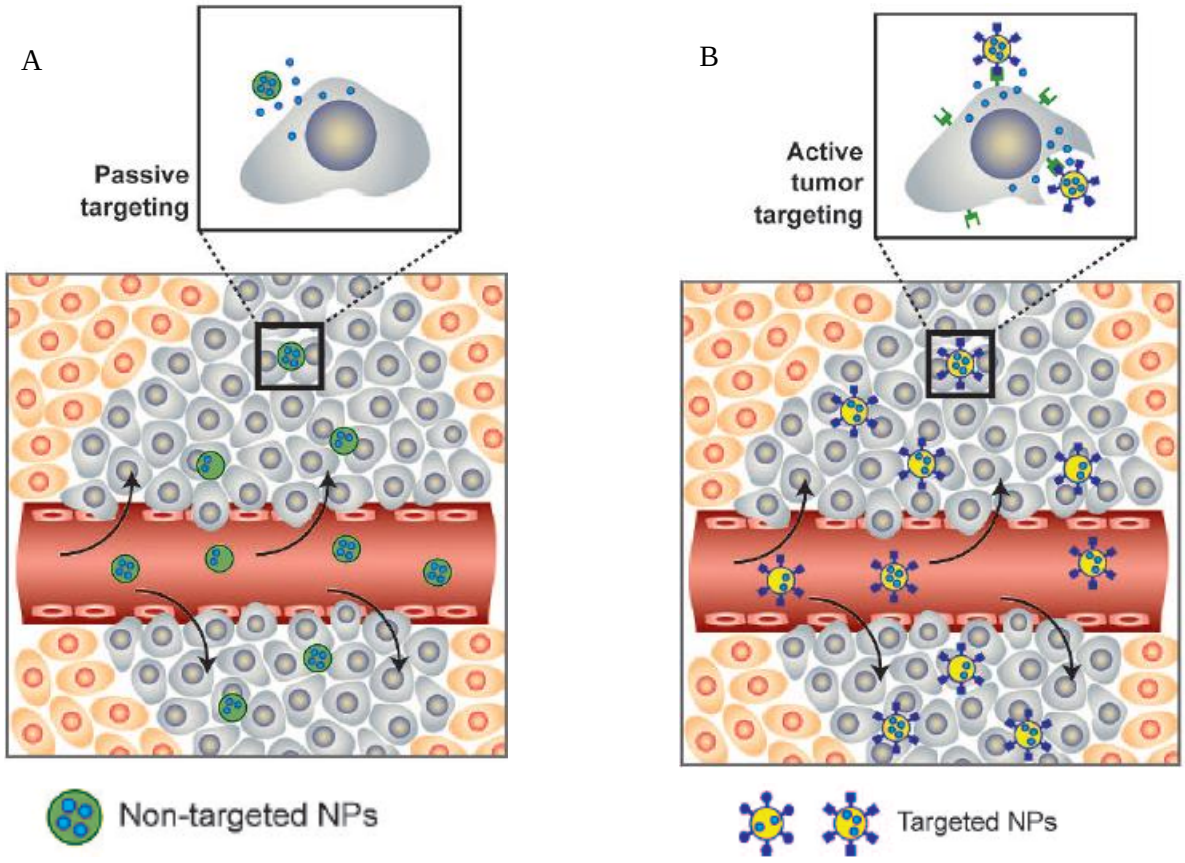


Figure 6: Passive targeting vs active targeting within a tumor micro-environment. (A) During passive targeting, non-targeted NPs extravasate from blood vessels into the leaky tumour vasculature where the drug is released. (B) In the example above targeted NPs displaying targeting ligands bind to specific cell receptors over-expressed on tumour cells to deliver their payload. Reprinted (adapted) with permission from (Farokhzad and Langer, 2009). Copyright 2009 American Chemical society.

## 1.5 Potential applications of virus-based NPs

VNPs/VLPs are useful tools for achieving biomedical applications (Comas-Garcia et al., 2020). Figure 7 provides a schematic highlighting a wide variety of these applications (Comas-Garcia et al., 2020). Two prominent applications – drug delivery and imaging, have been chosen for further discussion.

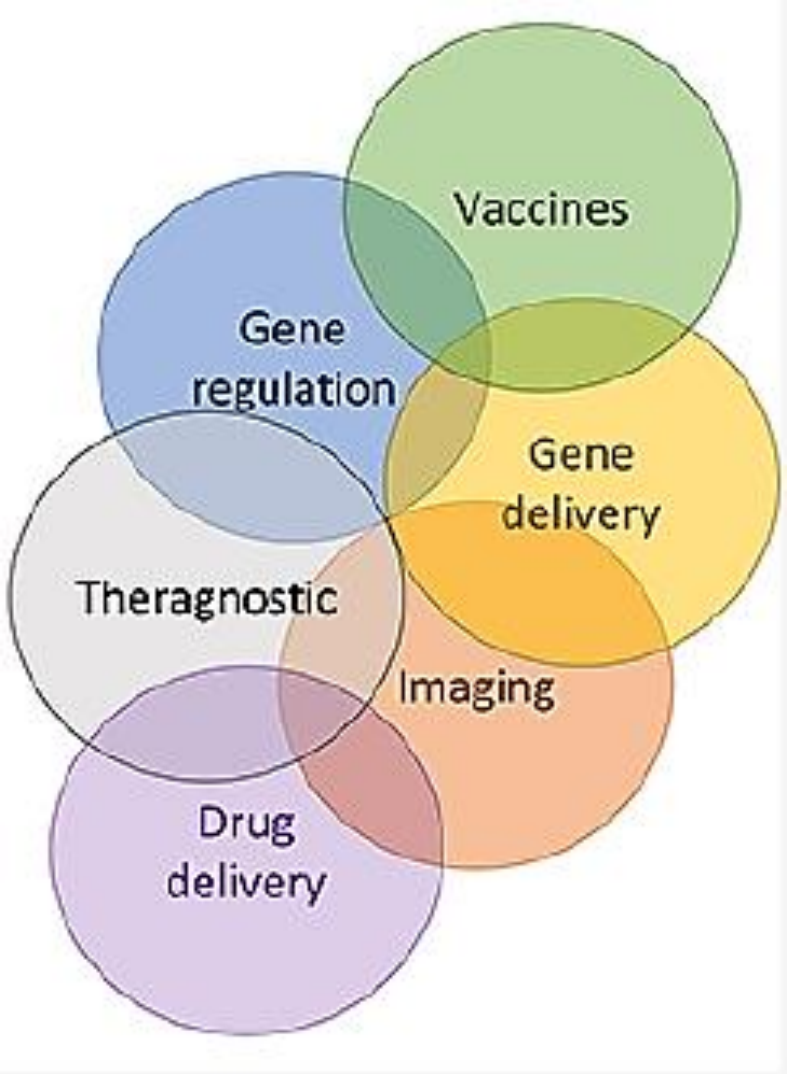


Figure 7: Schematic visualization of several biomedical applications which can be achieved with the help of VLPs. Reprinted (adapted) with permission from (Comas-Garcia et al., 2020). Copyright 2020 American Chemical Society.

### 1.5.1 Drug delivery

VLPs have the ability to encapsulate and/or attach cargo to their exterior surface and undergo passive/active targeting. Consequently, VLPs can be used to achieve targeted delivery and eventual release of a drug cargo within a particular cell, tissue or organ (Lua et al., 2014).

### 1.5.1.1 Why virus-based NPs are good drug delivery vehicles

VLPs possess numerous properties that are advantageous for drug delivery applications. They are biodegradable (Koudelka et al., 2015), display minimal toxicity and high biocompatibility (Rohovie et al., 2017, Schoonen and van Hest, 2014). The nanoscale size of VLPs aids their cellular endocytic uptake (Koudelka et al., 2015) and their size uniformity results in more consistent accumulation at a desired location (Ikwuagwu and Tullman-Ercek, 2022). VLPs also efficiently protect encapsulated drug cargo from enzymatic degradation during delivery (Benjamin et al., 2020). Thus, VLP-mediated delivery results in greater drug bioavailability at a target destination and minimizes the amount of doses required to achieve an effective treatment outcome (Nooraei et al., 2021).

### 1.5.1.2 Delivery of chemotherapeutic agents for cancer treatment

Chemotherapy is the most commonly utilized treatment option in the fight against cancer. During chemotherapy, small molecule drugs known as chemotherapeutic agents eliminate or limit the proliferation of cancer cells (Shahrivarkevishahi et al., 2022). Chemotherapeutic agents are generally administered systemically (Sun and Cui, 2020), which results in their wide-spread distribution throughout the whole body (Rohovie et al., 2017). However, systemic administration of chemotherapeutic agents which tend to display broad cytotoxicity, can result in many unwanted side effects (Oun et al., 2018). Systemically administered chemotherapeutic agents lack effective targeting specificity which results in a low delivery success rate (Sun and Cui, 2020). To overcome this obstacle normally requires an excessive (‘maximum-tolerated’) drug dose (Unzueta et al., 2015). However, doing so generates off-target toxicities which are damaging to normal tissues, thus limiting the therapeutic efficiency of chemotherapeutic agents (Yan et al., 2015). By using VNPs/VLPs one is able to achieve targeted accumulation of chemotherapeutic agents within tumor tissues, thereby limiting damage to normal tissues (Feng, 2004), reducing the required number of drug doses and improving the cancer treatment outcome (Chung et al., 2020). Many studies have investigated the applicability of VNPs/VLPs for the delivery of a vast array of chemotherapeutic agents including Doxorubicin (DOX) (Pitek et al., 2018, Ashley et al., 2011, Chen et al., 2016a), cisplatin (Franke et al., 2017), and phenathriplatin (Czapar et al., 2016) to name a few. In one such study, researchers used a bioconjugation strategy to load DOX in the central channel of TMV VNPs and also conjugated serum albumin (SA) to its exterior surface to improve biocompatibility. Thereafter, the efficacy of free DOX vs SA-TMV VNPs containing DOX was assessed in a mouse MDA-MB-231

tumor model. It was found that free DOX did not have any impact on the survivability of the mice compared to the control group that were injected with PBS alone. On the other hand, mice which received treatment with SA-TMV VNPs containing DOX, displayed significantly delayed tumour growth and by the end of the study 80% of the mice remained alive (Pitek et al., 2018). By looking at this study, it is apparent that virus-based NP delivery of a chemotherapeutic agent, facilitates a notable improvement in the the effectiveness of a cancer treament compared to treatment with a 'free' chemotherapeutic agent.

## 1.5.2 Imaging

Molecular imaging is a rapidly expanding field of study which has many applications that can be used to aid the diagnosis and treatment of diseases such as cancer in its early stages (Suffian and Al-Jamal, 2022, Chung et al., 2020). Molecular imaging enables one to detect/visualize disease location (Sun and Cui, 2020) and monitor the progression of tumour angiogenesis (Suffian and Al-Jamal, 2022). In-vitro or in-vivo imaging can be achieved by loading fluorescent dyes or probes to the interior and/or exterior surface of VLPs (Doll et al., 2013).

### 1.5.2.1 Why virus-based NPs are advantageous for imaging applications

Imaging agents can be attached to VLPs via bioconjugation to repeating functional groups present on the monodisperse and multivalent VLP CPs (Chen et al., 2016b). Due to the monodispersity of VLP CPs, imaging agents can be attached to VLPs with uniform spacing (Li et al., 2010). When dyes or fluorescent probes are loaded in such an organized manner, quenching of their fluorescent signal can be somewhat avoided (Doll et al., 2013), and imaging resoluton can be improved (Li et al., 2010). The multivalency of VLP CPs facilitates attachment of a targeting ligand to a second functional group. This enables targeted localization of VLPs containing an imaging agent to a specific location in the body (Schwarz and Douglas, 2015). VLPs are available in a wide variety of sizes and shapes and this can be taken advantage of by selecting VLPs that display high retention times. By doing this, one can improve the accumulation of VLPs at a desired location and lengthen the duration of imaging (Yildiz et al., 2011).

### 1.5.2.2 Optical imaging

Optical imaging with VLPs involves the utilization of fluorescent VLPs to specifically label a desired tissue or cell (Chung et al., 2020). The fluorescent signal emitted by the VLP can be

detected using confocal microscopy, thus enabling one to visualize the location of a fluorescent VLP. Furthermore, fluorescence enables one to analyse the in-vivo biodistribution of VLPs and quantify VLP uptake using flow cytometry (Li et al., 2009). Cowpea mosaic virus (CPMV) particles have been extensively investigated for their applicability in optical imaging applications (Chung et al., 2020). In an early study, NHS-ester chemistry was used to successfully conjugate a fluorophore, Alexa Fluor 555 (A555) to CPMV particles. CPMV-A555 particles were injected into living mice and chick embryos and microscopy enabled visualization of vascular endothelial cells and blood flow up to a depth of 500 µM. Furthermore, optical imaging using CPMV-A555 particles facilitated the long-term mapping of tumor vasculature (Lewis et al., 2006). It was later found that a natural interaction between CPMV particles and vimentin, a mammalian surface protein allowed imaging of tumour endothelium (Koudelka et al., 2009). A subsequent study found that this interaction facilitated the uptake of CPMV particles in many different types of human cancer cell lines which over-expressed vimentin and enabled in-vivo tumour homing (Steinmetz et al., 2011). More recent studies involving optical imaging with CPMV particles have focussed on achieving more specific targeting of tumour neovasculature by modication with targeting ligands (Cho et al., 2017). Amongst several others, brome-mosaic virus (BMV) VLPs, M13 bacteriophage VLPs and cowpea chlorotic mottle-virus (CCMV) VLPs have also been used for optical imaging applications (Jung et al., 2011, Carrico et al., 2012, Cadena-Nava et al., 2011).

# 1.6 Production of VNPs and VLPs

Viral capsid proteins are typically produced by viral transfection or in heterologous expression systems (Sun and Cui, 2020). A high titre of VNPs can be produced after viral infection of the natural hosts, whereas heterologous expression is more suitable to produce VLPs (Yildiz et al., 2011). Heterologous expression in the context of VLP production occurs as follows: Initially, the desired viral capsid protein gene(s) of interest are included on a suitable expression vector. Thereafter, the vector is introduced within a heterologous expression system which produces the viral capsid proteins required for VLP formation (Sun and Cui, 2020, Mejía-Méndez et al., 2022). The choice of heterologous expression system is of utmost importance to ensure proper folding and accurate post-translational modifications (PTMs) of the VLP capsid proteins (Fuenmayor et al., 2017). One should also consider requirements surrounding the long-term technical feasibility, stability and price of the production process when deciding on the most appropriate heterologous expression system for VLP production (Ding et al., 2018).

Heterologous expression systems which have been successfully used to produce VLPs include mammalian, yeast, insect, bacterial and plants cells (Kushnir et al., 2012).

## 1.6.1 What is plant molecular farming?

Plant molecular farming (PMF), a relatively modern branch of biotechnology, describes the production of recombinant proteins or other biologics in plants for pharmaceutical or industrial purposes (Rybicki, 2020, Obembe et al., 2011). The PMF process spans from the growth of the plant itself and includes the subsequent harvesting, transportation, storage, as well as the downstream protein extraction and purification processes (De Wilde et al., 2002). Recovery and utilization of the recombinant protein instead of the plant itself is the main aim of the PMF process (Ma et al., 2003, Stoger et al., 2014, Tschofen et al., 2016). Proteins may be used as a crude extract but are often purified following extraction and the plant host is merely discarded at the end of the process (Fischer and Buyel, 2020). The well-studied *Nicotiana benthamiana* is often the preferred plant host for production of recombinant proteins due to its ease of transformation and capacity for elevated levels of heterologous gene expression (Norkunas et al., 2018). The two different avenues to produce pharmaceuticals including VLPs in-planta are via stable transformation (transgenic expression) or by transient expression (Marsian and Lomonossoff, 2016).

## 1.6.2 Stable transformation

Stable transformation occurs when a foreign (exogenous) gene of interest is incorporated into the host plants nuclear or chloroplast genome using recombinant methods (Obembe et al., 2011, Ma and Wang, 2012, Chen et al., 2013a). This process results in the generation of a transgenic plant of altered genetic makeup which will then express the 'transgene' integrated within the host genome. The stably transformed plant will thereafter possess previously absent inheritable traits (Obembe et al., 2011). Stable transformation enables efficient upscaling and continuous long-term production of recombinant proteins since the transgene will be passed down from the host and maintained across multiple generations (Tremblay et al., 2010). However, stable transformation is a highly time-consuming process and the production of transgenic plants expressing usable levels of the protein of interest can take many months (Ma and Wang, 2012).

## 1.6.3 Transient expression

Transient expression of recombinant proteins offers an attractive alternative to stable transformation. The virus infection method and agroinfiltration are the two different

approaches that have been used to transiently express recombinant proteins in-planta (Obembe et al., 2011, Ma and Wang, 2012). The viral infection method utilizes plant viruses such as tobacco mosaic virus (TMV) and potato virus X (PVX) as vectors for the delivery of foreign genes into the plant host (Porta and Lomonossoff, 2002). These plant virus derived vectors can successfully infect tobacco plants and do not integrate into the plant genome, thereby enabling in-planta transient expression of a target protein (Obembe et al., 2011). Agroinfiltration takes advantage of the soil-borne *Agrobacterium* pathogen, *Agrobacterium tumefaciens* to facilitate transient expression of foreign gene(s) in-planta. (Marsian and Lomonossoff, 2016). In nature, *A. tumefaciens* causes crown gall disease by transferring a portion of its Ti (tumour-inducing) plasmid known as T-DNA to the plant nucleus (Chilton et al., 1977). This T-DNA region can be replaced with a foreign gene of interest thereby 'disarming' the Ti plasmid (Marsian and Lomonossoff, 2016, Kaur et al., 2021). One can additionally insert plant virus regulatory sequences such as promoters and enhancers in the modified Ti plasmid to create a high-yielding expression cassette (Sainsbury and Lomonossoff, 2014). A second plasmid containing the virulence (*vir*) genes is responsible for mediating transfer of the T-DNA region into the plant cells. Together these two plasmids create a binary vector system for *Agrobacterium*-mediated transient expression in-planta (Figure 8). (Simpson et al., 1986). *A. tumefaciens* suspension(s) containing the binary vector system are 'infiltrated' into the interstitial spaces of intact leaves (Kapila et al., 1997). This results in the transfection of millions of plant cells and short-term transient expression of the transgene without stable integration into the plant genome (Kaur et al., 2021). In contrast to stable transformation, transient expression enables rapid production of recombinant proteins within days or weeks. Furthermore, transient expression does not require costly equipment and supplies and is therefore a much cheaper alternative to stable transformation for achieving recombinant protein production in-planta (Ma and Wang, 2012).

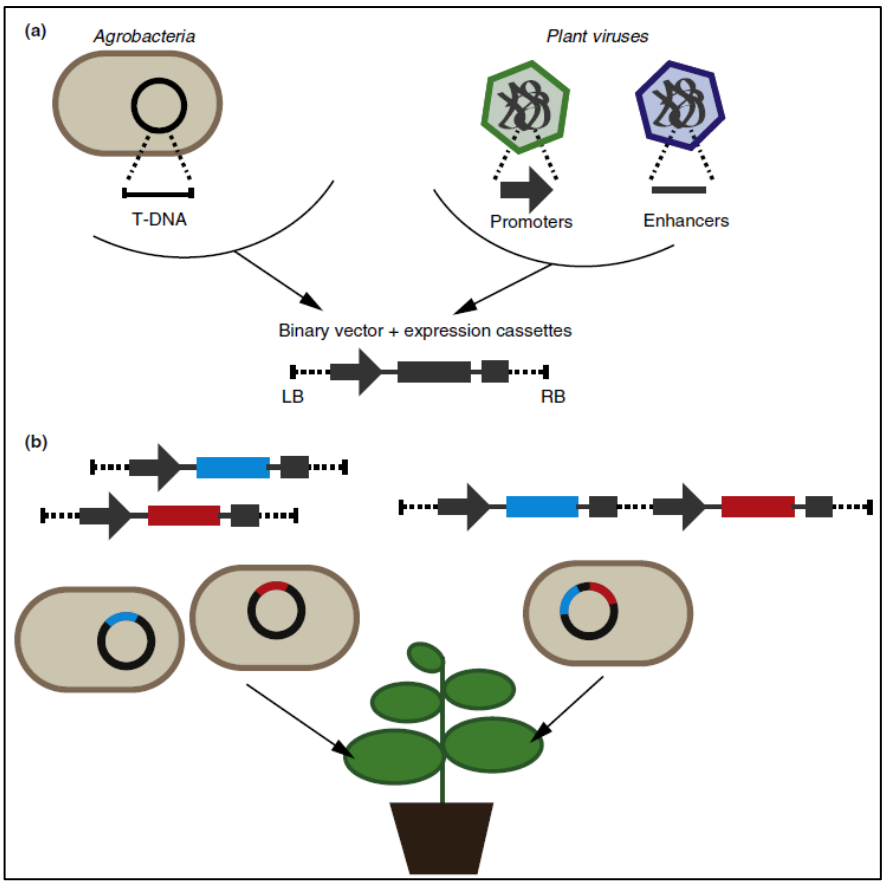


Figure 8: Schematic representation of binary vector system production. (a) Disarming of Ti plasmid and creation of foreign gene expression cassette with plant virus regulatory elements (b). Infiltration of *A. tumefaciens* suspension(s) to facilitate transient expression of the foreign gene in-planta (Sainsbury and Lomonossoff, 2014).

## 1.6.4 PMF vs other heterologous expression systems

Historically, mammalian, bacterial and to a lesser degree insect and yeast cells have been chosen as the preferred heterologous expression systems to produce recombinant proteins. However, plants have since gained traction as an alternative expression system offering a number of potential benefits. (Obembe et al., 2011). Critical PTMs such as glycosylation required for the biological functioning of mammalian proteins can be performed by plants (Ma et al., 2003, Tremblay et al., 2010). Plant expression systems offer a greater safety profile than mammalian cells as they do not allow replication of mammalian viruses, thereby avoiding potential contamination with human pathogens. The culturing of plant cells is much cheaper than using mammalian and insect cells as sunlight is the major source of energy required for plant growth. Finally, the robust and inert nature of plants simplifies handling and purification of recombinant proteins from plant tissues (Ma and Wang, 2012).

# 1.7 Production of AHSV VLPs and CLPs

In previous research conducted within our lab, transient expression was utilized to produce African horse sickness virus (AHSV) VLPs (Dennis, 2019). The AHSV virion is a non-enveloped, icosahedral particle approximately 80 nm in diameter with a complex, highly organized structure (Figure 9) (Dennis et al., 2019). Three distinct, concentric protein layers surround the segmented AHSV genome which is composed of 10 linear dsRNA molecules (Mellor et al., 1998, Mellor and Hamblin, 2004). The AHSV genome encodes a total of twelve proteins, seven of which comprise the structure of the native virion and five which are non-structural proteins (Roy et al., 1994). The outer capsid layer of the AHSV virion is composed of two major structural proteins, VP2 and VP5 (Figure 9). VP2 is the most variable viral protein and contains epitopes responsible for inducing production of specific neutralizing antibodies (Burrage et al., 1993, Roy et al., 1996). The core particle consists of an outer VP7 layer and an inner VP3 layer. VP7 trimers bind the surface of VP3 in a perpendicular fashion enclosing the AHSV genome and a replicase complex of three minor structural proteins, VP1, VP4 and VP6 (Figure 9). Dennis et al showed that transient co-expression of AHSV VP2, VP3, VP5 and VP7 in *N. benthamiana*, yielded successful production of AHSV VLPs (Dennis et al., 2019). Furthermore, AHSV core-like particles (CLPs) which consist of only the AHSV structural proteins that make up the AHSV 'core', i.e., AHSV VP3 and VP7, have been produced in expression systems such as insect cells and plants (Dennis, 2019, Maree et al., 2016). For AHSV CLPs, the inner core is formed by AHSV VP3, whereas the outer core is formed by AHSV VP7 (Maree et al., 2016).

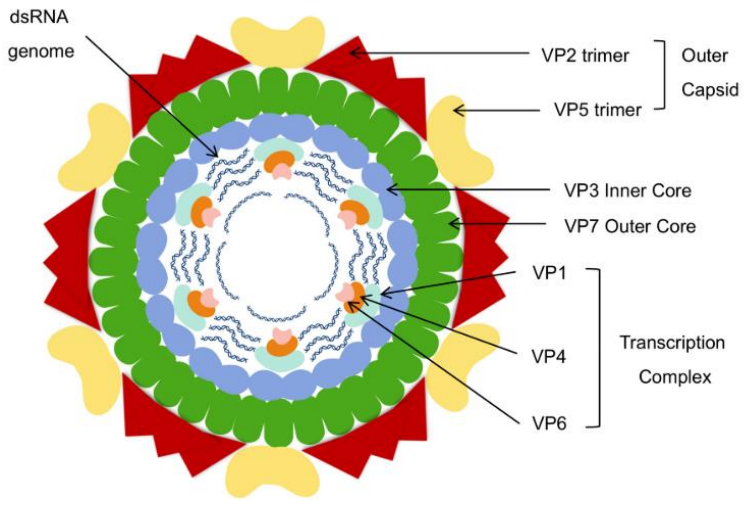


Figure 9: Schematic displaying the structural and genomic organization of the African horse sickness virus (Dennis et al., 2019)

## 1.8 Project aim

The main aim of this project was to test whether AHSV CLPs made in plants could be employed to encapsulate a fluorescent protein, namely enhanced green fluorescent protein (EGFP) as a proof of concept that such particles had cargo carrying potential. Several objectives were carried out to address this:

- The first major objective involved the production of a plasmid construct encoding the fusion of the fluorescent protein, EGFP, to the AHSV protein VP3 which comprises the inner core of the AHSV CLPs to facilitate genetic-based cargo loading of enhanced green fluorescent protein (EGFP) inside the AHSV CLPs.
- The second major objective was to produce AHSV CLPs containing EGFP by *Agrobacterium*-mediated transient co-expression of the construct encoding the EGFP-VP3 fusion, as well as the AHSV VP7 protein in *N. benthamiana* plants.
- The third objective was to optimize production of AHSV CLPs encapsulating EGFP.
- The fourth objective was to conduct a preliminary test to determine whether these particles could bind to an αvβ3 integrin receptor.

# Chapter 2: Cloning of *egfp*-AHSV-*VP3* into pEAQ and pRIC plant expression vectors

## 2.1 Introduction

The pEAQ-*HT* vector (Figure 10) is a plasmid that has been specifically designed to facilitate in-planta recombinant protein production in an efficient and timely manner (Peyret and Lomonossoff, 2013). The pEAQ-*HT* vector is created by combining the non-replicating cowpea mosaic virus hypertranslational (CPMV-*HT*) expression system with the pEAQ vector (Saxena et al., 2016). The pEAQ-*HT* vector utilizes the CPMV-*HT* expression system to enhance the translational efficiency of heterologous genes inserted between modified 3' and 5' untranslated regions (UTRs) of CPMV RNA-2 (Peyret and Lomonossoff, 2013, Sainsbury et al., 2009). As a result, the vector facilitates high level gene expression without the need for vector replication (Saxena et al., 2016, Peyret and Lomonossoff, 2013).

The pRIC4.0 vector (Figure 11) is an autonomously replicating geminivirus-based shuttle vector based on a mild strain of bean yellow dwarf virus (BeYDV-m) (Halley-Stott et al., 2007, Regnard et al., 2010). BeYDV utilizes Rep/Rep A and host-encoded proteins to undergo rolling circle replication (Hefferon and Dugdale, 2003). A common approach for designing a geminivirus-based replication vector involves replacement of the *rep* gene with the desired transgene. However, this approach requires co-transfection of another plasmid encoding production of the Rep protein to drive vector replication (Hefferon and Fan, 2004, Mor et al., 2003). The pRIC4.0 vector avoids this requirement by including both the *rep* gene and the desired transgene on the same plasmid. The pRIC4.0 vector specifically upregulates the expression of an inserted transgene by increasing its copy number via a replication process (Regnard et al., 2010).

This chapter describes the fusion of *egfp* to AHSV *VP3* and the cloning thereof into the two transient plant expression vectors pEAQ-*HT* and pRIC4.0 described above with the intention of subsequently comparing EGFP-VP3 expression levels to select the candidate that expresses the higher level of recombinant protein.

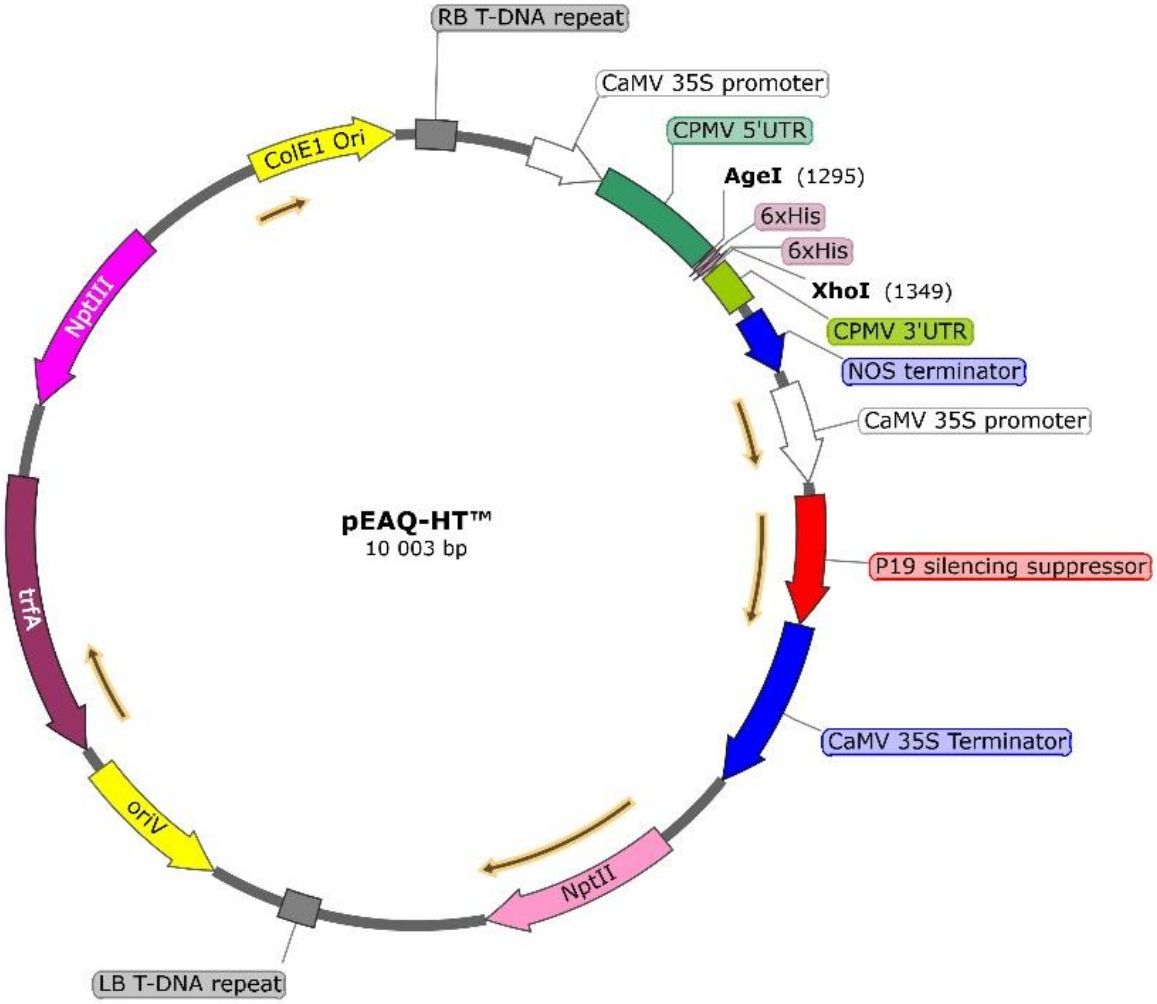


Figure 10: Plasmid map of the plant expression vector, pEAQ-*HT* (Sainsbury et al., 2009), compiled using SnapGene (GSL Biotech LLC, Chicago, IL USA) bioinformatics software and provided by Susan Dennis (BRU,UCT). LB and RB = left and right T-DNA borders, oriV = Prk2 replication origin, trfA = replication essential locus, Npt = neomycin phosphotransferase, ColE1 Ori = pBR322 replication origin, CaMV 35S = cauliflower mosaic virus, CPMV 5'/3' UTR = cowpea mosaic virus RNA-2 UTRs, NOS = nopaline synthase.

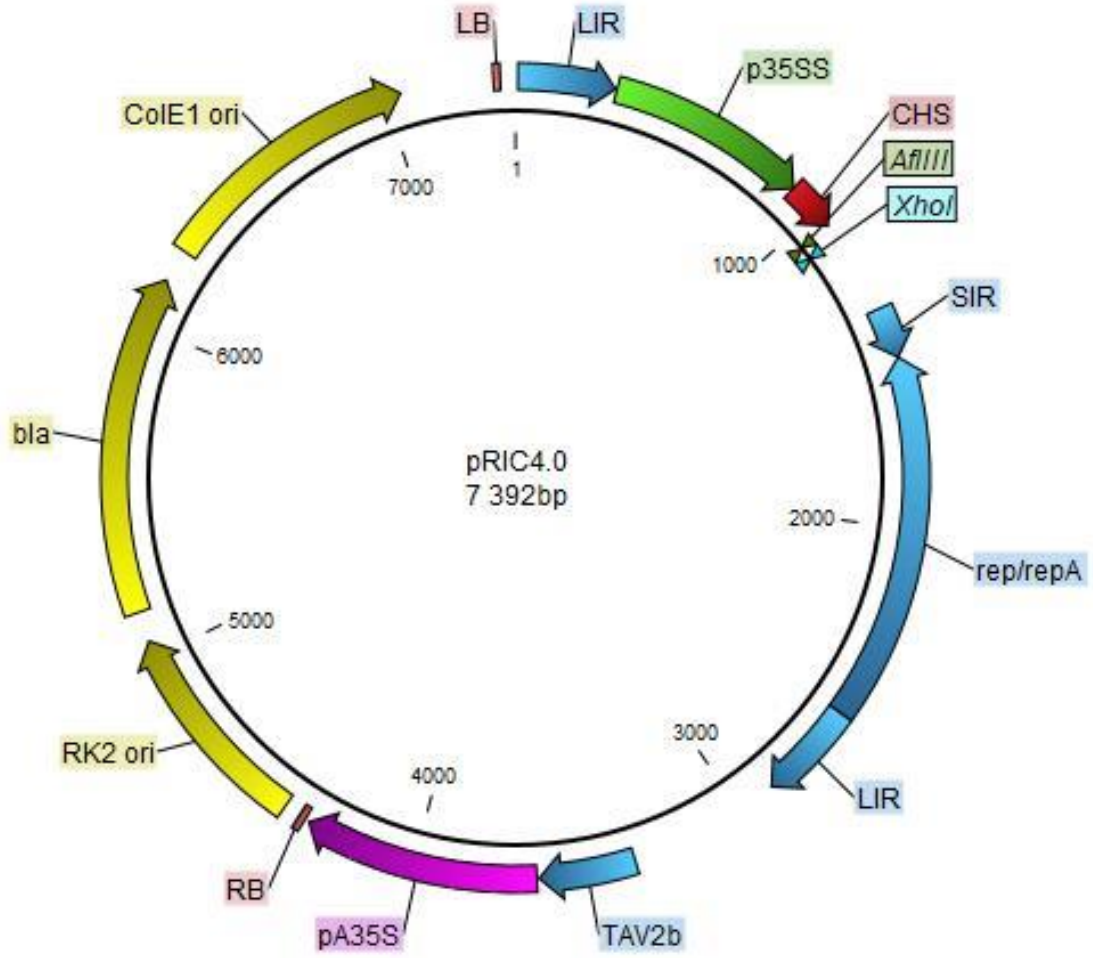


Figure 11: Plasmid map of the plant expression vector, pRIC4.0, compiled using CLC Mainbench bioinformatics software (Qiagen Bioinformatics, Aarhus, Denmark). LB and RB = left and right T-DNA borders, RK2 ori = origin of replication for *A. tumefaciens*, bla = ampicillin/carbenicillin resistance gene, ColE1 = origin of replication for *E. coli*, LIR/SIR = long/short intergenic region of BeYDV, p35SS = CaMV 35S promoter with duplicated transcriptional enhancer, CHS = chalcone synthase 5' untranslated region, pA35S = CaMV 35S polyadenylation signal, rep/repA = BeYDV rep gene, TAV2b = silencing suppressor cassette (Regnard et al., 2010).

# 2.2 Methods

## 2.2.1. Preparation of DNA for cloning

All the vectors (pEAQ-*HT*, pRIC4.0, pEGFP) and constructs (pEAQ-*HT*-VP3) required for cloning were sourced from the Biopharming Research Unit (BRU) culture collection (University of Cape Town, UCT) and were available in *E. coli* cells. To prepare DNA for cloning, DH5α *E. coli* cells (E. cloni$^{TM}$, Lucigen, Middleton, WI, USA) harbouring the desired constructs were initially inoculated into 10 mL Luria Bertani (LB) media containing the appropriate antibiotics (Supplementary table 1) and grown O/N at 37ºC in a shaking incubator. Plasmid DNA was miniprepped from the O/N cultures using the QIAprep® Spin Miniprep Kit (Qiagen, Hilden, Germany) according to the manufacturer's instructions. Restriction enzymes and buffers required for digestion reactions were sourced from ThermoFisher Scientific (USA). PCR and restriction digest products were resolved on a 1% Tris-borate EDTA (TBE) (2 mM EDTA, 89 mM boric acid, 89 mM Tris, pH 8.0) agarose gel containing 10 mg/mL EtBr and visualized under a long-wavelength ultraviolet (UV) light. The QIAquick® Gel Extraction kit (Qiagen, Hilden, Germany) was used to gel purify all DNA PCR and restriction digest products required for downstream cloning reactions.

## 2.2.2 In-fusion cloning

*Egfp* was fused to the 5' terminus of AHSV *VP3* by in-fusion cloning. Primers were designed to individually amplify *egfp* from pEGFP and AHSV *VP3* from pEAQ-*HT*-VP3 (Figure 12A). *Egfp* and AHSV *VP3* were then fused together (Figure 12B) and subsequently cloned into pEAQ-*HT* (Figure 12C) to yield pEAQ-*HT*-EGFP-VP3 (Figure 12D).

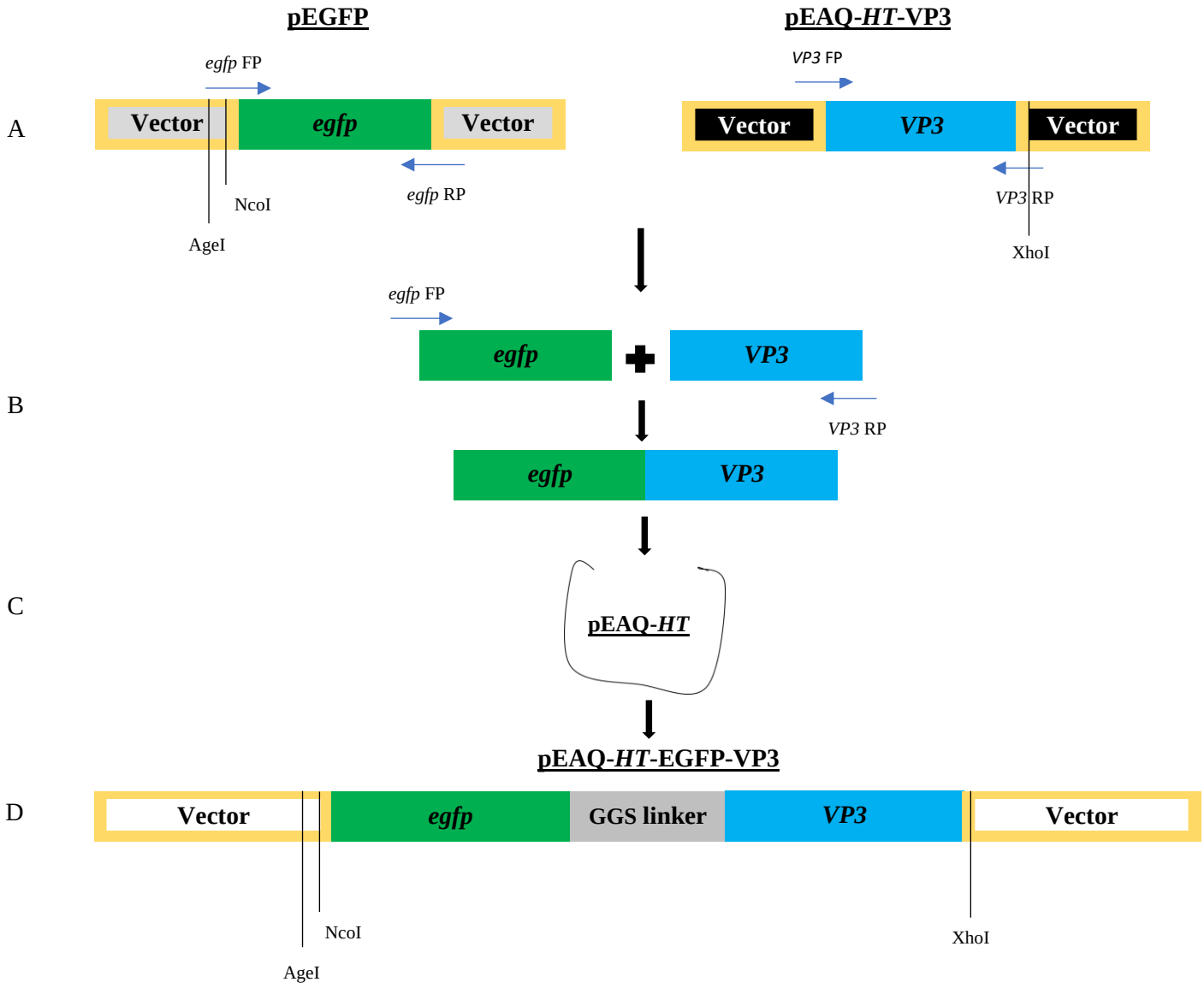


Figure 12: Schematic diagram of pEAQ-*HT*-EGFP-VP3 construct creation. (A) In-fusion cloning primers were designed (FP = forward primer, RP = reverse primer) to amplify *egfp* and *VP3* genes from pEGFP and pEAQ-*HT*-VP3 respectively. (B) Production of *egfp-VP3* by PCR of *egfp* and *VP3* genes using *egfp* FP and *VP3* RP. (C) In-fusion cloning of *egfp-VP3* into linearized pEAQ-*HT* vector. (D) Final pEAQ-*HT*-EGFP-VP3 construct with a glycine-glycine-serine (GGS) linker between *egfp* and *VP3*.

### 2.2.2.1 Design of in-fusion cloning primers

SnapGene (GSL Biotech LLC, Chicago, IL USA) bioinformatics software was used to design in-fusion cloning primers (Table 1) required for creation of the pEAQ-*HT*-EGFP-VP3 construct. These primers were synthesized by Inqaba Biotec$^{TM}$ (Pretoria, South Africa).

Table 1: In-fusion cloning primers for *egfp* and *VP3* amplification. FP = forward primer, RP= reverse primer, red nucleotides = AgeI restriction site, purple nucleotides = NcoI restriction site, orange nucleotides = XhoI restriction site, green box = GGS linker.

| Primer | Sequence |
|---|---|
| *egfp* FP | 5' TGCCCAAATTCGCG**ACCGGTCCATGG**TGAGCAAGGGCGAGGA 3' |
| *egfp* RP | 5' GCTTCCTCCGGACTTGTACAGCTCGTCCATGCCGAGA 3' |
| *VP3* FP | 5' AGCTGTACAAGTCCGGAGGAAGCATGTCAGGAAATGAGAGGATTCAGGA 3' |
| *VP3* RP | 5' TTAAAGGC**CTCGAG**CTATATAGTTGGTCTTG 3' |

### 2.2.2.2 PCR amplification of *egfp* and AHSV *VP3*

pEAQ-*HT*-VP3 (BRU, UCT (Dennis, 2019)) and pEGFP (BRU,UCT) plasmid DNA were mini-prepped from O/N DH5α *E. coli* cell cultures as described in **2.2.1**. Plasmid mini preps were subsequently diluted in dd$H_20$ and 10 ng of pEAQ-*HT*-VP3 and pEGFP DNA were added to two separate PCR reactions. Both PCR reactions included 1x CloneAmp HiFi PCR premix (Takara Bio), 0.5 µM forward primer, 0.5 µM reverse primer and template DNA (pEAQ-*HT*-VP3 or pEGFP). The *VP3* gene was amplified from pEAQ-*HT*-VP3 and the *egfp* gene was amplified from pEGFP using the appropriate primers (Table 1) and PCR cycle conditions (Table 2). The resulting *egfp* and *VP3* PCR amplification products were visualized, and gel purified as described in **2.2.1**. Purified *egfp* and *VP3* DNA fragments were then added to a new PCR reaction containing 1x CloneAmp HiFi PCR premix (Takara Bio) and 0.5 µM of the *egfp* forward primer and *VP3* reverse primer (Table 1) to generate an *egfp*-*VP3* fusion product which was amplified using the appropriate PCR cycle conditions (Table 2), resolved on an agarose gel, and purified as described in **2.2.1**.

Table 2: PCR cycle conditions for the amplification of *egfp* from pEGFP, *VP3* from pEAQ-*HT*-VP3 and *egfp-VP3* from the amplified *egfp* and *VP3* gene fragments. The expected size of each fragment following amplification using the in-fusion cloning primers is also indicated.

| DNA | PCR conditions | Expected size of amplified fragment |
|---|---|---|
| *egfp* | Denaturation at 98°C for 30 sec<br>Denaturation at 98°C for 10 sec<br>Annealing at 60°C for 30 sec } x 35<br>Extension at 72°C for 1 min<br>Elongation at 72°C for 10 min | 751 bp |
| *VP3* | Denaturation at 98°C for 30 sec<br>Denaturation at 98°C for 10 sec<br>Annealing at 60°C for 30 sec } x 35<br>Extension at 72°C for 1 min<br>Elongation at 72°C for 10 min | 2755 bp |
| *egfp-VP3* | Denaturation at 98°C for 30 sec<br>Denaturation at 98°C for 10 sec<br>Annealing at 60°C for 30 sec } x 35<br>Extension at 72°C for 3 min and 30 sec<br>Elongation at 72°C for 10 min | 3483 bp |

### 2.2.2.3 In-fusion cloning of *egfp-VP3* into pEAQ-*HT*

The pEAQ-*HT* vector (received from G. Lomonossoff, John Innes Centre, UK (Sainsbury et al., 2009)) was linearized using AgeI and XhoI restriction enzymes, resolved and purified from an agarose gel as described in **2.2.1**. The in-fusion®HD Cloning kit (Clontech, Mountain View, CA, USA) was then utilized to carry out the in-fusion cloning reaction of *egfp-VP3* into the linearized pEAQ-*HT* vector (Table 3). The in-fusion cloning reaction was incubated for 15 min at 50ºC and then placed on ice for an additional 15 min.

Table 3: Reaction components for in-fusion cloning of *egfp-VP3* into the pEAQ-*HT* vector.

| Reaction Component | In-fusion cloning of *egfp-VP3* into pEAQ-*HT* |
|---|---|
| Purified PCR fragment | 2 uL of *egfp-VP3* |
| Linearized vector | pEAQ-*HT* (±50ng) |
| 5x In-Fusion HD Enzyme Premix | 2 uL |
| Deionized Water | to 10 uL |

## 2.2.3 Restriction enzyme (RE) digest-based cloning

After creation of the pEAQ-*HT*-EGFP-VP3 construct using in-fusion cloning, *egfp-vp3* was subcloned into pRIC4.0 to yield pRIC4.0-EGFP-VP3.

### 2.2.3.1 Ligation of *egfp-VP3* into pRIC4.0

pEAQ-*HT*-EGFP-VP3 and pRIC4.0 DNA were mini-prepped from O/N DH5α *E. coli* cell cultures. The pEAQ-*HT*-EGFP-VP3 construct was subjected to NcoI/XhoI digestion and the pRIC4.0 vector was linearized by AflIII/XhoI digestion. The digest products were resolved on an agarose gel and the *egfp-VP3* gene fragment from pEAQ-*HT*-EGFP-VP3, and the linearized pRIC4.0 vector were purified as described in **2.2.1**. To ligate *egfp-VP3* into pRIC4.0 and create pRIC4.0-EGFP-VP3, 50 ng of pRIC4.0, 93 ng of *egfp-VP3*, a ligase buffer and T4 DNA ligase were mixed, and the ligation reaction mixture was then transformed into competent DH5α *E. coli* cells.

## 2.2.4 *E. coli* transformation and *Agrobacterium* electroporation

In-fusion **(section 2.2.2.3)** and ligation **(section 2.2.3.1)** reaction mixtures were transformed into competent DH5α *E. coli* cells using the transformation protocol as described in Sambrook *et al*., (1989). Transformed cells were added to 400 µL LB broth, incubated at 37ºC for 1hr, and 100 µL was plated onto LB agar supplemented with the appropriate antibiotics (Supplementary table 1). Plates were then incubated at 37ºC O/N to allow colony growth. Two *Agrobacterium tumefaciens* strains, AGL-1 and GV3101::pMP90RK were obtained from the BRU culture collection (University of Cape Town, UCT) and these cells were made electrocompetent using the protocol described in Shen and Forde (1989). Approximately 400 ng of mini-prepped pEAQ-*HT*-EGFP-VP3 DNA was mixed with 100 µL thawed AGL-1 cells, whereas 400 ng of mini-prepped pRIC4.0-EGFP-VP3 DNA was mixed with 100 µL thawed GV3101::pMP90RK cells. Each mixture was added to a separate 0.1 cm electroporation cuvette (Molecular BioProducts, USA) and a Gene Pulser (Bio-Rad, USA) was used to perform electroporation under the following conditions: 1.8 kV, 25µF and 200 Ω. After electroporation, cuvettes were placed on ice and 900 µL LB was added to the electroporation mixture. 1 mL of the total mixture was then added to a fresh Eppendorf tube and incubated at 27ºC for 2 hrs, thereafter 35 µL was plated onto LB agar supplemented with the appropriate antibiotics (Supplementary table 1) to allow *A. tumefaciens* colony growth.

## 2.2.5 Colony PCR screening and restriction digest confirmation

To confirm the presence of pEAQ-*HT*-EGFP-VP3 or pRIC4.0-EGFP-VP3 constructs in *E. coli/A. tumefaciens* transformants, a colony PCR (cPCR) screen utilizing the appropriate vector-specific primers (Table 4A) and PCR cycle conditions (Table 4B) was performed. To further confirm the success of *E. coli* transformation or *Agrobacterium* electroporation, DNA was first mini prepped from potential positive transformants as described in **2.2.1**. The DNA was then digested with various combinations of restriction enzymes to confirm the presence of expected banding patterns.

Table 4: (A) vector-specific (pEAQ and pTRAc) primers used to screen *E. coli* or *A. tumefaciens* colonies for the presence of pEAQ and pRIC (pRIC contains a similar backbone to pTRAc vector series) (Regnard et al., 2010) constructs respectively. FP = forward primer, RP = reverse primer. (B) PCR cycle conditions for cPCR confirmation of pEAQ and pRIC constructs in *E. coli* and *A. tumefaciens* cells and expected *egfp-VP3* fragment size.

A

| | |
|---|---|
| pEAQ FP | 5’ TTCTTCTTCTTGCTGATTGG 3’ |
| pEAQ RP | 5’ CACAGAAAACCGCTCACC 3’ |
| pTRAC FP | 5’ CATTTCATTTGGAGAGGACACG 3’ |
| pTRAC RP | 5’GAACTACTCACACATTATTCTGG 3’ |

B

| DNA | PCR cycle conditions | Expected size of amplified *egfp-VP3* fragment |
|---|---|---|
| pEAQ-*HT*-EGFP-VP3 | Denaturation at 95°C for 5 min<br>Denaturation at 95°C for 30 sec<br>Annealing at 51°C for 30 sec<br>Extension at 72°C for 2 min (x 30)<br>Elongation at 72°C for 7 min | 3673 bp |
| pRIC4.0-EGFP-VP3 | Denaturation at 95°C for 5 min<br>Denaturation at 95°C for 30 sec<br>Annealing at 48°C for 30 sec<br>Extension at 72°C for 1 min (x 30)<br>Elongation at 72°C for 7 min | 3614 bp |

# 2.3 Results

## 2.3.1 Fusion of *egfp* and AHSV *VP3*

To facilitate fusion of the *egfp* and *VP3* genes during the in-fusion cloning reaction, modification of their gene termini was required. This was achieved by using specially designed in-fusion cloning primers to carry out the PCR amplification reactions (Table 1). pEAQ-*HT*-VP3 and pEGFP DNA served as templates in separate individual PCR reactions for *VP3* and *egfp*, respectively. After amplification of *VP3* and *egfp*, PCR products were visualized on an agarose gel. Bands corresponding to the size of the *egfp* gene (751 bp) and *VP3* gene (2755 bp) were visualized in lanes 1-3 and 4-6, respectively (Figure 13A). *Egfp* and *VP3* DNA fragments were excised from the gel, purified, and used as combined templates in a new PCR reaction. PCR products were then resolved on an agarose gel to confirm successful amplification of the fused *egfp-VP3* DNA fragment from the *egfp* and *VP3* gene templates. Bands corresponding to the size of the *egfp-VP3* DNA fragment (3483 bp) and a 750-1000 bp non-specific amplification product were visualized in lanes 1-2 (Figure 13B).

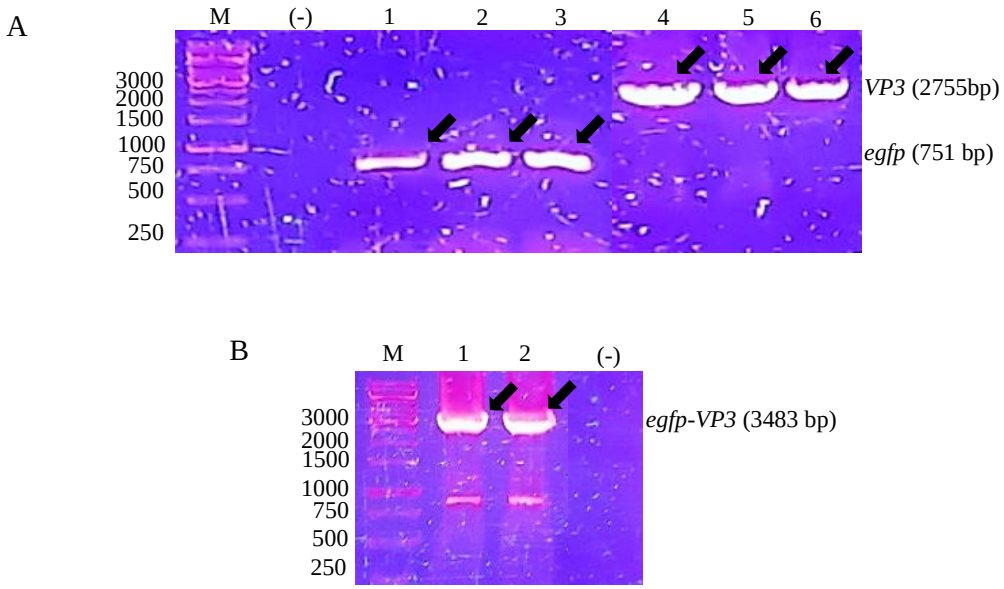


Figure 13: Production of recombinant *egfp-VP3* gene. (A) PCR amplification of *egfp* and *VP3*: (-) = no template control, 1-3 = *egfp* (751 bp) amplified from pEGFP using *egfp* forward and reverse primers, 4-6 = *VP3* (2755bp) amplified from pEAQ-*HT*-VP3 using *VP3* forward and reverse primers. Black arrows indicate excised *egfp* and *VP3* DNA fragments. (B) PCR amplification of *egfp-VP3*: (-) = no template control, 1-2 = *egfp-VP3* (3483 bp) amplified from *egfp* and *VP3* templates using the *egfp* forward primer and *VP3* reverse primer, and a non-specific 750-1000 bp product. Black arrows indicate the excised *egfp-VP3* DNA fragments.

## 2.3.2 In-fusion cloning of *egfp-VP3* into pEAQ-*HT*

After amplification of the *egfp-VP3* gene fragment, the pEAQ-*HT* vector was linearized by AgeI/XhoI restriction digestion (Data not shown). The pEAQ-*HT*-EGFP-VP3 construct was then created by inserting *egfp-VP3* into pEAQ-*HT* via the in-fusion cloning reaction and the in-fusion cloning reaction mixture was then transformed into DH5α *E. coli* cells.

## 2.3.3 Restriction digest of pEAQ-*HT*-EGFP-VP3 and pRIC4.0

To create pRIC4.0-EGFP-VP3, pRIC4.0 was linearized with AflIII/XhoI to yield a 7392 bp fragment (Figure 14A). pEAQ-*HT*-EGFP-VP3 was digested to yield 3 fragments: the 3450 bp fragment represented the *egfp-VP3* fragment (Figure 14B).

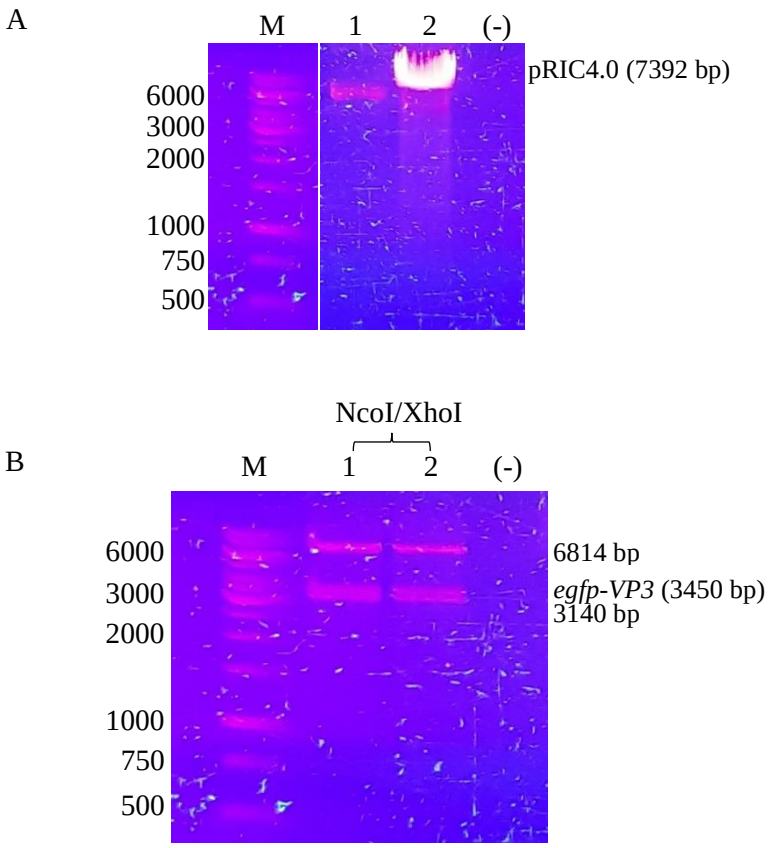


Figure 14: Restriction digestion of pRIC4.0 and pEAQ-*HT*-EGFP-VP3 to obtain DNA fragments for sub-cloning. (A) Linearization of the pRIC4.0 vector. Lane 1 = undigested pRIC4.0 vector control, Lane 2 = pRIC4.0 vector digested by AflIII/XhoI restriction enzymes, (-) = no template control. (B) NcoI/XhoI restriction digestion of pEAQ-*HT*-EGFP-VP3 to obtain *egfp-VP3* DNA fragment. Lane 1-2 = digest products corresponding to sizes of 3140 bp, 3450 bp and 6814 bp, (-) = no template control.

## 2.3.4 Ligation of *egfp-VP3* into pRIC4.0

The 3450 bp *egfp-VP3* fragment was then ligated into the linearized pRIC4.0 vector to create the pRIC4.0-EGFP-VP3 construct, and the ligation reaction mixture was transformed into DH5α *E. coli* cells.

## 2.3.5 Confirmation of successful *E. coli* transformation

### 2.3.5.1 Colony PCR screening

After *E. coli* transformation, cPCR was used to screen colonies for the presence of the final construct. A total of 8 colonies were screened to detect the presence of the pEAQ-*HT*-EGFP-VP3 construct in *E. coli* transformed with the in-fusion cloning reaction mixture. Bands corresponding to the expected size of the *egfp-VP3* DNA fragment (3673 bp) were visualized in only 4 of the 8 screened colonies (Figure 15A, C1, C2, C4 and C6). In the other 4 colonies, non-specific DNA fragments were amplified (Figure 15A, C3,C5,C7,C8). A total of 10 colonies were screened to detect the presence of the pRIC4.0-EGFP-VP3 construct in *E. coli* cells transformed with the ligation reaction mixture. DNA fragments corresponding to the size of *egfp-VP3* (3614 bp) were visualized in 4 of the 10 screened colonies (Figure 15B, C2, C4, C7 and C9). In the remaining colonies, either no DNA fragment was visualized (Figure 15B, C5) or several smaller non-specific DNA fragments were visualized (Figure 15B, C1, C3, C6, C8 and C10).

A

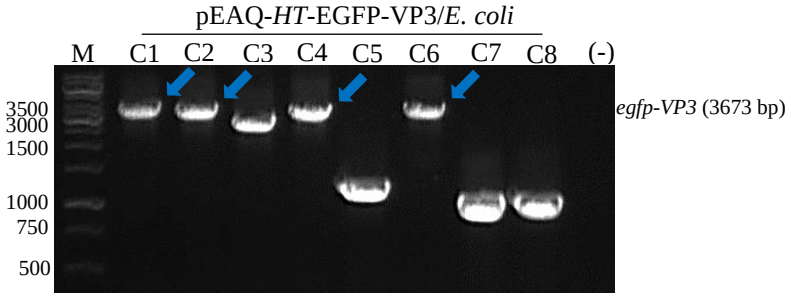


B

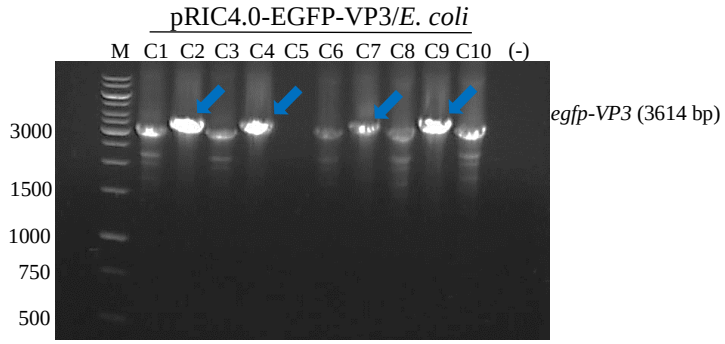

Figure 15: cPCR screening to confirm successful transformation of *E. coli*. (A) cPCR using pEAQ vector specific primers to confirm the presence of pEAQ-*HT*-EGFP-VP3 in transformed *E. coli* colonies (C1-C8). (-) = no template control. Blue arrows indicate amplified *egfp-VP3* DNA fragments (3673 bp). (B) cPCR using pTRAc primers to confirm the presence of pRIC4.0-EGFP-VP3 in transformed *E. coli* colonies (C1-C10). (-) = no template control. Blue arrows indicate amplified *egfp-VP3* DNA fragments (3614 bp).

### 2.3.5.2 Restriction digest confirmation

To further confirm the presence of the pEAQ-*HT*-EGFP-VP3 or pRIC4.0-EGFP-VP3 constructs in transformed DH5α *E. coli* cells, DNA was mini-prepped from potentially positive colonies based on the *E. coli* cPCR results. DNA mini-prepped from two colonies (C2 and C4)(Figure 15A), were subjected to two digest reactions (AgeI/XhoI and NcoI/XhoI) to further confirm the presence of pEAQ-*HT*-EGFP-VP3 in these colonies. For both colonies, AgeI/XhoI digestion yielded two DNA fragments around the expected size (9949 bp and 3455 bp) and NcoI/XhoI digestion yielded three DNA fragments around the expected size (6819 bp, 3449 bp and 3136 bp) (Figure 16A). DNA mini-prepped from four colonies (C2,C4,C7,C9)(Figure 15B), was subjected to two digest reactions (EcoRV and HindIII/PstII) to further confirm the presence of pRIC4.0-EGFP-VP3 in these colonies. For all four colonies, EcoRV digestion yielded three DNA fragments of the expected size (7886 bp, 2318 bp and 567 bp), and HindIII/PstII digestion also yielded three DNA fragments of the expected size (7401 bp, 3111 bp and 298 bp)(Figure 16B).

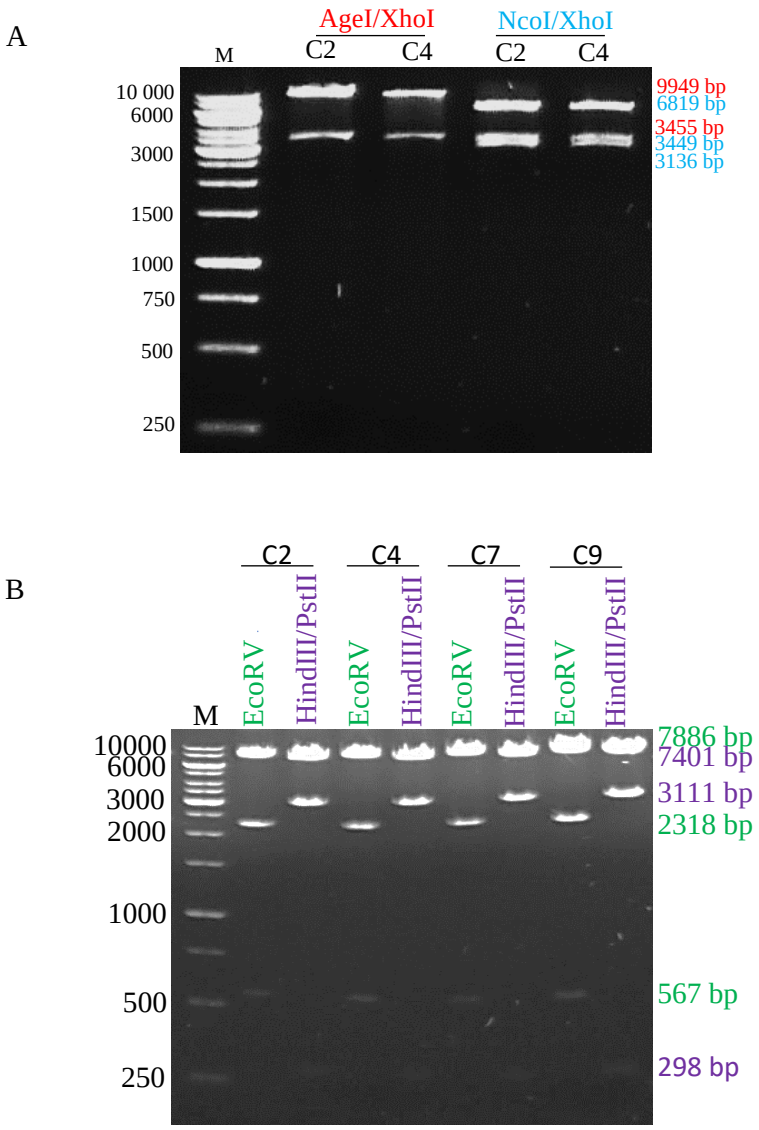


Figure 16: RE digest reactions to confirm successful *E. coli* transformation. (A) Confirming the presence of the pEAQ-*HT*-EGFP-VP3 construct in DNA extracted from colonies 2 and 4. Lanes 1 and 2 = AgeI/XhoI digest products of colonies 2 and 4. Sizes of Re digest products highlighted in red. Lanes 3 and 4 = NcoI/XhoI digest products of colony 2 and 4. Sizes of Re digest products highlighted in blue. (B) Confirming the presence of the pRIC4.0-EGFP-VP3 construct in DNA extracted from colonies 2,4,7 and 9. Lanes 1,3,5 and 7 = EcoRV digest products of colonies 2,4,7 and 9 respectively. Re digest products highlighted in green. Lanes 2,4,6 and 8 = HindIII/PstII digest products of colonies 2,4,7 and 9 respectively. Re digest products highlighted in purple.

## 2.3.6 Confirmation of successful *Agrobacterium* electroporation

### 2.3.6.1 Colony PCR screening

After confirming transformation of *E. coli* with either pEAQ-*HT*-EGFP-VP3 or pRIC4.0-EGFP-VP3, DNA from positive *E. coli* transformants was electroporated into *A. tumefaciens* cells. To determine whether AGL-1 cells were successfully electroporated with the pEAQ-*HT*-EGFP-VP3 construct, five AGL-1 colonies were screened. Bands corresponding to the size of the *egfp-VP3* gene fragment (3673 bp) and a non-specific DNA fragment of approximately 1500 bp were amplified from all five colonies (Figure 17A, C1-C5). To determine whether GV3101::pMP90RK cells were successfully electroporated with the pRIC4.0-EGFP-VP3 construct, ten GV3101::pMP90RK colonies were screened. Bands corresponding to the expected size of the *egfp-VP3* gene fragment (3614 bp) were amplified from all 10 colonies (Figure 17B, C1-C10).

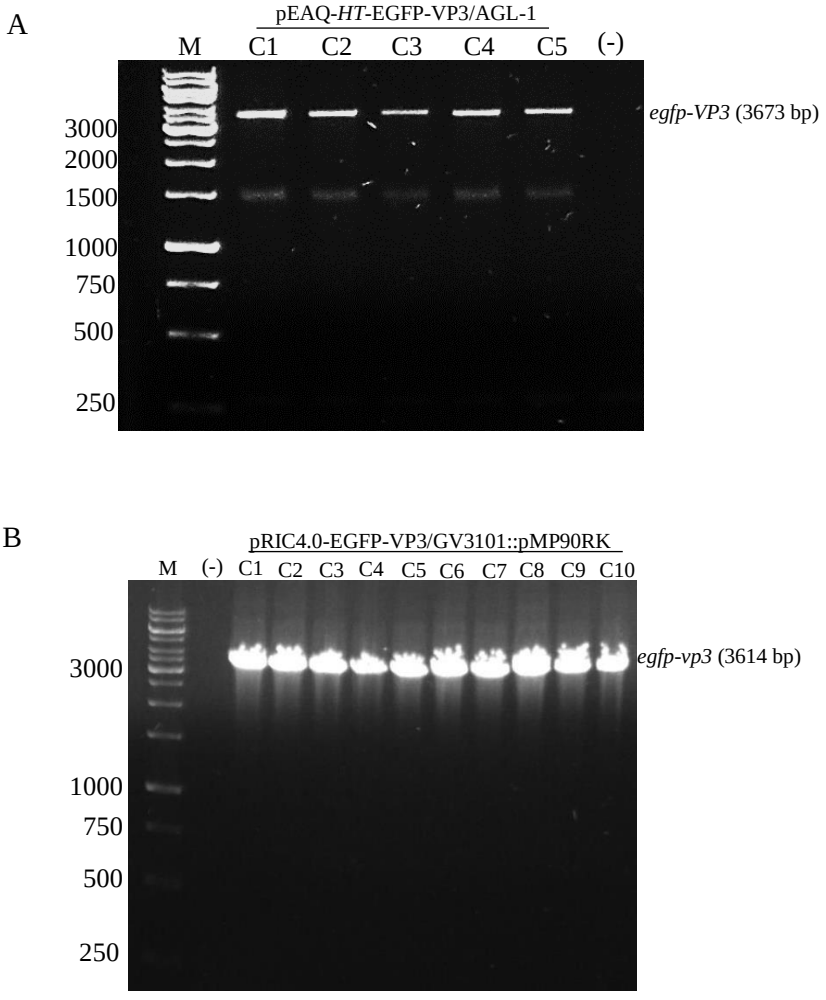

Figure 17: cPCR screening to confirm successful electroporation of *A. tumefaciens* cells (A) cPCR using pEAQ vector specific primers to confirm the presence of pEAQ-*HT*-EGFP-VP3 in electroporated AGL-1 colonies (C1-C5). (-) = no template control, C1-C5 = amplified *egfp-VP3* DNA fragment (3673 bp) (B) cPCR using pTRAc primers to confirm the presence of pRIC4.0-EGFP-VP3 in electroporated GV3101::pMP90RK colonies (C1-C10). (-) = no template control, C1-C10 = amplified *egfp-VP3* DNA fragment (3614 bp).

# 2.4 Discussion

To facilitate potential encapsulation of EGFP inside AHSV CLPs, it was of utmost importance to first design and make constructs capable of encoding an EGFP-VP3 fusion protein. The in-fusion cloning technique which enables attachment of two or more DNA fragments that have a 15 bp overlap at their termini (Zhu et al., 2007), was successfully utilized to create the pEAQ-*HT*-EGFP-VP3 construct. The primers used for initial amplification of the *egfp* and AHSV *VP3* genes were designed in a way that enabled successful fusion of *egfp* to AHSV *VP3* with incorporation of a glycine-glycine-serine (GGS) linker between these two genes. Incorporation of a linker region was done to ensure successful covalent attachment of functional domains of the EGFP and AHSV VP3 proteins. The GGS linker was specifically incorporated as glycine-serine based linkers have been shown to increase the stability and folding of several recombinant fusion proteins (Chen et al., 2013b). This was done to ensure that the functionality of the EGFP protein was not hindered, thereby ensuring that fluorescence of this protein occurred. Although successful amplification of *egfp-VP3* was achieved, a tool such as Primer-BLAST which enables target specific primer design could be used in the future to help design primers that minimize the amplification of the observed non-specific PCR products (Ye et al., 2012). By engineering the primers used to amplify *egfp* and AHSV *VP3* with a 15 bp overlap with the ends of the linearized pEAQ-*HT* vector, insertion of *egfp-VP3* into pEAQ-*HT* was seamlessly achieved via the in-fusion cloning reaction. Compared to traditional cloning approaches, in-fusion cloning requires no restriction digestion, phosphatase treatment or ligation, and cloning is achieved in a single reaction (Clontech, 2012). The presence of pEAQ-*HT*-EGFP-VP3 was confirmed in *E. coli* cells transformed with the in-fusion reaction mixture, via cPCR and restriction digest confirmation reactions, thereby confirming the success of in-fusion cloning. By employing restriction digestion, the *egfp-VP3* fragment was successfully cut from pEAQ-*HT*-EGFP-VP3, and a ligation reaction was used to successfully subclone this fragment into a linearized pRIC4.0 vector as evident by the results of cPCR and restriction

digest confirmation reactions which confirmed the presence of the pRIC4.0-EGFP-VP3 construct in *E. coli* cells transformed with the ligation reaction mixture.

Overall, these results showed successful utilization of two different cloning strategies for production of two constructs that could then later be assessed in terms of their ability to produce the EGFP-VP3 fusion protein required for assembly of an AHSV CLP containing the EGFP protein.

# Chapter 3: Production, purification, and analysis of AHSV CLPs encapsulating EGFP

## 3.1 Introduction

African horse sickness virus (AHSV) and bluetongue virus (BTV) belong to the Orbivirus genus which is found within the Reoviridae family of viruses (Basak et al., 1996). Morphologically, purified AHSV (Chapter 1, Figure 9) and BTV particles are almost identical in structure (Murphy et al., 1971, Burroughs et al., 1994), and both are comprised of a double capsid layer (Basak et al., 1996). The outer capsid layer of AHSV and BTV is made up of the structural proteins, VP2 and VP5, whereas their inner capsid layer or 'core' encapsulates the viral genome and is made up of the structural proteins, VP3 and VP7, and the minor proteins VP1,VP4 and VP6 (Chapter 1, Figure 9) (Basak et al., 1996). Multiple studies have demonstrated that if one expresses the structural proteins of AHSV or BTV in a heterologous expression system such as plants or insect cells, empty virus like particles (VLPs) and core-like particles (CLPs) can be produced (Dennis, 2019, Maree et al., 2016, Thuenemann et al., 2013, Hewat et al., 1992, Hewat et al., 1994, French and Roy, 1990). Baculovirus-mediated expression of the VP3 and VP7 structural proteins of BTV in insect cells was shown to result in the spontaneous self-assembly of empty CLPs (French and Roy, 1990). French et al later showed that expression of all four BTV structural proteins - VP3, VP7, VP5 and VP2 using a baculovirus expression system in insect cells resulted in the production of empty BTV VLPs (French et al., 1990). A later study found that BTV VLPs showed potential as an inherently safe vaccine candidate against BTV in sheep (Stewart et al., 2012). BTV VLPs and CLPs have also been successfully produced in plants via *Agrobacterium*-mediated transient expression of the BTV structural proteins in a study geared towards investigating a more cost-effective BTV vaccine production strategy (Thuenemann et al., 2013). Similarly to BTV, empty AHSV CLPs composed of VP3 and VP7 have been produced using a baculovirus expression system in insect cells (Maree et al., 2016). Furthermore, AHSV VLPs have also been produced using a plant expression system to develop an AHSV vaccine candidate (Dennis, 2019). While most research involving these VLPs and CLPs revolves around the production of potential vaccine candidates against the native virus, these particles have also shown great potential in the field of nanotechnology (Thuenemann and Lomonossoff, 2018). A study by Kar et al found that by fusing GFP to the N-terminus of BTV VP3, one could produce fluorescent CLPs upon co-expression with BTV VP7 in insect cells. Unfortunately, this GFP fusion was found to be

unstable and encapsulation of GFP within the CLP internal cavity could not be confirmed (Kar et al., 2005). A later study successfully used plants to produce BTV CLPs encapsulating GFP (Brillault et al., 2017). Furthermore, this study showed that an arginine-glycine-aspartate (RGD) motif present on an exposed surface loop of BTV VP7 may enable these particles to target a human integrin receptor, highlighting their potential biomedical application as a delivery vehicle of small molecules and proteins to human target cells (Brillault et al., 2017). The RGD motif has specifically shown a high binding affinity toward upregulated integrin receptors, particularly αvβ3 and αvβ5, and has been utilized to target diagnostic and therapeutic molecules to cancer cells that overexpress these integrin receptors (Lee et al., 2016, Brillault et al., 2017). This chapter initially describes the plant-based production of an AHSV EGFP-VP3 fusion protein using the pEAQ-*HT*-EGFP-VP3 and pRIC4.0-EGFP-VP3 constructs described in chapter 2. The chapter further describes the plant-based production of empty AHSV CLPs and AHSV CLPs encapsulating EGFP as well as the purification and analysis of these particles. Finally, this chapter describes a preliminary test to determine whether the RGD motif present on an exposed surface loop of AHSV VP7, enables AHSV CLPs encapsulating EGFP to interact with an αvβ3 integrin receptor.

# 3.2 Methods

## 3.2.1 *Agrobacterium*-mediated transient protein expression

### 3.2.1.1 Single infiltration

Recombinant AGL-1 (pEAQ-*HT* and pEAQ-*HT*-EGFP-VP3)**(section 2.3.2)** and GV3101::pMP90RK (pRIC4.0 and pRIC4.0-EGFP-VP3) **(section 2.3.4)** starter cultures were prepared by inoculating 1 mL glycerol stocks into 10 mL LB broth containing the appropriate antibiotics (Supplementary table 1) and grown O/N at 27º C with agitation. The starter cultures were then inoculated into 50 mL induction media (2.5 g/L tryptone, 5 g/L NaCl, 12.5 g/L yeast extract, 1.95 g/L morpholinoethanesulfonic acid (MES), pH = 5.6) supplemented with the appropriate antibiotics (Supplementary table 1), 200 µM acetosyringone and grown O/N at 27º C with agitation. Finally, the 50 mL pre-cultures were inoculated into 500 mL induction media supplemented with the appropriate antibiotics (Supplementary table 1), 200 µM acetosyringone and grown O/N at 27°C with agitation. The optical density ($OD_{600}$) values of the final 500 mL cultures were measured at a wavelength of 600 nm using a spectrophotometer. To create single infiltration suspensions with desired optical density values, individual cultures were diluted

using a resuspension solution (5 mM MES, 20 mM $MgCl_2$, 200 µM acetosyringone). Thereafter, infiltration suspensions were incubated for 2 h at room temperature to allow acetosyringone to activate *vir* gene expression. The pEAQ-*HT*/AGL-1 and pRIC4.0/GV3101::pMP90RK cultures were diluted to a final $OD_{600}$ = 0.5 and *N. benthamiana* plants were infiltrated with each of these infiltration suspensions. The pEAQ-*HT*-EGFP-VP3/AGL-1 and pRIC4.0-EGFP-VP3/GV3101::pMP90RK cultures were diluted to a final $OD_{600}$ = 0.25 or 0.5 and *N. benthamiana* plants were infiltrated with each of these infiltration suspensions. To vacuum infiltrate the leaves of approximately 4-week-old *N. benthamiana* plants, the plants were submerged in the appropriate infiltration suspensions and a 100 kPa vacuum was applied. After vacuum infiltration, the plants were incubated in a growth room at 22°C and subjected to a 16-h light, 8-h dark cycle until the day of harvest.

### 3.2.1.2 Co-infiltration

For co-expression, recombinant AGL-1 cultures of pEAQ-*HT*-VP3 **(section 2.2.2.2)**, pEAQ-*HT*-EGFP-VP3 **(section 2.3.2)** and pEAQ-*HT*-VP7 (BRU, UCT, (Dennis, 2019)) were prepared to a final 500 mL volume and their $OD_{600}$ values were measured as described in **3.2.1.1.** To create co-infiltration suspensions, individual cultures were first mixed and then diluted to the desired $OD_{600}$ value using resuspension solution. To produce empty CLPs, pEAQ-*HT*-VP3/AGL-1 was mixed with pEAQ-*HT*-VP7/AGL-1 and diluted in resuspension solution to create a VP3:VP7 co-infiltration suspension with a final $OD_{600}$ = 1.0 ($OD_{600}$ of 0.5 each). To produce CLPs encapsulating EGFP ('EGFP CLPs'), pEAQ-*HT*-EGFP-VP3/AGL-1 was mixed with pEAQ-*HT*-VP7/AGL-1 and diluted in resuspension solution to create an EGFP-VP3:VP7 co-infiltration suspension with a final $OD_{600}$ = 1.0 ($OD_{600}$ = 0.5 each). Vacuum infiltration was carried out as described in **3.2.1.1,** with *N. benthamiana* plants being infiltrated with the VP3:VP7 co-infiltration suspension and *N. benthamiana* plants being infiltrated with the EGFP-VP3:VP7 co-infiltration suspension.

## 3.2.2. Small extraction and analysis of EGFP-VP3 expression

### 3.2.2.1 Small scale homogenization and protein extraction

Expression of EGFP-VP3 in *N. benthamiana* plants infiltrated with pEAQ-*HT*-EGFP-VP3/AGL-1 or pRIC4.0-EGFP-VP3/GV3101::pMP90RK was monitored by harvesting leaf discs at 4-, 5- and 6-days post-infiltration (DPI). One leaf disc per plant, was harvested from a total of 4 plants infiltrated with either pEAQ-*HT*-EGFP-VP3/AGL-1 or pRIC4.0-EGFP-

VP3/GV3101::pMP90RK at 4,5 and 6 DPI and collected into a 1.5 mL tube. The leaf disc samples were weighed and homogenized in 3 volumes of 1x PI buffer (1 x PBS [ 2 mM $KH_2PO_4$, 2.7 mM KCl, 10 mM $Na_2HPO_4$, 137 mM NaCl, pH 7.4], containing 1 x Complete™, EDTA-free protease inhibitor cocktail [Roche, Basel, Switzerland]) using a micro pestle. Homogenates were incubated for 1 h at 4°C with gentle agitation and then clarified by centrifugation at 13 000 rpm for 10 min in a table-top microcentrifuge. Total soluble protein (TSP) was then collected into a new 1.5 mL tube and stored at -20°C. Protein samples were also prepared from leaf discs harvested at 5 DPI from *N. benthamiana* plants infiltrated with either pEAQ-*HT*/AGL-1 or pRIC4.0/GV3101::pMP90RK (empty vectors -> negative controls) using the same methodology as described above.

### 3.2.2.2 Protein analysis

The concentration of each sample collected between 4 and 6 DPI, was determined by performing a Bradford assay using bovine serum albumin (BSA)(Sigma-Aldrich, MO, USA) as a standard. To determine EGFP-VP3 protein expression levels at different optical densities between 4 and 6 DPI, 50 uL of each sample was first mixed with 12.5 uL sample application buffer (SAB)(Sambrook et al., 1989) and denatured for 10 min at 95°C. Equal amounts of each sample as determined by Bradford assay, were then loaded into the wells of a 10% SDS polyacrylamide gel and separated by electrophoresis for 1 h at 200V. The PageRuler™ Plus Prestained Protein Ladder (Thermo Fisher Scientific) was loaded (6 ul/well) as a molecular weight marker. A Trans-blot® SD semi-dry transfer cell (Bio-Rad, Irvine, CA) set to 15V was used to transfer protein samples from the SDS polyacrylamide gel onto a HyBond™ C Extra nitrocellulose membrane (AEC-Amersham, South Africa) over 1 h 30 min. For western blot analysis, membranes were first transferred to blocking buffer (1x PBS, 5% fat free dairy milk, 0.1% Tween-20®) and blocked for 30 min at room temperature with gentle agitation. The membranes were then probed O/N at 4°C with an anti-AHSV horse serum (received from C. Potgieter Deltamune (Pty) Ltd., South Africa) diluted (1:5000) in blocking buffer or an anti-GFP antibody (Abcam) diluted (1:2000) in blocking buffer. The membranes were then washed 3 times in blocking buffer at room temperature for 5 min. Thereafter, membranes were probed for 1 h at 37°C with an anti-horse alkaline phosphatase (AP) conjugated secondary antibody (Sigma-Aldrich, St Louis, MO, USA) diluted (1:10 000) in blocking buffer or goat anti-mouse AP conjugated secondary antibody (Sigma-Aldrich) diluted (1:10 000) in blocking buffer. Membranes were then washed 3x in blocking buffer (without milk) for 15 min at room temperature. A chromogenic substrate, 5-bromo-4-chloro-3-indolyl-phosphate/nitroblue

tetrazolium chloride (BCIP-NBT 1-component, KPL, Milford, Ma, USA) was then added to the membrane for protein detection.

## 3.2.3 Qualitative and quantitative EGFP expression analysis

The in-vivo imaging system (IVIS®) was used together with the Lumina II imaging and living image software (Version 3.2, Caliper Life science) to detect and quantify EGFP fluorescent signals in the leaves of *N. benthamiana* plants infiltrated with the EGFP-VP3:VP7 co-infiltration suspension. At both 4 and 8 DPI, the oldest/bottom two leaves were harvested. Leaf 1 was classified as the leaf closest to the bottom of the plant, whereas leaf 2 was classified as the leaf second closest to the bottom of the plant. To visualize EGFP fluorescent signals, leaves were placed (one leaf at a time), in the IVIS® Lumina II imaging chamber and the imaging mode was set to 'Fluorescent' and exposure time was set to 'Auto'. Thereafter, the EGFP filter set which includes an excitation filter (445-490 nm) and an emission filter (515-575 nm) was selected, and an image of each leaf was acquired showing any EGFP-derived fluorescence. After an image was acquired, EGFP fluorescence was displayed in terms of 'efficiency'. The 'efficiency' number for each pixel in the generated image represented the fraction of fluorescent photons compared to each incident excitation photon and therefore had no units. A region of interest (ROI) was marked across the entire surface area of each leaf (indicated by a red circle), and average efficiency within the ROI was calculated. This measurement effectively determined the efficiency per pixel across the area ($cm^2$) of the ROI marked on each leaf. This strategy was used to quantify and compare EGFP fluorescent signals in leaves harvested at 4 and 8 DPI.

## 3.2.4 Large scale extraction and analysis of CLPs produced at 4 DPI

### 3.2.4.1 Large scale homogenization and protein extraction

The production of CLPs in *N. benthamiana* plants infiltrated with a VP3:VP7 or an EGFP-VP3:VP7 co-infiltration suspension was assessed by harvesting whole leaves at 4 DPI. Approximately 10 g of leaf material was homogenized in 3 volumes (w/v) of 1 x PI buffer (containing 1 x Complete™, EDTA-free protease inhibitor cocktail [Roche, Basel, Switzerland]) using a T25 digital ULTRA-TURRAX® homogeniser (IKA® Works., Inc., NC, USA). Homogenates were subsequently filtered through two layers of Miracloth™ (Calbiochem, Massachusetts, USA) into 50 mL tubes and the filtrate was then clarified by

centrifugation at 16 000x g (BeckmanT Coulter Avanti® J25TI centrifuge) for 10 min at 10°C. The homogenates were then added to new 50 mL tubes and incubated O/N at 4°C to allow CLPs to mature.

### 3.2.4.2 Density gradient purification of CLPs

CLPs were purified by ultracentrifugation through a discontinuous iodixanol density gradient. Iodixanol (Optiprep™; Sigma Aldrich, St Louis, MO, USA) solutions (20-40 %) prepared in 1x PI buffer were incrementally layered within an ultracentrifuge tube to create an 8 mL step gradient which was overlaid with approximately 30 mL of clarified plant lysate (Figure 18). Ultracentrifugation was then performed at 22 500 rpm for 3 h in an SW32 Ti rotor ultracentrifuge (Beckman, Brea, CA). After ultracentrifugation, the bottom of the VP3:VP7 and EGFP-VP3:VP7 gradient tubes were pierced with a needle and fractions of 500 uL were collected. Fractions collected around the 30-40% interface (F6-F8) of the VP3:VP7 and EGFP-VP3:VP7 iodixanol density gradients were mixed with 50 uL SAB (Sambrook et al., 1989) and denatured for 10 min at 95°C. These fractions were electrophoresed (30 uL/well) through a 10% SDS-polyacrylamide gel which was then stained with Coomassie blue stain (0.1% Brilliant Blue R-250, 10% glacial acetic acid, 50% methanol) for 1 h at 37°C to visualize proteins. The proteins present in VP3:VP7 and EGFP-VP3:VP7 F6, were also analysed by an anti-AHSV and anti-GFP western blot analysis as described in **3.2.2.2.**

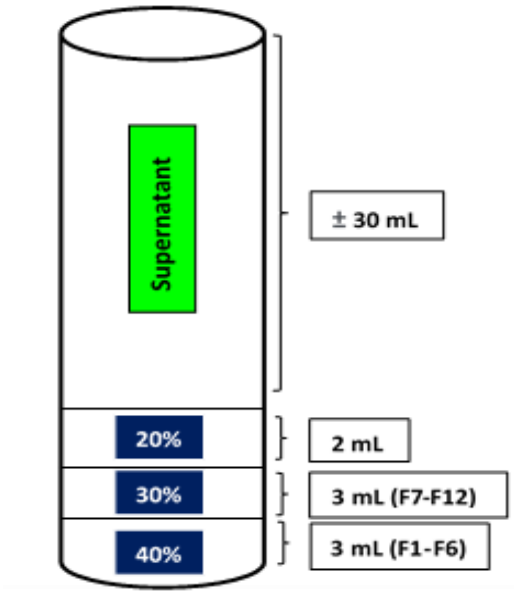


Figure 18: Schematic diagram of the 20-40% iodixanol density gradient used to purify CLPs (Empty CLPs or 'EGFP CLPs'). The approximate location where each collected 500 uL fraction ('F') falls within the density gradient is also indicated.

## 3.2.5 Extraction and analysis of ‘EGFP CLPs’ harvested at 4 and 8 DPI

### 3.2.5.1 Extraction and purification of ‘EGFP CLPs’

‘EGFP CLPs’ were extracted and purified from whole leaves infiltrated with the EGFP-VP3:VP7 co-infiltration suspension as described in **3.2.4**, at 4 and 8 DPI. However, this time leaves were homogenized in a CLP extraction buffer (50 mM bicine, pH 8.4 with NaOH, 140 mM NaCl, 0.1% (w/v) NLS sodium salt, 1 mM DTT), and the 20-40% iodixanol solutions were prepared using a CLP purification buffer (20 mM NaCl, 20 Mm Tris-HCl, pH8.4) instead of a 1x PI buffer. At 4 DPI, instead of fraction collection, a 2 mL syringe was used to draw out a visible green band from the EGFP-VP3:VP7 gradient tube, whereas at 8 DPI, fractions of 500 uL were collected as described in **3.2.4.2.**

### 3.2.5.2 Gel densitometry

To quantify the concentration of ‘EGFP CLPs’ collected at 4 vs 8 DPI after modifying the extraction and purification buffer, gel densitometry was performed. To achieve this, the ‘EGFP CLP’ samples were separated by SDS-PAGE and subsequently stained with Coomassie blue. Several dilutions of a BSA standard with a known concentration were also subjected to electrophoresis on the same gel. After Coomassie blue staining, the SynGene reader (GeneTools version 3.07.03) software was used to quantify the amount of protein present in each individual BSA protein band across the dilution range. A BSA standard curve was then constructed and used to calculate the approximate concentration of the AHSV proteins present in the ‘EGFP CLP’ samples harvested at 4 and 8 DPI.

## 3.2.6 Transmission electron microscopy

Glow-discharged carbon-coated copper grids were floated on 20 uL drops of density gradient fractions and incubated at room temperature for 5 min. The grids were then subjected to two successive washes in 10 uL drops of sterile $dH_20$. Thereafter, particles were negatively stained by floating the grid on a 10 uL drop of uranyl acetate (UA) for 30 sec. Filter paper was used to remove excess UA and the grids were negatively stained a final time by floating them on a 20 uL drop of UA for 1 second. An FEI Tecnai G2 20 Twin TEM with a bottom mounted digital camera (EMU, UCT) was used to view the grids.

## 3.2.7 Native PAGE

Native PAGE was used to characterize purified 'EGFP CLP', and empty CLP samples collected from EGFP-VP3:VP7 and VP3:VP7 density gradients, respectively. CLP samples (75 uL) were first mixed with 75 uL of 2x sample buffer (62.5 mM Tris-HCl, pH 6.8, 25% glycerol [v/v], 1% bromophenol blue [w/v]). Thereafter, CLP samples were loaded into the wells (30 uL/well) of a native polyacrylamide gel (lacking SDS) and electrophoresis was performed at 200 V for 1 hr. After native PAGE, anti-AHSV and anti-GFP western blot analysis was performed as described in **3.2.2.2.** The tubes containing the purified 'EGFP CLP', and empty CLP samples were also imaged using the IVIS® in-vivo imaging system as described in **3.2.3** to detect EGFP fluorescence.

## 3.2.8 Solid-state binding assay

The potential binding of 'EGFP CLPs' to an integrin receptor was tested by performing a solid-state binding assay. The integrin receptor, αvβ3 (Chemicon®), was first diluted to 5 µg/mL in 20 mM Tris-HCl (pH 7.4) containing 1 mM $MgCl_2$, 1 mM $MnCl_2$, 2 mM $CaCl_2$ and 150 mM NaCl. The first 3 wells (A1-A3) of a black 96-well plate were then coated (100 uL/well) O/N at 4°C with the diluted integrin receptor mixture. The first 6 wells (A1-A6) were blocked (100 uL/well) for 90 min at 37°C with 1% (w/v) BSA diluted in CLP purification buffer **(section 3.2.5.1)**. Thereafter, 100 uL 'EGFP CLP' samples diluted to 5 µg/mL in purification buffer were applied to the first 6 wells (A1-A6) and the plate was incubated for 30 min at 37°C. The black 96-well plate was then subjected to 3 successive washes with 1x PBS. The GloMax®-Multi+ Detection System with Instinct™ Software was used to take a fluorescent reading of the plate at excitation/emission wavelengths of 490/510-575 nm respectively.

# 3.3 Results

## 3.3.1 Optimization of EGFP-VP3 expression

The transient expression of constructs encoding EGFP-VP3 protein alone was first tested to confirm expression of the protein. Samples from leaves of *N. benthamiana* plants infiltrated with either pEAQ-*HT*-EGFP-VP3/AGL-1 or pRIC4.0-EGFP-VP3/GV3101::pMP90RK and harvested at 4,5 and 6 DPI were compared.

No major necrotic symptoms were observed in leaves infiltrated with pEAQ-*HT*-EGFP-VP3/AGL-1 harvested between 4 and 6 DPI. However, between 5 and 6 DPI, leaves infiltrated with pRIC4.0-EGFP-VP3/GV3101::pMP90RK began to show necrotic symptoms. These symptoms included the appearance of necrotic brown spots at 5 DPI ($OD_{600}$ = 0.5), as well as major browning across the leaf surface area at 6 DPI ($OD_{600}$ = 0.25 and 0.5) (Figure 19).

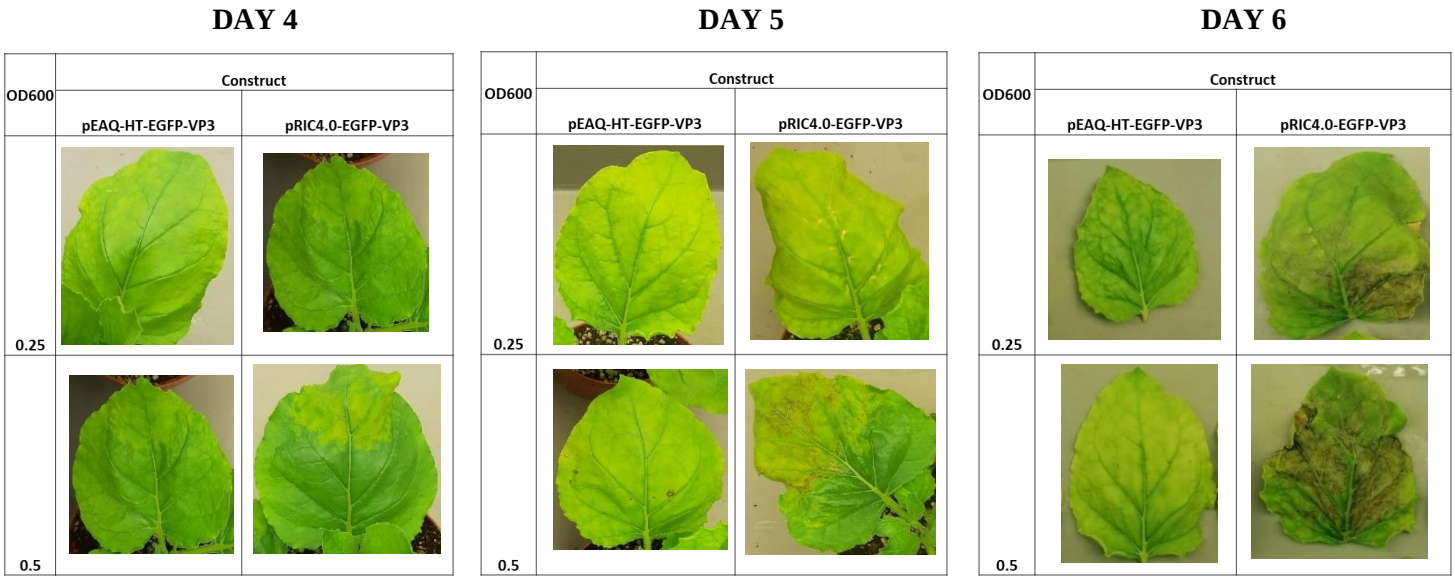


Figure 19: Leaf images of *N. benthamiana* plants infiltrated with pEAQ-*HT*-EGFP-VP3/AGL-1 or pRIC4.0-EGFP-VP3/GV3101::pMP90RK ($OD_{600}$ = 0.25/0.5) between 4 and 6 DPI.

To establish conditions for optimal EGFP-VP3 expression, a western blot analysis was performed on crude extracts obtained from leaves harvested between 4 and 6 DPI to compare EGFP-VP3 protein band intensities as a qualitative measure of expression levels. For leaves infiltrated with pEAQ-*HT*-EGFP-VP3/AGL-1, a band corresponding to the expected size of EGFP-VP3 (130.3 kDa) (black arrows) was detected in samples from leaves infiltrated at both $OD_{600}$ values and harvested at 4-6 DPI when probing with anti-AHSV (Figure 20A) or anti-GFP (Figure 20B). The EGFP-VP3 (130.3 kDa) band intensity was the strongest at 4 DPI when probing with anti-AHSV sera (Figure 20A). For plants infiltrated with pRIC4.0-

EGFP-VP3/GV3101::pMP90RK, a band corresponding to the expected size of EGFP-VP3 (130.3 kDa) was only detected at 4 DPI ($OD_{600}$ = 0.25 and 0.5) and faintly at 5 DPI ($OD_{600}$ = 0.5) when probing with anti-AHSV sera (Figure 20C). However, when probing with anti-GFP sera, the EGFP-VP3 (130.3 kDa) band was the most intense at 5 DPI ($OD_{600}$ = 0.5) and very faint at both 4 and 6 DPI (Figure 20D). Finally, the darkest band intensity overall of EGFP-VP3 from leaves infiltrated with pEAQ-*HT*-EGFP-VP3/AGL-1 compared to the leaves infiltrated with pRIC4.0-EGFP-VP3/GV3101::pMP90RK suggested that the pEAQ-*HT* construct was more suitable for achieving a higher EGFP-VP3 expression level. Besides the bands corresponding to the expected size of EGFP-VP3, many other non-specific bands were detected after conducting the anti-AHSV and anti-GFP western blot analysis, suggesting the occurrence of non-specific binding.

A

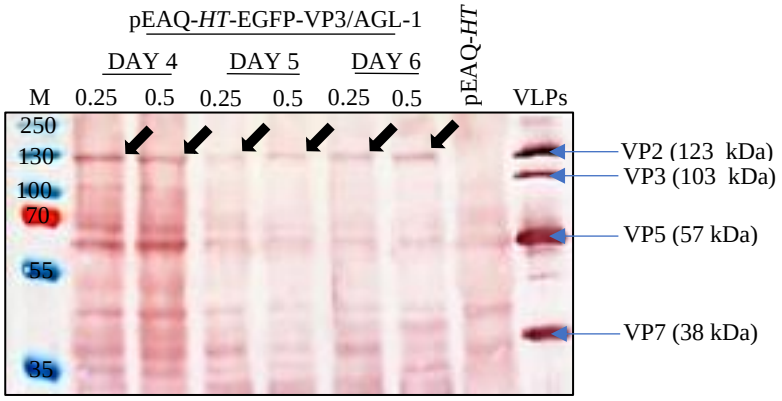
pEAQ-*HT*-EGFP-VP3/AGL-1
DAY 4
DAY 5
DAY 6
pEAQ-*HT*
M 0.25 0.5 0.25 0.5 0.25 0.5
VLPs
250
130
100
70
55
35
VP2 (123 kDa)
VP3 (103 kDa)
VP5 (57 kDa)
VP7 (38 kDa)

B

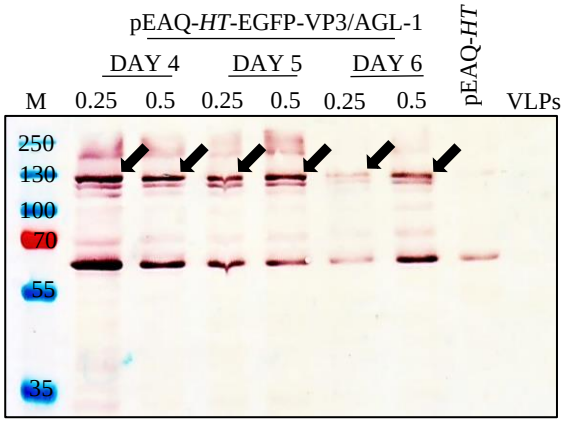
pEAQ-*HT*-EGFP-VP3/AGL-1
DAY 4
DAY 5
DAY 6
pEAQ-*HT*
M 0.25 0.5 0.25 0.5 0.25 0.5
VLPs
250
130
100
70
55
35

C

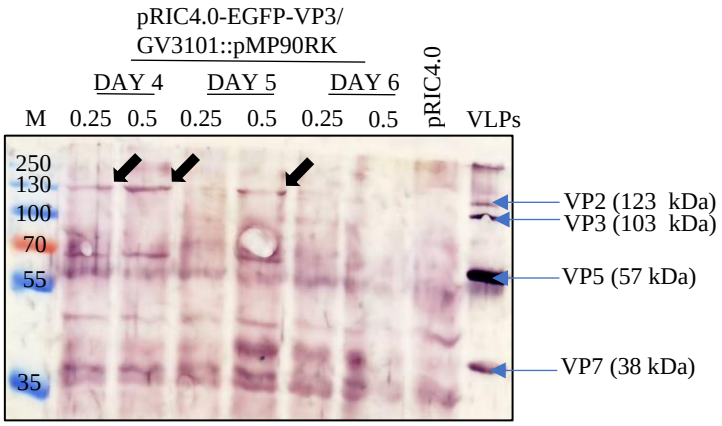
pRIC4.0-EGFP-VP3/
GV3101::pMP90RK
DAY 4
DAY 5
DAY 6
pRIC4.0
M 0.25 0.5 0.25 0.5 0.25 0.5
VLPs
250
130
100
70
55
35
VP2 (123 kDa)
VP3 (103 kDa)
VP5 (57 kDa)
VP7 (38 kDa)

D

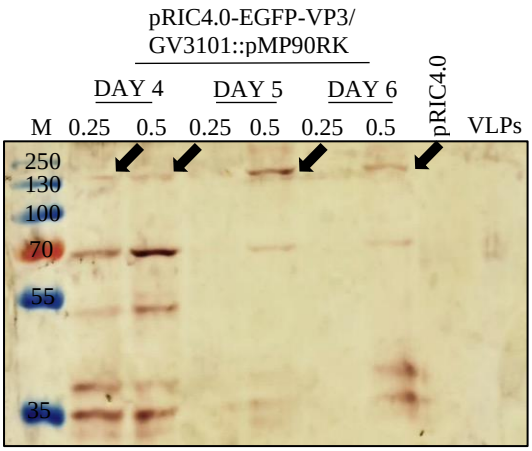
pRIC4.0-EGFP-VP3/
GV3101::pMP90RK
DAY 4
DAY 5
DAY 6
pRIC4.0
M 0.25 0.5 0.25 0.5 0.25 0.5
VLPs
250
130
100
70
55
35

Figure 20: Optimization of *N. benthamiana* based EGFP-VP3 protein expression. Anti-AHSV (A) and anti-GFP (B) reducing western blot analysis of proteins extracted from leaf discs of plants infiltrated with pEAQ-*HT*-EGFP-VP3/AGL-1 at an $OD_{600}$ = 0.25 or 0.5 between 4 and 6 DPI. EGFP-VP3 (130.3 kDa) is indicated by black arrows. pEAQ-*HT* = crude leaf extracts from leaves infiltrated with AGL-1 harbouring pEAQ-*HT* lacking any insert = negative control. Anti-AHSV (C) and anti-GFP (D) reducing western blot analysis of proteins extracted from leaf discs of plants infiltrated with pRIC4.0-EGFP-VP3/GV3101::pMP90RK at an $OD_{600}$ = 0.25 or 0.5 between 4 and 6 DPI. EGFP-VP3 (130.3 kDa) is indicated by black arrows. pRIC4.0 = leaves infiltrated with GV3101::pMP90RK harbouring pRIC4.0 lacking any insert = negative control. VLPs = denatured AHSV VLP sample comprising AHSV VP2 (123 kDa), VP3 (103 kDa), VP5 (57 kDa) and VP7 (38 kDa) = positive control (A-D).

## 3.3.2 Purification of CLPs

pEAQ-*HT*-EGFP-VP3/AGL-1 was used for further co-infiltration experiments to produce EGFP-VP3 and infiltrated with VP7 on a larger scale to determine their ability to assemble into CLPs. Due to time and reagent constraints, CLP production was assessed only after harvesting infiltrated leaves at 4 DPI to confirm successful CLP assembly. Constructs encoding AHSV VP3 and VP7 (VP3:VP7) were co-infiltrated to generate empty CLPs as a control and constructs encoding AHSV EGFP-VP3 and VP7 (EGFP-VP3:VP7) were co-infiltrated to generate 'EGFP CLPs'. Their production was assessed in samples prepared from *N. benthamiana* leaves co-infiltrated with either VP3:VP7 or EGFP-VP3:VP7 suspensions ($OD_{600}$ = 1.0), respectively which were harvested at 4 DPI. Crude leaf extracts were loaded onto a density gradient and subjected to an ultracentrifugation step to concentrate putative assembled CLPs.

After ultracentrifugation, a small, fluorescent green band (black arrow) was observed near the 30-40% interface of the EGFP-VP3:VP7 gradient (Figure 21A). However, in comparison, no band was visible at the **corresponding** location of the gradient loaded with the VP3:VP7 sample (Figure 21B). Fractions collected from the 30-40% interface region (F6-F8) of the EGFP-VP3:VP7 gradient, separated by SDS-PAGE and subsequently stained with Coomassie blue showed the presence of EGFP-VP3 (130.3 kDa) and VP7 (38 kDa) proteins, with proteins in F6 having the most intense band (Figure 21C). VP3 (103 kDa) and VP7 (38 kDa) proteins were detected by Coomassie staining, within fractions collected from the 30-40% interface (F6-F8) of the VP3:VP7 gradient (Figure 21D). An anti-GFP and anti-AHSV western blot analysis was performed on F6 collected from both the EGFP-VP3:VP7 and VP3:VP7 gradients. When probing with anti-GFP, EGFP-VP3 (130.3 kDa) was only detected within EGFP-VP3:VP7 F6,

whereas no proteins were detected within VP3:VP7 F6. However, when probing with anti-AHSV sera, VP7 (38 kDa) was detected in VP3:VP7 and EGFP-VP3:VP7 F6, whereas VP3 (103 kDa) and EGFP-VP3 (130.3 kDa) proteins were detected in VP3:VP7 F6 and EGFP-VP3:VP7 F6, respectively (Figure 21E). TEM analysis of EGFP-VP3:VP7 F6 (Figure 21F) and VP3:VP7 F6 (Figure 21G) confirmed the presence of CLPs in both cases, approximately 70 nm in diameter.

A

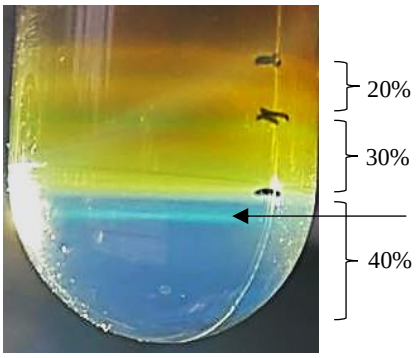
EGFP-VP3:VP7
20%
30%
40%

B

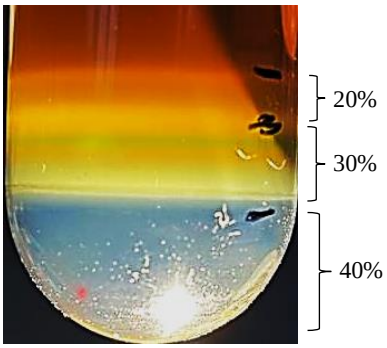
VP3:VP7
20%
30%
40%

C

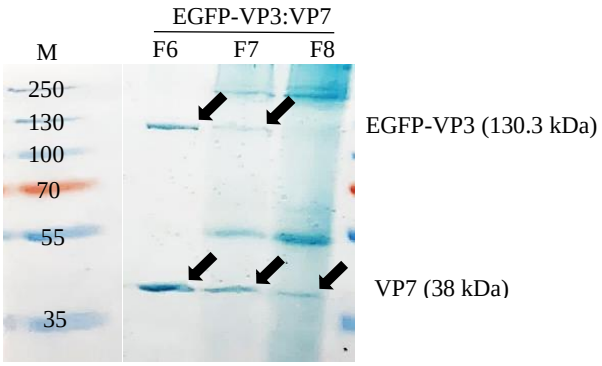
EGFP-VP3:VP7
M
F6
F7
F8
250
130
100
70
55
35
EGFP-VP3 (130.3 kDa)
VP7 (38 kDa)

D

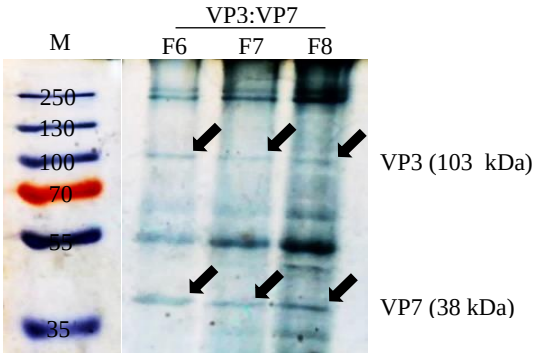
VP3:VP7
M
F6
F7
F8
250
130
100
70
55
35
VP3 (103 kDa)
VP7 (38 kDa)

E

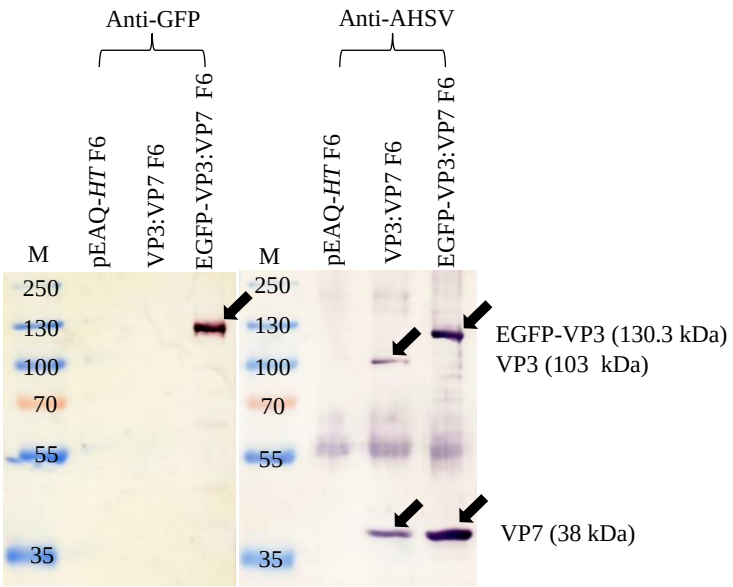
Anti-GFP
Anti-AHSV
pEAQ-HT F6
VP3:VP7 F6
EGFP-VP3:VP7 F6
M
250
130
100
70
55
35
EGFP-VP3 (130.3 kDa)
VP3 (103 kDa)
VP7 (38 kDa)

F

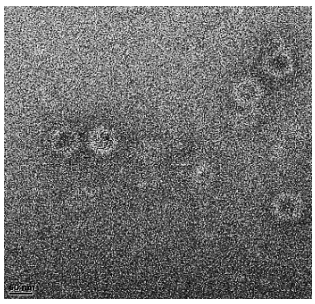
EGFP-VP3:VP7

G

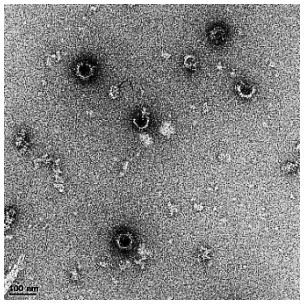
VP3:VP7 F6

Figure 21: Purification of empty CLPs and 'EGFP CLPs' from samples harvested at 4 DPI via 20-40% density gradient ultracentrifugation. Fractions of 500 uL were collected from EGFP-VP3:VP7 (A) and VP3:VP7 (B) iodixanol density gradients. Black arrow = the fluorescent green band observed near the 30-40% interface of the EGFP-VP3:VP7 (A) iodixanol density gradient. Coomassie staining of F6-F8 collected from the EGFP-VP3:VP7 (C) and VP3:VP7 (D) iodixanol density gradients. (E) Anti-GFP and Anti-AHSV reducing western blot analysis for comparison of VP3:VP7 F6 and EGFP-VP3:VP7 F6. pEAQ-*HT* F6 = negative control. TEM analysis of EGFP-VP3:VP7 F6 (F) and VP3:VP7 F6 (G). Scale bars = 200 nm.

## 3.3.3 Encapsulation of EGFP inside 'EGFP CLPs'

To confirm encapsulation of EGFP inside the 'EGFP CLPs', EGFP fluorescence was first qualitatively assessed in the tubes containing fraction 6 (F6) samples of EGFP-VP3:VP7 and VP3:VP7. No EGFP fluorescence was detected in the tube containing VP3:VP7 CLPs (Figure 22A), however EGFP fluorescence was detected in the tube containing EGFP-VP3:VP7 CLPs (Figure 22B). VP3:VP7 F6 and EGFP-VP3:VP7 F6 samples were subsequently separated on a native polyacrylamide gel to separate the CLPs and western blotted using anti-AHSV sera and anti-GFP antibody. This was done to substantiate the TEM results by providing further proof that the CLPs obtained from both fractions were isolated as intact particles of the same size. The anti-AHSV western blot showed a single band in both fractions at the same location on the polyacrylamide gel, suggesting purification of intact CLPs that were the same size (Figure 22C – anti-AHSV lanes). However, when probing with anti-GFP, the same band could no longer be detected in EGFP-VP3:VP7 F6 (Figure 22C – anti-GFP lanes), suggesting encapsulation of the EGFP protein within the CLP interior.

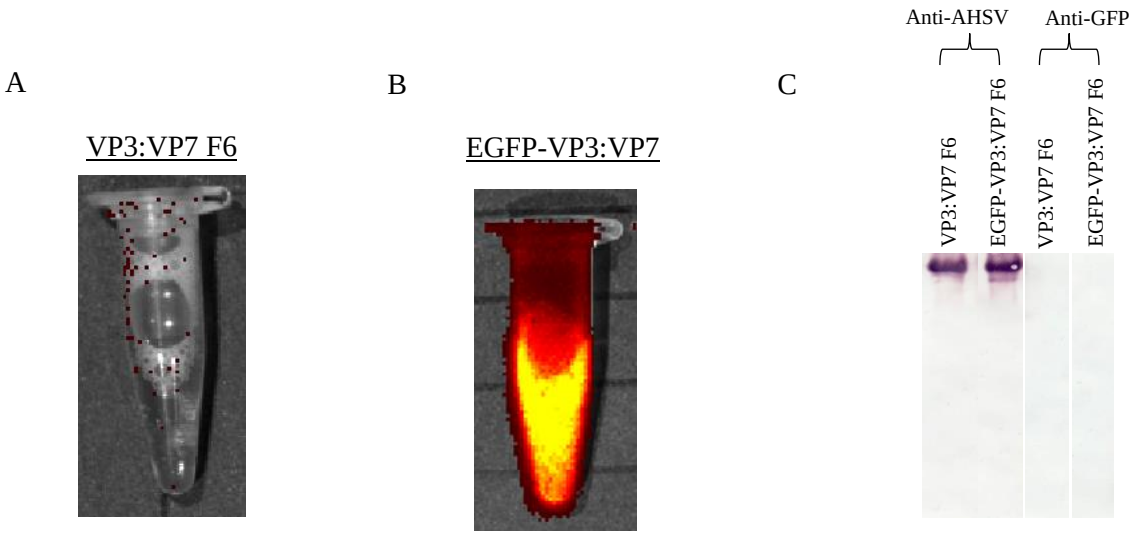

Figure 22: Confirmation of EGFP encapsulation within 'EGFP CLPs'. Images of Eppendorf tubes containing VP3:VP7 F6 (A) or EGFP-VP3:VP7 F6 (B) using the EGFP filter settings of the IVIS® in-vivo imaging system for detection of any EGFP derived fluorescent signals. (C) Anti-AHSV and anti-GFP western blot analysis of VP3:VP7 F6 and EGFP-VP3:VP7 F6 after native PAGE separation of proteins.

## 3.3.4 'EGFP CLP' production in leaves harvested at 4 vs 8 DPI

Once production of CLPs that successfully encapsulated the EGFP protein was established, an attempt was made to increase the CLP yield. To accomplish this, a CLP extraction and purification buffer, successfully used in other research to extract and purify BTV CLPs encapsulating a GFP protein (Brillault et al., 2017) was tested and used instead of the 1x PI buffer. CLP production was additionally compared at day 4 and day 8 post-infiltration.

### 3.3.4.1 Optimization of 'EGFP CLP' production

An attempt was made to increase the yield of purified 'EGFP CLPs' by modifying the CLP extraction and purification buffers to more optimal parameters. 'EGFP CLP' levels were then compared between infiltrated leaves sampled at 4 and 8 DPI. The fluorescent band, indicative of 'EGFP CLPs' was obtained after density gradient ultracentrifugation, CLP morphology was assessed by TEM and protein amounts on Coomassie-stained gels were then measured by gel densitometry. At 4 DPI, a very thick, bright fluorescent green band was visualized near the 30-40% interface of the EGFP-VP3:VP7 iodixanol density gradient (Figure 23A). On the other hand, at 8 DPI a much thinner, fainter fluorescent green band was visualized near the 30-40% interface of the EGFP-VP3:VP7 iodixanol density gradient (Figure 23B). TEM analysis of the 1 mL fraction containing the large fluorescent green band ('E4') directly syringed out from the EGFP-VP3:VP7 gradient at 4 DPI, showed the presence of many CLPs approximately 70 nm in diameter (Figure 23C). TEM analysis of the fraction ('E8') collected from the EGFP-VP3:VP7 gradient at 8 DPI, showed far less CLPs than was observed at 4 DPI (Figure 23D). Gel densitometry was used to estimate the concentration of purified 'EGFP CLPs' obtained at 4 DPI ('E4', Figure 23E) and at 8 DPI ('E8', Figure 23F). It was calculated that 10g of leaf material harvested at 4 DPI yielded approximately 142 µg of highly purified 'EGFP CLPs', whereas 10g of leaf material harvested at 8 DPI, yielded only 7 µg of highly purified 'EGFP CLPs'.

A

EGFP-VP3:VP7

DAY 4

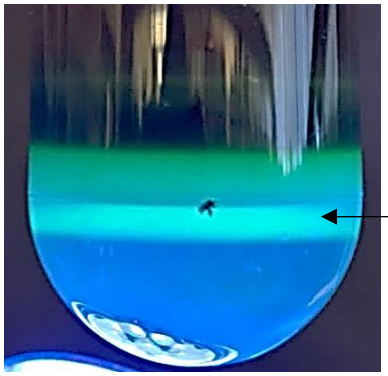

E4

B

EGFP-VP3:VP7

DAY 8

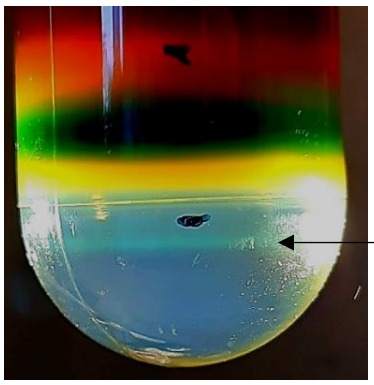

E8

C

'E4'

DAY 4

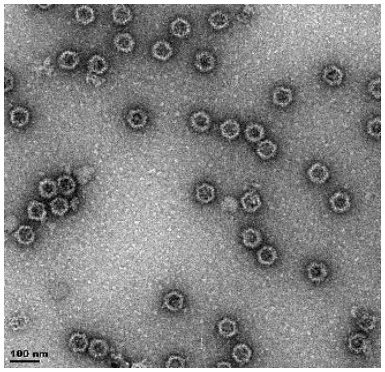

D

'E8'

DAY 8

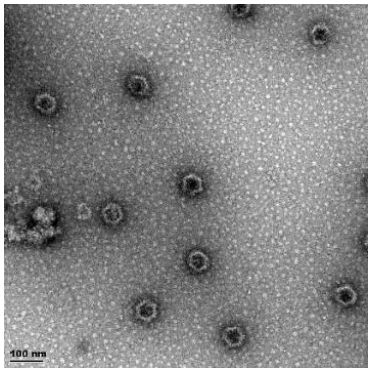

E

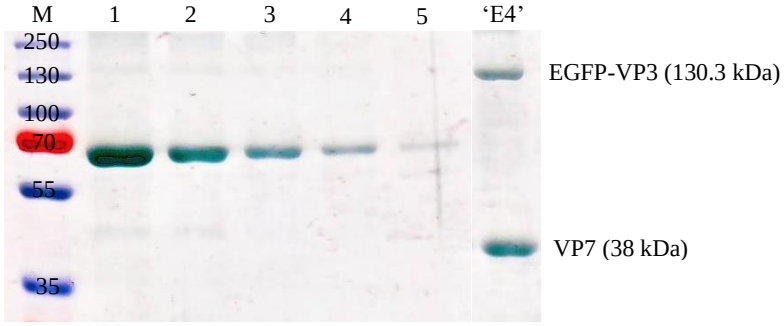


F

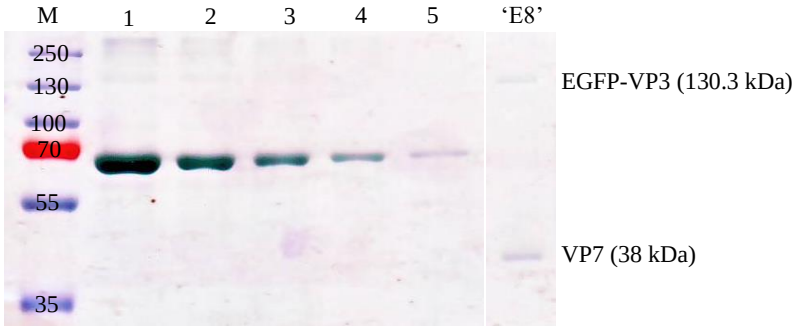

Figure 23: Purification and analysis of 'EGFP CLPs' after modification of the extraction and purification buffer. Comparison of the EGFP-VP3:VP7 iodixanol density gradient obtained at 4 (A) and at 8 (B) DPI. TEM analysis comparison of the 1 mL fraction ('E4') obtained from the EGFP-VP3:VP7 gradient at 4 DPI (C) and the 500 µL fraction ('E8') obtained from the EGFP-VP3:VP7 gradient at 8 DPI (D). Gel densitometry of the 'EGFP CLP' sample obtained at 4 DPI – 'E4' (E) and the 'EGFP CLP' sample obtained at 8 DPI – 'E8' (F). Known amounts of Bovine serum albumin (BSA) 7.5 µg (lane 1), 3.75 µg (lane 2), 1.875 µg (lane 3), 0.9375 µg (lane 4) and 0.46857 µg (lane 5) were simultaneously run on SDS-PAGE gels with the 'EGFP CLP' samples (E-F). The concentration of the EGFP-VP3 (130.3 kDa) and VP7 (38 kDa) protein band present in each 'EGFP CLP' sample was then quantified using a BSA standard curve to determine 'EGFP CLP' yield.

### 3.3.4.2 Analysis of EGFP-derived fluorescence in infiltrated leaves

After infiltration of *N. benthamiana* plants with an EGFP-VP3:VP7 co-infiltration suspension to produce 'EGFP CLPs', EGFP-derived fluorescent signals in leaves harvested at 4 and 8 DPI were compared using the IVIS® in-vivo imaging system. At 4 DPI, the oldest leaf (leaf 1) and second oldest leaf (leaf 2) showed no signs of necrosis and strong EGFP-derived fluorescence was observed across the surface area of each leaf (Figure 24A). In comparison, at 8 DPI, the oldest leaf (leaf 1) showed major necrotic symptoms such as wilting and browning around the leaf edges, and much weaker EGFP fluorescence was observed compared to leaf 1 harvested at 4 DPI. The second oldest leaf (leaf 2) showed only minor necrotic symptoms such as a few leaf spots at 8 DPI and EGFP-derived fluorescence could still be observed across the leaf surface area but was absent in the small regions of necrosis (Figure 24B). Quantitative analysis of EGFP-derived fluorescence within a region of interest (ROI) covering the surface area of each leaf, showed that the average efficiency of EGFP expression in the oldest leaf (leaf 1) was approximately 9.9 x greater at 4 DPI than at 8 DPI. Furthermore, the average efficiency of EGFP expression in the second oldest leaf (leaf 2) was approximately 2.18 x greater at 4 DPI than at 8 DPI (Figure 24C).

A

4 DPI

Leaf 1

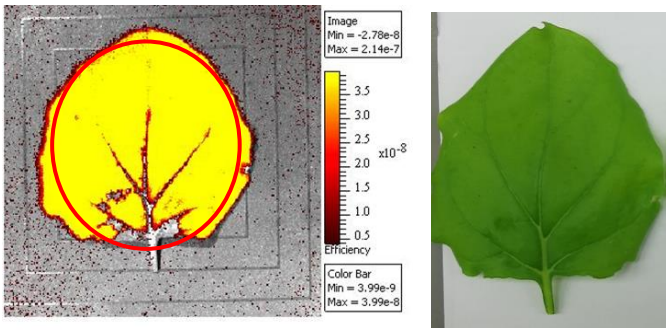


Leaf 2

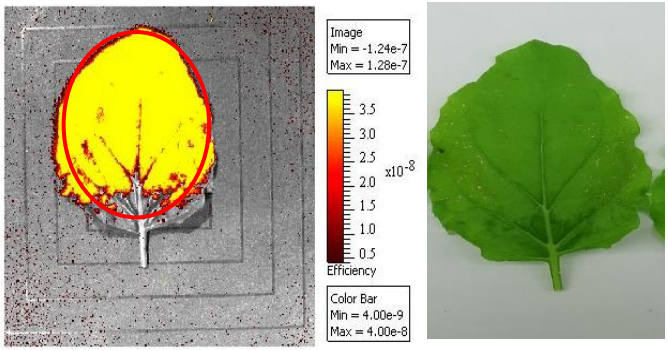


B

8 DPI

Leaf 1

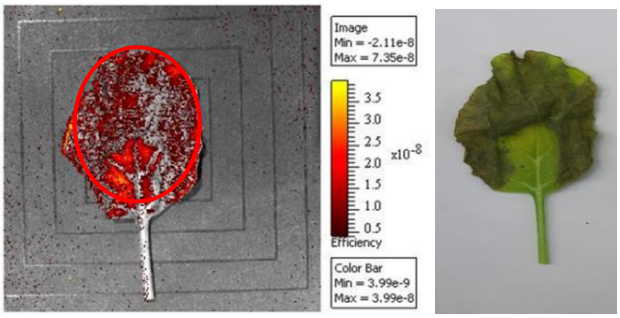


Leaf 2

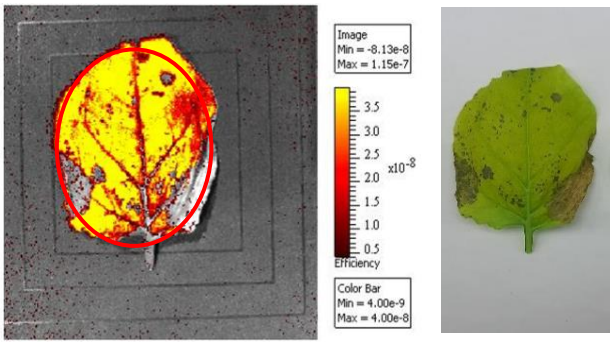

C

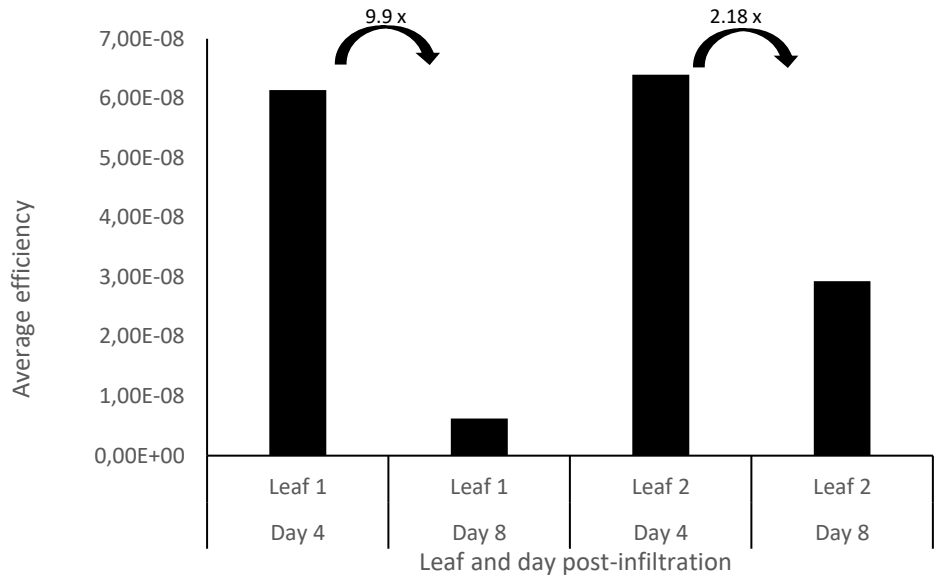


Figure 24: Qualitative and quantitative analysis of EGFP fluorescence in leaves infiltrated with an EGFP-VP3:VP7 co-infiltration suspension at 4 vs 8 DPI. Photographic and fluorescence emission image (generated using the IVIS® in-vivo imaging system) of leaf 1 (oldest leaf) and leaf 2 (second oldest leaf) for detection of EGFP-derived fluorescence at 4 (A) and 8 (B) DPI. (C) Average efficiency of EGFP expression (calculated using the Lumina II imaging software) within the marked ROI (indicated by a red circle) spanning the surface area of leaf 1 and leaf 2, at 4 and 8 DPI.

## 3.3.5 Interaction of 'EGFP CLPs' with an integrin receptor

A solid-state binding assay was used to assess the potential binding of the purified 'EGFP CLPs' to a human integrin receptor, αvβ3, against a BSA background. No difference in EGFP fluorescence readings were observed between the wells that had been coated with integrin ('EGFP CLPs' + αvβ3) and uncoated ('EGFP CLPs') (Figure 25).

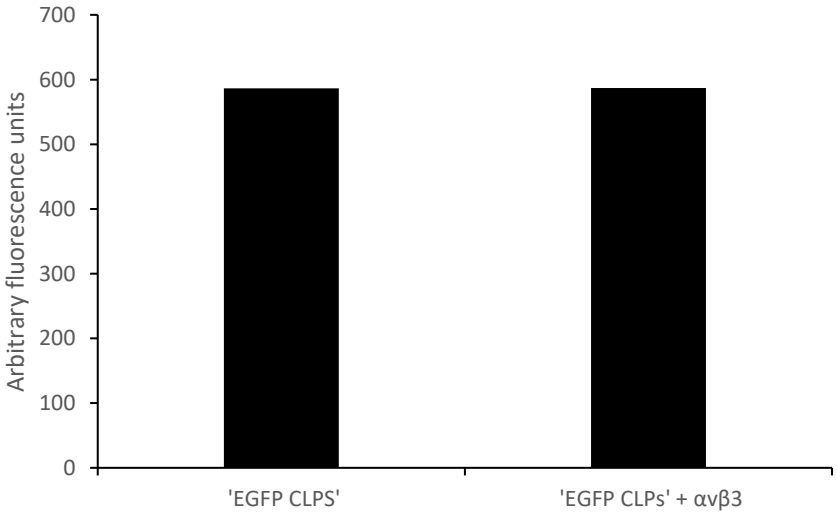

Figure 25: Assessment of binding potential between ‘EGFP CLPs’ and the human integrin receptor, αvβ3 determined by detection of the fluorescent cargo. ‘EGFP CLPs’ = average fluorescence reading over three wells not coated with the integrin receptor after adding the purified ‘EGFP CLPs’. ‘EGFP CLPs’ + αvβ3 = average fluorescence reading over three wells coated with the integrin receptor after adding the purified ‘EGFP CLPs’. Fluorescence readings were taken at an excitation/emission wavelength of 490/510-575 nm respectively using the GloMax®- Multi+ Detection System.

## 3.4 Discussion

To ensure successful production of AHSV CLPs encapsulating EGFP, co-expression of EGFP-VP3 and AHSV VP7 was necessary. To this end, 2 constructs encoding EGFP-VP3 protein (pRIC4.0-EGFP-VP3 and pEAQ-*HT*-EGFP-VP3) were assessed and compared for their ability to express EGFP-VP3. The non-specific bands observed after conducting the anti-AHSV western blot analysis could have been caused by the non-specific detection of various plant proteins present in the crude extract from the harvested *N. benthamiana* plants. It is possible that the horse blood from which the anti-AHSV serum was prepared contained antibodies against plant proteins due to the horse eating a diet that potentially contained some plant material. This could have ultimately been a major reason for the detection of non-specific proteins when probing with the anti-AHSV sera. The non-specific bands observed after conducting either the anti-AHSV or anti-GFP western blot analysis could also potentially be attributed to the non-specific binding of the primary antibody to a non-specific target protein. This could explain why in addition to the specific EGFP-VP3 target protein, there was also detection of many non-specific protein bands on the blots. The higher EGFP-VP3 expression levels in plants infiltrated with pEAQ-*HT*-EGFP-VP3/AGL-1 than in plants infiltrated with pRIC4.0-EGFP-VP3/GV3101::pMP90RK (estimated by comparing equal total soluble protein volumes separated by SDS-PAGE) suggested that the pEAQ-*HT*-EGFP-VP3 construct was more suitable for co-expression with AHSV VP7 to obtain a higher 'EGFP CLP' yield. Furthermore, while EGFP-VP3 expression levels were higher at 4 DPI, this protein was still expressed at 5 and 6 DPI in plants infiltrated with pEAQ-*HT*-EGFP-VP3/AGL-1 at both $OD_{600}$ values. This showed that the pEAQ-*HT*-EGFP-VP3 construct was also suitable for maintaining transient production of EGFP-VP3 for at least 3 days. In contrast, the decline in EGFP-VP3 expression levels in plants infiltrated with pRIC4.0-EGFP-VP3/GV3101::pMP90RK after 4-5 DPI, suggested that the pRIC4.0-EGFP-VP3 construct could only maintain transient EGFP-VP3 expression for a relatively short time frame before a notable decrease in expression levels occurred. It was also apparent that the level of EGFP-VP3 expression could potentially be linked to the physiological state of the infiltrated leaves. At 6 DPI, a significant increase in necrotic symptoms in leaves of *N. benthamiana* plants infiltrated with pRIC4.0-EGFP-VP3/GV3101::pMP90RK correlated with a notable decrease in EGFP-VP3 expression levels. In contrast, the leaves of *N. benthamiana* plants infiltrated with pEAQ-*HT*-EGFP-VP3/AGL-1 showed no necrosis between 4 and 6 DPI and correlated with relatively consistent EGFP-VP3 expression levels within the same timeframe. This further suggested that the pEAQ-*HT*-EGFP-

VP3 construct could potentially express EGFP-VP3 beyond 6 DPI, as the leaves were still in a healthy condition at that point compared to their original state. After taking the above findings into consideration, the pEAQ-*HT*-EGFP-VP3 construct was selected as the most desirable choice for co-expression with AHSV VP7 to produce 'EGFP CLPs'; this was because overall findings of the small-scale expression study showed that this vector allowed for greater EGFP-VP3 expression levels on multiple days post infiltration and induced less stress on infiltrated leaves thereby preserving their physiological state.

After density gradient ultracentrifugation, the presence of a narrow, slightly fluorescent green band near the 30-40% interface of the EGFP-VP3:VP7 gradient suggested successful production of AHSV CLPs. This was considered a reasonable assumption, as a prior study found that AHSV VLPs, which are very similar in size to AHSV CLPs, accumulated near the 30-40% interface of an iodixanol density gradient (Dennis, 2019). Furthermore, the green colour of this band, suggested successful encapsulation of EGFP inside the AHSV CLPs. The observed absence of any band (specifically a fluorescent green band) at the corresponding location in the VP3:VP7 gradient was expected as these CLPs would be empty and not contain the fluorescent EGFP protein. Detection of EGFP-VP3 and VP7 proteins of the expected size on a Coomassie stained gel in EGFP-VP3:VP7 F6, a fraction sampled from the visible fluorescent green band in the EGFP-VP3:VP7 gradient, provided further evidence suggesting that the fluorescent green band comprised concentrated 'EGFP CLPs'. On the contrary, detection of only VP3 and VP7 on a Coomassie stained gel in fractions collected from the 30-40% interface of the VP3:VP7 gradient, suggested production of empty CLPs. Anti-GFP and anti-AHSV western blot analysis of EGFP-VP3:VP7 and VP3:VP7 F6, showed a clear difference in the constituent proteins present in each of these fractions, further suggesting that 'EGFP CLPs' were purified by co-expression of EGFP-VP3 and VP7, whereas empty CLPs were purified by co-expression of VP3 and VP7. TEM analysis of the appropriate samples confirmed the presence of CLPs in both EGFP-VP3:VP7 and VP3:VP7 F6 fractions. This proved that fusion of EGFP to AHSV VP3 did not impact self-assembly of the proteins into CLPs. The presence of CLPs in both EGFP-VP3:VP7 and VP3:VP7 F6 fractions, further confirmed that there was no difference in the banding location of these particles within the iodixanol density gradient. This result was not expected since density gradient centrifugation, also known as isopycnic gradient centrifugation works by separating particles based on their density (Brakke, 1951). This centrifugation technique results in the movement of particles through a density gradient medium until a point is reached where the density of the particle is

equivalent to that of the surrounding medium (Brakke, 1961). Since the density of the iodixanol gradient used to purify CLPs increased from the top to the bottom of the centrifuge tube (Figure 18), denser particles should have collected nearer the bottom of the centrifuge tube. Therefore, one would expect 'EGFP CLPS' to band at a location further down the centrifuge tube than the presumably empty CLPs which should theoretically be of a lower density due to the lack of encapsulated EGFP. However, since both particles were collected from the same interface of the iodixanol density gradient, it shows that any density differences between these CLPs were negligible. This result aligned with a previous study by Brillault et al that found no visible difference in the banding location of empty BTV CLPs and BTV CLPs encapsulating GFP (Brillault et al., 2017).

Although all the results up to this point, suggested that the CLPs purified from the EGFP-VP3:VP7 gradient encapsulated EGFP, this was confirmed by detection of an EGFP fluorescent signal in EGFP-VP3:VP7 F6 using the IVIS® in-vivo imaging system. Furthermore, the complete lack of detection of an EGFP fluorescent signal in VP3:VP7 F6 supported this conclusion by showing that in comparison, the CLPs purified from the VP3:VP7 gradient lacked EGFP. The detection of a single band from both EGFP-VP3:VP7 and VP3:VP7 F6 fractions on a native gel after probing with anti-AHSV (Figure 22C), suggested the presence of singular intact particles after density gradient purification. The lack of detection of a band for the EGFP-VP3:VP7 F6 sample on the native gel when probing with anti-GFP (Figure 22C) suggested that the antibody could not access the EGFP protein, providing the final confirmation that EGFP was encapsulated within the CLP interior. Detection of EGFP fluorescence, despite encapsulation of the EGFP protein within the CLP interior, could be attributed to the presence of pores in the VP3 protein (Dennis et al., 2019), providing a potential reason why the fluorescent signal could still be detected from within the CLP interior. Since the mobility of proteins through a native page gel is dependent on their size (Li and Arakawa, 2019), the migration of the protein band in each fraction to the same point on the native page gel confirmed the observation by TEM analysis that both the empty CLPs and 'EGFP CLPs' were of the same diameter size.

Although 'EGFP CLPs' were successfully produced and then purified by density gradient ultracentrifugation at 4 DPI, there were still questions surrounding whether the 'EGFP CLP' yield could be optimized. In a study conducted by Brillault et al, GFP was successfully encapsulated within BTV CLPs, however in this study different CLP extraction and purification buffers were used and the leaves were harvested at 8 DPI (Brillault et al., 2017).

To assess ‘EGFP CLP’ production on multiple days would be time consuming and costly, consequently a potential way to quickly predict ‘EGFP CLP’ yield in the leaves of *N. benthamiana* plants prior to extraction and purification was highly desirable. Interestingly, another research group found that the IVIS® in-vivo imaging system could be used to qualitatively and quantitatively monitor GFP expression in the leaves of *N. benthamiana* plants (Stephan et al., 2011). Thus, this imaging system was considered a good way to detect any differences qualitatively and quantitatively in EGFP fluorescence at 4 vs 8 DPI within leaves co-infiltrated with an EGFP-VP3:VP7 suspension to make ‘EGFP CLPs’. In doing so, one could later determine whether there was any correlation between the level of EGFP fluorescence and the eventual yield of purified ‘EGFP CLPs’. Unfortunately, due to time constraints this experiment could only be performed once. Despite this, the results obtained provided qualitative and quantitative evidence that EGFP fluorescence was greater at 4 DPI, when the leaves were healthy, compared to 8 DPI, when the leaves were more necrotic. Since EGFP formed part of the fusion protein EGFP-VP3 in this experiment, the results obtained here suggested greater EGFP-VP3 expression and consequently a potentially higher ‘EGFP CLP’ yield at 4 DPI compared to 8 DPI.

Modification of the CLP extraction and purification buffers to those used by Brillault et al, resulted in a much wider fluorescent green band than had previously been seen at 4 DPI within the EGFP-VP3:VP7 gradient when 1x PI buffer was used for extraction and purification. This suggested that the extraction and purification buffer used to purify BTV CLPs encapsulating GFP, could also be used to greatly improve the yield of AHSV ‘EGFP CLPs’. One major difference between the 1x PI buffer and the buffer used to extract BTV CLPs in the study conducted by Brillault et al was the buffer pH. In another study it was also found that AHSV VLP stability was greater when extraction was carried out using the Bicine-based extraction buffer used here compared to a 1x PBS buffer and this was attributed to the higher pH of the Bicine-based extraction buffer (Dennis et al., 2018). Thus, it is possible that AHSV ‘EGFP CLPs’ were stabilized more when extracted using the Bicine-based extraction buffer, a higher pH buffer, compared to the 1x PI buffer, a lower pH buffer, leading to an increased AHSV ‘EGFP CLP’ yield. The presence of NLS, a detergent, in the Bicine-based extraction buffer and the absence of this detergent in the 1x PI buffer could also possibly explain the difference in AHSV ‘EGFP CLP’ yield. Detergents offer a hydrophobic environment for proteins and consequently have been shown to increase protein stability (Stangl et al., 2012). Thus, the presence of NLS in the Bicine-based extraction buffer may have also contributed to increasing

AHSV ‘EGFP CLP’ stability during the extraction process, resulting in an overall greater AHSV ‘EGFP CLP’ yield compared to when 1x PI buffer which did not contain NLS, was used to extract AHSV ‘EGFP CLPs’.

The presence of a fluorescent green band within the EGFP-VP3:VP7 gradient at 8 DPI, suggested that ‘EGFP CLPs’ could still be produced at 8 DPI, however the band was thinner than at 4 DPI, suggesting a lower ‘EGFP CLP’ yield. TEM analysis showed that more CLPs were purified from the EGFP-VP3:VP7 gradient at 4 DPI than at 8 DPI, further supporting that ‘EGFP CLP’ yield was greater at 4 DPI. Finally, densitometric analysis quantitatively confirmed that at 4 DPI, a significantly greater ‘EGFP CLP’ yield was obtained than at 8 DPI.

Interestingly, the ‘EGFP CLP’ yield obtained at 4 and 8 DPI as determined by densitometric analysis showed a correlation with the quantitatively determined EGFP fluorescence levels in leaves harvested at 4 and 8 DPI. High EGFP fluorescence in leaves harvested at 4 DPI correlated with a high ‘EGFP CLP’ yield, whereas much lower levels of EGFP fluorescence in leaves harvested at 8 DPI, correlated with a significantly decreased ‘EGFP CLP’ yield at 8 DPI. This showed that one could potentially use the IVIS® in-vivo imaging system to determine which DPI might be most suitable for obtaining the greatest yield of ‘EGFP CLPs’ based on the level of EGFP fluorescence quantitatively determined in the infiltrated leaves.

After optimizing conditions for ‘EGFP CLP’ purification, a possible interaction between these purified particles and a human integrin receptor, αvβ3, was assessed by performing a solid-state binding assay and detecting for the presence of the fluorescent EGFP cargo. Due to funding and time constraints this experiment could only be performed once. Furthermore, due to the high cost of the integrin receptor, testing the interaction between empty CLPs and αvβ3 was deemed unnecessary as the assay relied upon the presence of a fluorescent protein to confirm any interaction with the αvβ3 receptor. Thus, it was decided to conserve the available integrin receptor and only test the interaction between αvβ3 and ‘EGFP CLPs’. Successful binding would be reflected by high EGFP fluorescence readings in wells coated with αvβ3 compared to the control wells not coated with αvβ3. One would expect such results since the ‘EGFP CLPs’ would have no place to bind in the control wells that were not coated with αvβ3 after blocking with BSA and would be subsequently removed from the 96 well plate after the assay wash step . Thus, in the control wells, one would expect only low background readings when measuring for EGFP fluorescence due to the absence of ‘EGFP CLPs’. On the other hand, if ‘EGFP CLPs’ could indeed bind to αvβ3, they would not be removed from the wells

coated with this receptor after carrying out the wash step, and binding would be confirmed by the detection of significantly increased EGFP fluorescence relative to the control wells. The lack of any measurable difference in the fluorescence readings between the control wells and the wells that were coated with αvβ3, suggested strongly that there was no binding between the 'EGFP CLPs' and αvβ3. This result was unexpected, since both BTV CLPs and AHSV CLPs possess an RGD motif on the VP7 protein (Tan et al., 2001), an amino acid motif shown to have a high binding affinity for the αvβ3 receptor (Lee et al., 2016). However, unlike BTV CLPs, which were shown to interact with an αvβ3 receptor in a prior study (Brillault et al., 2017), the same could not be said for the AHSV 'EGFP CLPs' based on the results of the solid-state binding assay.

Despite the result of the solid-state binding assay seemingly indicating that there was no binding between the AHSV 'EGFP CLPs' and αvβ3, this could not be confirmed with certainty due to two potential shortcomings with the assay itself. It was considered a possibility that the wells may not have been successfully coated with the αvβ3 receptor. To achieve standard coating of the assay plate requires successful hydrophobic interactions between the assay plate and non-polar amino acids of the protein to be immobilized (Biesiadecki and Jin, 2011). Thus, if there was weak hydrophobic absorption of the αvβ3 receptor to the assay plate, the receptor may have not been successfully immobilized. If this were the case, the AHSV 'EGFP CLPs' would have nothing to bind to, and one would not see any difference in fluorescence readings with the control wells. To avoid this possibility, a microtiter assay plate with altered surface chemistry could have been used to enhance the hydrophobic absorption of the αvβ3 receptor to the plate surface (Biesiadecki and Jin, 2011). However, due to funding and time constraints, such a plate could not be acquired when conducting this assay. The second potential shortcoming of the solid-state binding assay may have been related to detection of EGFP fluorescence. EGFP fluorescence was measured with a top-reading fluorescence microplate reader since the available assay plate had a solid black bottom, and thus fluorescence readings needed to be taken from the top of the assay plate. It is possible that the 'EGFP CLPs' did indeed bind to the αvβ3 receptor, but the EGFP fluorescent signal may have been too weak to detect when measuring from the top of the assay plate. Under these circumstances, one would be unable to distinguish between any signal from the control wells and the wells coated with αvβ3 when measuring for EGFP fluorescence. If this were the case, the detection of EGFP fluorescence could potentially be enhanced by obtaining a black 96 well-plate with a clear bottom and measuring EGFP fluorescence from the bottom of the plate using a bottom-reading

fluorescence microplate reader. However, such a plate could not be obtained when conducting the solid-state binding assay. On the other hand, if we assume that the results of the assay were accurate, the lack of binding between the 'EGFP CLPs' and αvβ3, could potentially be attributed to a difference in the position of the RGD motif on AHSV VP7 compared to BTV VP7. On AHSV VP7, an alanine-glycine-glutamine (AGQ) motif replaces the RGD motif found at the same location within the BTV VP7 protein (Basak et al., 1996). Despite this, an RGD motif is still present on a highly flexible VP7 loop (Tan et al., 2001), however this RGD motif is located at a lower part of the AHSV VP7 top domain than the AGQ segment which has replaced the RGD motif found in the BTV VP7 protein (Basak et al., 1996). Consequently, it is possible that this RGD motif could be somewhat less accessible to αvβ3 than the AGQ segment, which could explain the lack of binding between the AHSV 'EGFP CLPs' and the αvβ3 receptor. If this were the case, it would suggest that unlike BTV CLPs, AHSV CLPs may not have potential as a delivery vehicle for specific targeting of cells overexpressing αvβ3.

# Chapter 4: Conclusion

During this study, several objectives were achieved. The initial objective of this study focussed on the production of plasmid constructs capable of expressing the EGFP-VP3 fusion protein required for later co-expression experiments. As described in chapter 2, two different constructs capable of encoding EGFP-VP3 were successfully produced using two distinct cloning techniques. By utilizing in-fusion cloning, EGFP-VP3 was successfully amplified and then cloned into the pEAQ-*HT* plant expression vector without the need for restriction digestion or any ligation reactions. By utilizing restriction digest-based cloning, EGFP-VP3 was successfully sub-cloned from pEAQ-*HT*-EGFP-VP3 into the pRIC4.0 plant expression vector.

The second objective focussed on the production of CLPs encapsulating an EGFP cargo by *Agrobacterium*-mediated transient co-expression of the EGFP-VP3 fusion protein and the AHSV VP7 protein in *N. benthamiana* plants. As described in chapter 3, this study showed that both the pEAQ-*HT* and pRIC4.0 constructs were suitable for production of EGFP-VP3, but the pEAQ-*HT*-EGFP-VP3 construct emerged as a more viable option for achieving higher, longer-lasting EGFP-VP3 expression levels. Moving on, the second objective of the study was successfully achieved after co-expression of pEAQ-*HT*-EGFP-VP3 and pEAQ-*HT*-VP7 resulted in spontaneous formation of CLPs that successfully encapsulated EGFP. The CLPs were successfully purified using density gradient ultracentrifugation and one was able to immediately differentiate empty CLPs from those encapsulating EGFP by the colour of the concentrated band of particles found near the 30-40% interface of the density gradient. This confirmed the suitability of the pEAQ-*HT* vector series for facilitating production of well-assembled AHSV CLPs that encapsulate a fluorescent cargo, as had been achieved using BTV CLPs (Brillault et al., 2017).

The third objective of this study focussed on optimizing conditions for producing AHSV CLPs that encapsulated EGFP. It was found that one could use the BTV extraction and purification buffer used by Brillault et al, to increase the yield of purified AHSV CLPs encapsulating the EGFP protein. Furthermore, this study showed how one can use an in-vivo imaging system to determine quantitative expression levels of a fluorescent protein in infiltrated *N. benthamiana* leaves and highlighted how one could potentially use this information to determine which harvesting day may yield the greatest number of CLPs encapsulating the fluorescent cargo prior to carrying out particle extraction and purification processes.

The final objective of this study sought to determine whether purified AHSV CLPs encapsulating EGFP could potentially bind to a human integrin receptor, αvβ3, by conducting a solid-state binding assay. Unfortunately, this study was unable to definitively confirm whether 'EGFP CLPs', interact with the αvβ3 receptor, as has been proven with BTV CLPs encapsulating GFP. To ensure accurate and reliable solid-state binding assay results, the assay could be repeated in the future using a black 96 well plate modified to enhance binding and with a clear bottom so that detection of any EGFP fluorescence can be enhanced by using a bottom-reading fluorescence microplate reader.

In terms of future work, it will be important to first repeat certain experiments, including the fluorescent imaging of leaves using the IVIS® in-vivo imaging system and the solid-state binding assay (both of which could only be performed once due to funding and time constraints), to confirm the results of both these experiments. Thereafter, the potential of these 'EGFP CLPs' to successfully target and deliver their EGFP payload to cells can be preliminarily investigated. This work would involve incubation of these particles with a cell line previously established as a model for RGD-mediated targeting such as MCF-7, a human breast adenocarcinoma cell line (Brillault et al., 2017). Confocal microscopy could then be used to assess whether the particles are internalized by detecting for EGFP fluorescence. If successful, this would open the possibility of using these particles for optical imaging applications such as specific labelling of a desired cell or tissue and fluorescent signals could also be used to determine in-vivo biodistribution patterns of these CLPs. Alternatively, once the ability of these particles to target and internalize their payload within cells overexpressing the αvβ3 receptor has been proven, a therapeutic molecule could be encapsulated within the AHSV CLP instead of the EGFP protein. By doing this, the ability of these particles to act as drug delivery vehicles can be studied and this may potentially lead to more effective disease treatment in the future such as an improved cancer treatment outcome.

To conclude, the work performed herein showed successful production of a nanoparticle capable of encapsulating a foreign cargo molecule. This work is significant as successful encapsulation is an essential step along the path towards development of a potential delivery vehicle for diagnostic and/or therapeutic molecules. Specifically, this work showed how one can utilize *N. benthamiana* as a heterologous expression system to produce AHSV CLPs encapsulating a fluorescent protein, EGFP.

# Bibliography


ALBANESE, A., TANG, P. S. & CHAN, W. C. 2012. The effect of nanoparticle size, shape, and surface chemistry on biological systems. *Annual review of biomedical engineering,* 14**,** 1-16.

ALJABALI, A. A., SHUKLA, S., LOMONOSSOFF, G. P., STEINMETZ, N. F. & EVANS, D. J. 2013. Cpmv-dox delivers. *Molecular pharmaceutics,* 10**,** 3-10.

ASHLEY, C. E., CARNES, E. C., PHILLIPS, G. K., DURFEE, P. N., BULEY, M. D., LINO, C. A., PADILLA, D. P., PHILLIPS, B., CARTER, M. B. & WILLMAN, C. L. 2011. Cell-specific delivery of diverse cargos by bacteriophage MS2 virus-like particles. *ACS nano,* 5**,** 5729-5745.

ATTIA, M. F., ANTON, N., WALLYN, J., OMRAN, Z. & VANDAMME, T. F. 2019. An overview of active and passive targeting strategies to improve the nanocarriers efficiency to tumour sites. *Journal of Pharmacy and Pharmacology,* 71**,** 1185-1198.

BADRI NARAYANAN, K. & SOO HAN, S. 2017. Genetic modifications of icosahedral plant virus-based nanoparticles for vaccine and immunotherapy applications. *Current Protein and Peptide Science,* 18**,** 1141-1151.

BALKE, I. & ZELTINS, A. 2019. Use of plant viruses and virus-like particles for the creation of novel vaccines. *Advanced Drug Delivery Reviews,* 145**,** 119-129.

BASAK, A. K., GOUET, P., GRIMES, J., ROY, P. & STUART, D. 1996. Crystal structure of the top domain of African horse sickness virus VP7: comparisons with bluetongue virus VP7. *Journal of virology,* 70**,** 3797-3806.

BENDAHMANE, M., KOO, M., KARRER, E. & BEACHY, R. N. 1999. Display of epitopes on the surface of tobacco mosaic virus: impact of charge and isoelectric point of the epitope on virus-host interactions11Edited by N-H Chua. *Journal of Molecular Biology,* 290**,** 9-20.

BENJAMIN, C., BROHLIN, O., SHAHRIVARKEVISHAHI, A. & GASSENSMITH, J. J. 2020. Virus like particles: fundamental concepts, biological interactions, and clinical applications.

BIESIADECKI, B. J. & JIN, J.-P. 2011. A high-throughput solid-phase microplate protein-binding assay to investigate interactions between myofilament proteins. *Journal of Biomedicine and Biotechnology,* 2011.

BRAKKE, M. K. 1951. Density gradient centrifugation: a new separation technique1. *Journal of the American Chemical Society,* 73**,** 1847-1848.

BRAKKE, M. K. 1961. Density gradient centrifugation and its application to plant viruses. *Advances in Virus Research.* Elsevier.

BRASCH, M., PUTRI, R. M., DE RUITER, M. V., LUQUE, D., KOAY, M. S. T., CASTÓN, J. R. & CORNELISSEN, J. J. L. M. 2017. Assembling Enzymatic Cascade Pathways inside Virus-Based Nanocages Using Dual-Tasking Nucleic Acid Tags. *Journal of the American Chemical Society,* 139**,** 1512-1519.

BRIGGER, I., DUBERNET, C. & COUVREUR, P. 2012. Nanoparticles in cancer therapy and diagnosis. *Advanced Drug Delivery Reviews,* 64**,** 24-36.

BRILLAULT, L., JUTRAS, P. V., DASHTI, N., THUENEMANN, E. C., MORGAN, G., LOMONOSSOFF, G. P., LANDSBERG, M. J. & SAINSBURY, F. 2017. Engineering Recombinant Virus-like Nanoparticles from Plants for Cellular Delivery. *ACS Nano,* 11**,** 3476-3484.

BROWN, N. & BHELLA, D. 2016. Are viruses alive. *Microbiol. Today,* 43**,** 58-61.

BROWN, S. D., FIEDLER, J. D. & FINN, M. G. 2009. Assembly of Hybrid Bacteriophage Qβ Virus-like Particles. *Biochemistry,* 48**,** 11155-11157.

BURRAGE, T. G., TREVEJO, R., STONE-MARSCHAT, M. & LAEGREID, W. W. 1993. Neutralizing epitopes of African horsesickness virus serotype 4 are located on VP2. *Virology,* 196**,** 799-803.

BURROUGHS, J., O'HARA, R., SMALE, C., HAMBLIN, C., WALTON, A., ARMSTRONG, R. & MERTENS, P. 1994. Purification and properties of virus particles, infectious subviral particles, cores and VP7 crystals of African horsesickness virus serotype 9. *Journal of general virology,* 75**,** 1849-1857.

CADENA-NAVA, R. D., HU, Y., GARMANN, R. F., NG, B., ZELIKIN, A. N., KNOBLER, C. M. & GELBART, W. M. 2011. Exploiting Fluorescent Polymers To Probe the Self-Assembly of Virus-like Particles. *The Journal of Physical Chemistry B,* 115**,** 2386-2391.

CARREIRA, A., MENÉNDEZ, M., REGUERA, J., ALMENDRAL, J. M. & MATEU, M. G. 2004. In vitro disassembly of a parvovirus capsid and effect on capsid stability of heterologous peptide insertions in surface loops. *Journal of Biological Chemistry,* 279**,** 6517-6525.

CARRICO, Z. M., FARKAS, M. E., ZHOU, Y., HSIAO, S. C., MARKS, J. D., CHOKHAWALA, H., CLARK, D. S. & FRANCIS, M. B. 2012. N-Terminal Labeling of Filamentous Phage To Create Cancer Marker Imaging Agents. *ACS Nano,* 6**,** 6675-6680.

CHAKRABORTI, S., LIN, T.-Y., GLATT, S. & HEDDLE, J. G. 2020. Enzyme encapsulation by protein cages. *RSC advances,* 10**,** 13293-13301.

CHARPILIENNE, A., NEJMEDDINE, M., BEROIS, M., PAREZ, N., NEUMANN, E., HEWAT, E., TRUGNAN, G. & COHEN, J. 2001. Individual Rotavirus-like Particles Containing 120 Molecules of Fluorescent Protein Are Visible in Living Cells* 210. *Journal of Biological Chemistry,* 276**,** 29361-29367.

CHEN, Q., LAI, H., HURTADO, J., STAHNKE, J., LEUZINGER, K. & DENT, M. 2013a. Agroinfiltration as an effective and scalable strategy of gene delivery for production of pharmaceutical proteins. *Advanced techniques in biology & medicine,* 1.

CHEN, X., ZARO, J. L. & SHEN, W.-C. 2013b. Fusion protein linkers: property, design and functionality. *Advanced drug delivery reviews,* 65**,** 1357-1369.

CHEN, Z., LI, N., CHEN, L., LEE, J. & GASSENSMITH, J. J. 2016a. Dual functionalized bacteriophage Qβ as a photocaged drug carrier. *Small,* 12**,** 4563-4571.

CHEN, Z., LI, N., LI, S., DHARMARWARDANA, M., SCHLIMME, A. & GASSENSMITH, J. J. 2016b. Viral chemistry: the chemical functionalization of viral architectures to create new technology. *Wiley Interdisciplinary Reviews: Nanomedicine and Nanobiotechnology,* 8**,** 512-534.

CHILTON, M.-D., DRUMMOND, M. H., MERLO, D. J., SCIAKY, D., MONTOYA, A. L., GORDON, M. P. & NESTER, E. W. 1977. Stable incorporation of plasmid DNA into higher plant cells: the molecular basis of crown gall tumorigenesis. *Cell,* 11**,** 263-271.

CHO, C.-F., YU, L., NSIAMA, T. K., KADAM, A. N., RATURI, A., SHUKLA, S., AMADEI, G. A., STEINMETZ, N. F., LUYT, L. G. & LEWIS, J. D. 2017. Viral nanoparticles decorated with novel EGFL7 ligands enable intravital imaging of tumor neovasculature. *Nanoscale,* 9**,** 12096-12109.

CHOI, B., KIM, H., CHOI, H. & KANG, S. 2018. Protein Cage Nanoparticles as Delivery Nanoplatforms. *Biomimetic Medical Materials: From Nanotechnology to 3D Bioprinting,* 1064**,** 27.

CHUNG, Y. H., CAI, H. & STEINMETZ, N. F. 2020. Viral nanoparticles for drug delivery, imaging, immunotherapy, and theranostic applications. *Advanced Drug Delivery Reviews,* 156**,** 214-235.

CLEMONS, T. D., SINGH, R., SOROLLA, A., CHAUDHARI, N., HUBBARD, A. & IYER, K. S. 2018. Distinction Between Active and Passive Targeting of Nanoparticles Dictate Their Overall Therapeutic Efficacy. *Langmuir,* 34**,** 15343-15349.

CLONTECH 2012. In-Fusion® HD cloning kit user manual. Clontech Mountain View.

COHRS, R. J., GILDEN, D. H., KINCHINGTON, P. R., GRINFELD, E. & KENNEDY, P. G. 2003. Varicella-zoster virus gene 66 transcription and translation in latently infected human ganglia. *Journal of virology,* 77**,** 6660-6665.

COMAS-GARCIA, M., COLUNGA-SAUCEDO, M. & ROSALES-MENDOZA, S. 2020. The Role of Virus-Like Particles in Medical Biotechnology. *Molecular Pharmaceutics,* 17**,** 4407-4420.

COMELLAS-ARAGONÈS, M., ENGELKAMP, H., CLAESSEN, V. I., SOMMERDIJK, N. A., ROWAN, A. E., CHRISTIANEN, P., MAAN, J. C., VERDUIN, B. J., CORNELISSEN, J. J. & NOLTE, R. J. 2007. A virus-based single-enzyme nanoreactor. *Nature nanotechnology,* 2**,** 635-639.

CZAPAR, A. E., ZHENG, Y.-R., RIDDELL, I. A., SHUKLA, S., AWUAH, S. G., LIPPARD, S. J. & STEINMETZ, N. F. 2016. Tobacco mosaic virus delivery of phenanthriplatin for cancer therapy. *ACS nano,* 10**,** 4119-4126.

DE WILDE, C., PEETERS, K., JACOBS, A., PECK, I. & DEPICKER, A. 2002. Expression of antibodies and Fab fragments in transgenic potato plants: a case study for bulk production in crop plants. *Molecular Breeding,* 9**,** 271-282.
DENNIS, S. J. 2019. *Development of plant-produced African horse sickness vaccines.* Faculty of Science.
DENNIS, S. J., MEYERS, A. E., HITZEROTH, I. I. & RYBICKI, E. P. 2019. African horse sickness: a review of current understanding and vaccine development. *Viruses,* 11**,** 844.
DENNIS, S. J., O'KENNEDY, M. M., RUTKOWSKA, D., TSEKOA, T., LOURENS, C. W., HITZEROTH, I. I., MEYERS, A. E. & RYBICKI, E. P. 2018. Safety and immunogenicity of plant-produced African horse sickness virus-like particles in horses. *Veterinary research,* 49**,** 1-6.
DESTITO, G., YEH, R., RAE, C. S., FINN, M. & MANCHESTER, M. 2007. Folic acid-mediated targeting of cowpea mosaic virus particles to tumor cells. *Chemistry & biology,* 14**,** 1152-1162.
DING, X., LIU, D., BOOTH, G., GAO, W. & LU, Y. 2018. Virus-Like Particle Engineering: From Rational Design to Versatile Applications. *Biotechnology Journal,* 13**,** 1700324.
DOLL, T. A. P. F., RAMAN, S., DEY, R. & BURKHARD, P. 2013. Nanoscale assemblies and their biomedical applications. *Journal of The Royal Society Interface,* 10**,** 20120740.
DOUGLAS, T. & YOUNG, M. 2006. Viruses: Making Friends with Old Foes. *Science,* 312**,** 873-875.
ESTRADA, L. H. & CHAMPION, J. 2015. Protein nanoparticles for therapeutic protein delivery. *Biomaterials science,* 3**,** 787-799.
FANG, J., NAKAMURA, H. & MAEDA, H. 2011. The EPR effect: Unique features of tumor blood vessels for drug delivery, factors involved, and limitations and augmentation of the effect. *Advanced Drug Delivery Reviews,* 63**,** 136-151.
FAROKHZAD, O. C. & LANGER, R. 2009. Impact of nanotechnology on drug delivery. *ACS nano,* 3**,** 16-20.
FENG, S.-S. 2004. Nanoparticles of biodegradable polymers for new-concept chemotherapy. *Expert review of medical devices,* 1**,** 115-125.
FISCHER, R. & BUYEL, J. F. 2020. Molecular farming – The slope of enlightenment. *Biotechnology Advances,* 40**,** 107519.
FRANKE, C. E., CZAPAR, A. E., PATEL, R. B. & STEINMETZ, N. F. 2017. Tobacco mosaic virus-delivered cisplatin restores efficacy in platinum-resistant ovarian cancer cells. *Molecular pharmaceutics,* 15**,** 2922-2931.
FRENCH, T., MARSHALL, J. & ROY, P. 1990. Assembly of double-shelled, viruslike particles of bluetongue virus by the simultaneous expression of four structural proteins. *Journal of virology,* 64**,** 5695-5700.
FRENCH, T. & ROY, P. 1990. Synthesis of bluetongue virus (BTV) corelike particles by a recombinant baculovirus expressing the two major structural core proteins of BTV. *Journal of Virology,* 64**,** 1530-1536.
FUENMAYOR, J., GÒDIA, F. & CERVERA, L. 2017. Production of virus-like particles for vaccines. *New Biotechnology,* 39**,** 174-180.
GLASGOW, J. E., CAPEHART, S. L., FRANCIS, M. B. & TULLMAN-ERCEK, D. 2012. Osmolyte-Mediated Encapsulation of Proteins inside MS2 Viral Capsids. *ACS Nano,* 6**,** 8658-8664.
HALLEY-STOTT, R., TANZER, F., MARTIN, D. & RYBICKI, E. 2007. The complete nucleotide sequence of a mild strain of Bean yellow dwarf virus. *Archives of virology,* 152**,** 1237.
HEFFERON, K. L. & DUGDALE, B. 2003. Independent expression of Rep and RepA and their roles in regulating bean yellow dwarf virus replication. *Journal of General Virology,* 84**,** 3465-3472.
HEFFERON, K. L. & FAN, Y. 2004. Expression of a vaccine protein in a plant cell line using a geminivirus-based replicon system. *Vaccine,* 23**,** 404-410.
HEWAT, E. A., BOOTH, T. F., LOUDON, P. T. & ROY, P. 1992. Three-dimensional reconstruction of baculovirus expressed bluetongue virus core-like particles by cryo-electron microscopy. *Virology,* 189**,** 10-20.

HEWAT, E. A., BOOTH, T. F. & ROY, P. 1994. Structure of correctly self-assembled bluetongue virus-like particles. *Journal of structural biology,* 112**,** 183-191.
HILL, B. D., ZAK, A., KHERA, E. & WEN, F. 2018. Engineering Virus-like Particles for Antigen and Drug Delivery. *Current Protein and Peptide Science,* 19**,** 112-127.
IKWUAGWU, B. & TULLMAN-ERCEK, D. 2022. Virus-like particles for drug delivery: a review of methods and applications. *Current Opinion in Biotechnology,* 78**,** 102785.
JEGERLEHNER, A., STORNI, T., LIPOWSKY, G., SCHMID, M., PUMPENS, P. & BACHMANN, M. F. 2002. Regulation of IgG antibody responses by epitope density and CD21-mediated costimulation. *European journal of immunology,* 32**,** 3305-3314.
JUAREZ, V., PASOLLI, H. A., HELLWIG, A., GARBI, N. & ARREGUI, A. C. 2012. Virus-Like Particles Harboring CCL19, IL-2 and HPV16 E7 Elicit Protective T Cell Responses in HLA-A2 Transgenic Mice. *Open Virology Journal,* 6**,** 270-276.
JUNG, B., RAO, A. L. & ANVARI, B. 2011. Optical nano-constructs composed of genome-depleted brome mosaic virus doped with a near infrared chromophore for potential biomedical applications. *Acs Nano,* 5**,** 1243-1252.
KACZMARCZYK, S. J., SITARAMAN, K., YOUNG, H. A., HUGHES, S. H. & CHATTERJEE, D. K. 2011. Protein delivery using engineered virus-like particles. *Proceedings of the National Academy of Sciences,* 108**,** 16998-17003.
KAPILA, J., DE RYCKE, R., VAN MONTAGU, M. & ANGENON, G. 1997. An Agrobacterium-mediated transient gene expression system for intact leaves. *Plant science,* 122**,** 101-108.
KAR, A. K., IWATANI, N. & ROY, P. 2005. Assembly and intracellular localization of the bluetongue virus core protein VP3. *Journal of virology,* 79**,** 11487-11495.
KAUR, M., MANCHANDA, P., KALIA, A., AHMED, F. K., NEPOVIMOVA, E., KUCA, K. & ABD-ELSALAM, K. A. 2021. Agroinfiltration mediated scalable transient gene expression in genome edited crop plants. *International Journal of Molecular Sciences,* 22**,** 10882.
KIM, C. H., AXUP, J. Y. & SCHULTZ, P. G. 2013. Protein conjugation with genetically encoded unnatural amino acids. *Current Opinion in Chemical Biology,* 17**,** 412-419.
KOUDELKA, K. J., DESTITO, G., PLUMMER, E. M., TRAUGER, S. A., SIUZDAK, G. & MANCHESTER, M. 2009. Endothelial targeting of cowpea mosaic virus (CPMV) via surface vimentin. *PLoS pathogens,* 5**,** e1000417.
KOUDELKA, K. J., PITEK, A. S., MANCHESTER, M. & STEINMETZ, N. F. 2015. Virus-based nanoparticles as versatile nanomachines. *Annual review of virology,* 2**,** 379.
KUSHNIR, N., STREATFIELD, S. J. & YUSIBOV, V. 2012. Virus-like particles as a highly efficient vaccine platform: diversity of targets and production systems and advances in clinical development. *Vaccine,* 31**,** 58-83.
LEE, E. J., LEE, N. K. & KIM, I.-S. 2016. Bioengineered protein-based nanocage for drug delivery. *Advanced Drug Delivery Reviews,* 106**,** 157-171.
LEE, L. A., NIU, Z. & WANG, Q. 2009. Viruses and virus-like protein assemblies—Chemically programmable nanoscale building blocks. *Nano Research,* 2**,** 349-364.
LEE, L. A. & WANG, Q. 2006. Adaptations of nanoscale viruses and other protein cages for medical applications. *Nanomedicine: Nanotechnology, Biology and Medicine,* 2**,** 137-149.
LEWIS, J. D., DESTITO, G., ZIJLSTRA, A., GONZALEZ, M. J., QUIGLEY, J. P., MANCHESTER, M. & STUHLMANN, H. 2006. Viral nanoparticles as tools for intravital vascular imaging. *Nature medicine,* 12**,** 354-360.
LI, C. & ARAKAWA, T. 2019. Application of native polyacrylamide gel electrophoresis for protein analysis: Bovine serum albumin as a model protein. *International journal of biological macromolecules,* 125**,** 566-571.
LI, F., ZHANG, Z. P., PENG, J., CUI, Z. Q., PANG, D. W., LI, K., WEI, H. P., ZHOU, Y. F., WEN, J. K. & ZHANG, X. E. 2009. Imaging viral behavior in mammalian cells with self-assembled capsid–quantum-dot hybrid particles. *Small,* 5**,** 718-726.

LI, K., NGUYEN, H. G., LU, X. & WANG, Q. 2010. Viruses and their potential in bioimaging and biosensing applications. *Analyst,* 135**,** 21-27.
LUA, L. H., CONNORS, N. K., SAINSBURY, F., CHUAN, Y. P., WIBOWO, N. & MIDDELBERG, A. P. 2014. Bioengineering virus-like particles as vaccines. *Biotechnology and bioengineering,* 111**,** 425-440.
LUDWIG, C. & WAGNER, R. 2007. Virus-like particles—universal molecular toolboxes. *Current opinion in biotechnology,* 18**,** 537-545.
MA, J. K., DRAKE, P. M. & CHRISTOU, P. 2003. The production of recombinant pharmaceutical proteins in plants. *Nature reviews genetics,* 4**,** 794-805.
MA, S. & WANG, A. 2012. Molecular farming in plants: an overview. *Molecular farming in plants: recent advances and future prospects***,** 1-20.
MA, Y., NOLTE, R. J. M. & CORNELISSEN, J. J. L. M. 2012. Virus-based nanocarriers for drug delivery. *Advanced Drug Delivery Reviews,* 64**,** 811-825.
MAREE, S., MAREE, F. F., PUTTERILL, J. F., DE BEER, T. A., HUISMANS, H. & THERON, J. 2016. Synthesis of empty African horse sickness virus particles. *Virus research,* 213**,** 184-194.
MARSIAN, J. & LOMONOSSOFF, G. P. 2016. Molecular pharming—VLPs made in plants. *Current Opinion in Biotechnology,* 37**,** 201-206.
MATEU, M. G. 2013. Assembly, stability and dynamics of virus capsids. *Archives of Biochemistry and Biophysics,* 531**,** 65-79.
MCNEALE, D., DASHTI, N., CHEAH, L. C. & SAINSBURY, F. 2022. Protein cargo encapsulation by virus-like particles: Strategies and applications. *Wiley Interdisciplinary Reviews: Nanomedicine and Nanobiotechnology***,** e1869.
MEJÍA-MÉNDEZ, J. L., VAZQUEZ-DUHALT, R., HERNÁNDEZ, L. R., SÁNCHEZ-ARREOLA, E. & BACH, H. 2022. Virus-like Particles: Fundamentals and Biomedical Applications. *International Journal of Molecular Sciences* [Online], 23.
MELLOR, P. S. & HAMBLIN, C. 2004. African horse sickness. *Veterinary research,* 35**,** 445-466.
MELLOR, P. S., RAWLINGS, P., BAYLIS, M. & WELLBY, M. P. 1998. Effect of temperature on African horse sickness virus infection in Culicoides. *African horse sickness.* Springer.
MOLINO, N. M. & WANG, S.-W. 2014. Caged protein nanoparticles for drug delivery. *Current Opinion in Biotechnology,* 28**,** 75-82.
MOR, T. S., MOON, Y. S., PALMER, K. E. & MASON, H. S. 2003. Geminivirus vectors for high-level expression of foreign proteins in plant cells. *Biotechnology and bioengineering,* 81**,** 430-437.
MURPHY, F., BORDEN, E., SHOPE, R. & HARRISON, A. 1971. Physicochemical and morphological relationships of some arthropod-borne viruses to bluetongue virus—a new taxonomic group. Electron microscopic studies. *Journal of General Virology,* 13**,** 273-288.
NASSAL, M., SKAMEL, C., KRATZ, P. A., WALLICH, R., STEHLE, T. & SIMON, M. M. 2005. A fusion product of the complete Borrelia burgdorferi outer surface protein A (OspA) and the hepatitis B virus capsid protein is highly immunogenic and induces protective immunity similar to that seen with an effective lipidated OspA vaccine formula. *European Journal of Immunology,* 35**,** 655-665.
NOORAEI, S., BAHRULOLUM, H., HOSEINI, Z. S., KATALANI, C., HAJIZADE, A., EASTON, A. J. & AHMADIAN, G. 2021. Virus-like particles: preparation, immunogenicity and their roles as nanovaccines and drug nanocarriers. *Journal of Nanobiotechnology,* 19**,** 59.
NORKUNAS, K., HARDING, R., DALE, J. & DUGDALE, B. 2018. Improving agroinfiltration-based transient gene expression in Nicotiana benthamiana. *Plant methods,* 14**,** 1-14.
OBEMBE, O. O., POPOOLA, J. O., LEELAVATHI, S. & REDDY, S. V. 2011. Advances in plant molecular farming. *Biotechnology Advances,* 29**,** 210-222.
OJHA, S. K., PATTNAIK, R., SINGH, P. K., DIXIT, S., MISHRA, S., PAL, S. & KUMAR, S. 2022. Virus as a Nanocarrier for Drug Delivery Redefining Medical Therapeutics-A Status Report. *Combinatorial Chemistry & High Throughput Screening,* 25**,** 1619-1629.

OUN, R., MOUSSA, Y. E. & WHEATE, N. J. 2018. The side effects of platinum-based chemotherapy drugs: a review for chemists. *Dalton transactions,* 47**,** 6645-6653.
PATTERSON, D. P., SCHWARZ, B., EL-BOUBBOU, K., VAN DER OOST, J., PREVELIGE, P. E. & DOUGLAS, T. 2012. Virus-like particle nanoreactors: programmed encapsulation of the thermostable CelB glycosidase inside the P22 capsid. *Soft Matter,* 8**,** 10158-10166.
PATTERSON, D. P., SCHWARZ, B., WATERS, R. S., GEDEON, T. & DOUGLAS, T. 2014. Encapsulation of an enzyme cascade within the bacteriophage P22 virus-like particle. *ACS chemical biology,* 9**,** 359-365.
PETROS, R. A. & DESIMONE, J. M. 2010. Strategies in the design of nanoparticles for therapeutic applications. *Nature reviews Drug discovery,* 9**,** 615-627.
PEYRET, H. & LOMONOSSOFF, G. P. 2013. The pEAQ vector series: the easy and quick way to produce recombinant proteins in plants. *Plant molecular biology,* 83**,** 51-58.
PITEK, A., HU, H., SHUKLA, S. & STEINMETZ, N. 2018. Cancer theranostic applications of albumin-coated tobacco mosaic virus nanoparticles. *ACS applied materials & interfaces,* 10**,** 39468-39477.
PLUMMER, E. M. & MANCHESTER, M. 2011. Viral nanoparticles and virus-like particles: platforms for contemporary vaccine design. *Wiley Interdisciplinary Reviews: Nanomedicine and Nanobiotechnology,* 3**,** 174-196.
POKORSKI, J. K. & STEINMETZ, N. F. 2011. The Art of Engineering Viral Nanoparticles. *Molecular Pharmaceutics,* 8**,** 29-43.
PORTA, C. & LOMONOSSOFF, G. P. 2002. Viruses as vectors for the expression of foreign sequences in plants. *Biotechnology and Genetic Engineering Reviews,* 19**,** 245-292.
RAMQVIST, T., ANDREASSON, K. & DALIANIS, T. 2007. Vaccination, immune and gene therapy based on virus-like particles against viral infections and cancer. *Expert opinion on biological therapy,* 7**,** 997-1007.
REGNARD, G. L., HALLEY-STOTT, R. P., TANZER, F. L., HITZEROTH, I. I. & RYBICKI, E. P. 2010. High level protein expression in plants through the use of a novel autonomously replicating geminivirus shuttle vector. *Plant biotechnology journal,* 8**,** 38-46.
ROHOVIE, M. J., NAGASAWA, M. & SWARTZ, J. R. 2017. Virus-like particles: Next-generation nanoparticles for targeted therapeutic delivery. *Bioengineering & Translational Medicine,* 2**,** 43-57.
ROTHER, M., NUSSBAUMER, M. G., RENGGLI, K. & BRUNS, N. 2016. Protein cages and synthetic polymers: a fruitful symbiosis for drug delivery applications, bionanotechnology and materials science. *Chemical Society Reviews,* 45**,** 6213-6249.
ROY, P., BISHOP, D. H. L., HOWARD, S., AITCHISON, H. & ERASMUS, B. 1996. Recombinant baculovirus-synthesized African horsesickness virus (AHSV) outer-capsid protein VP2 provides protection against virulent AHSV challenge. *Journal of General Virology,* 77**,** 2053-2057.
ROY, P., MERTENS, P. P. C. & CASAL, I. 1994. African horse sickness virus structure. *Comparative immunology, microbiology and infectious diseases,* 17**,** 243-273.
RUNNING, W. E., NI, P., KAO, C. C. & REILLY, J. P. 2012. Chemical Reactivity of Brome Mosaic Virus Capsid Protein. *Journal of Molecular Biology,* 423**,** 79-95.
RYBICKI, E. P. 2020. Plant molecular farming of virus-like nanoparticles as vaccines and reagents. *WIREs Nanomedicine and Nanobiotechnology,* 12**,** e1587.
SAINSBURY, F. & LOMONOSSOFF, G. P. 2014. Transient expressions of synthetic biology in plants. *Current Opinion in Plant Biology,* 19**,** 1-7.
SAINSBURY, F., THUENEMANN, E. C. & LOMONOSSOFF, G. P. 2009. pEAQ: versatile expression vectors for easy and quick transient expression of heterologous proteins in plants. *Plant biotechnology journal,* 7**,** 682-693.
SAMBROOK, J., FRITSCH, E. F. & MANIATIS, T. 1989. *Molecular cloning: a laboratory manual*, Cold spring harbor laboratory press.

SAXENA, P., THUENEMANN, E. C., SAINSBURY, F. & LOMONOSSOFF, G. P. 2016. Virus-derived vectors for the expression of multiple proteins in plants. *Recombinant proteins from plants: methods and protocols*, 39-54.

SCHLICK, T. L., DING, Z., KOVACS, E. W. & FRANCIS, M. B. 2005. Dual-surface modification of the tobacco mosaic virus. *Journal of the American Chemical Society,* 127, 3718-3723.

SCHOONEN, L. & VAN HEST, J. C. M. 2014. Functionalization of protein-based nanocages for drug delivery applications. *Nanoscale,* 6, 7124-7141.

SCHWARZ, B. & DOUGLAS, T. 2015. Development of virus-like particles for diagnostic and prophylactic biomedical applications. *WIREs Nanomedicine and Nanobiotechnology,* 7, 722-735.

SHAHGOLZARI, M., PAZHOUHANDEH, M., MILANI, M., YARI KHOSROUSHAHI, A. & FIERING, S. 2020. Plant viral nanoparticles for packaging and in vivo delivery of bioactive cargos. *Wiley Interdisciplinary Reviews: Nanomedicine and Nanobiotechnology,* 12, e1629.

SHAHRIVARKEVISHAHI, A., HAGGE, L. M., BROHLIN, O. R., KUMARI, S., EHRMAN, R., BENJAMIN, C. & GASSENSMITH, J. J. 2022. Virus-like particles: a self-assembled toolbox for cancer therapy. *Materials Today Chemistry,* 24, 100808.

SHARMA, J., UCHIDA, M., MIETTINEN, H. M. & DOUGLAS, T. 2017. Modular interior loading and exterior decoration of a virus-like particle. *Nanoscale,* 9, 10420-10430.

SHEN, W.-J. & FORDE, B. G. 1989. Efficient transformation of Agrobacterium spp. by high voltage electroporation. *Nucleic acids research,* 17, 8385.

SHIRBAGHAEE, Z. & BOLHASSANI, A. 2016. Different applications of virus-like particles in biology and medicine: Vaccination and delivery systems. *Biopolymers,* 105, 113-132.

SIMPSON, R. B., SPIELMANN, A., MARGOSSIAN, L. & MCKNIGHT, T. D. 1986. A disarmed binary vector from Agrobacterium tumefaciens functions in Agrobacterium rhizogenes. *Plant Molecular Biology,* 6, 403-415.

SMITH, M. T., HAWES, A. K. & BUNDY, B. C. 2013. Reengineering viruses and virus-like particles through chemical functionalization strategies. *Current Opinion in Biotechnology,* 24, 620-626.

STANGL, M., VEERAPPAN, A., KROEGER, A., VOGEL, P. & SCHNEIDER, D. 2012. Detergent properties influence the stability of the glycophorin A transmembrane helix dimer in lysophosphatidylcholine micelles. *Biophysical journal,* 103, 2455-2464.

STEELE, J. F., PEYRET, H., SAUNDERS, K., CASTELLS-GRAELLS, R., MARSIAN, J., MESHCHERIAKOVA, Y. & LOMONOSSOFF, G. P. 2017. Synthetic plant virology for nanobiotechnology and nanomedicine. *Wiley Interdisciplinary Reviews: Nanomedicine and Nanobiotechnology,* 9, e1447.

STEINMETZ, N. F. 2010. Viral nanoparticles as platforms for next-generation therapeutics and imaging devices. *Nanomedicine: Nanotechnology, Biology and Medicine,* 6, 634-641.

STEINMETZ, N. F., CHO, C.-F., ABLACK, A., LEWIS, J. D. & MANCHESTER, M. 2011. Cowpea mosaic virus nanoparticles target surface vimentin on cancer cells. *Nanomedicine,* 6, 351-364.

STEINMETZ, N. F., LIM, S. & SAINSBURY, F. 2020. Protein cages and virus-like particles: from fundamental insight to biomimetic therapeutics. *Biomaterials science,* 8, 2771-2777.

STEPHAN, D., SLABBER, C., GEORGE, G., NINOV, V., FRANCIS, K. P. & BURGER, J. T. 2011. Visualization of plant viral suppressor silencing activity in intact leaf lamina by quantitative fluorescent imaging. *Plant Methods,* 7, 1-10.

STEWART, M., DOVAS, C., CHATZINASIOU, E., ATHMARAM, T., PAPANASTASSOPOULOU, M., PAPADOPOULOS, O. & ROY, P. 2012. Protective efficacy of Bluetongue virus-like and subvirus-like particles in sheep: presence of the serotype-specific VP2, independent of its geographic lineage, is essential for protection. *Vaccine,* 30, 2131-2139.

STOGER, E., FISCHER, R., MOLONEY, M. & MA, J. K.-C. 2014. Plant molecular pharming for the treatment of chronic and infectious diseases. *Annual review of plant biology,* 65, 743-768.

SUFFIAN, I. F. B. M. & AL-JAMAL, K. T. 2022. Bioengineering of virus-like particles as dynamic nanocarriers for in vivo delivery and targeting to solid tumours. *Advanced Drug Delivery Reviews,* 180**,** 114030.

SUN, X. & CUI, Z. 2020. Virus-Like Particles as Theranostic Platforms. *Advanced Therapeutics,* 3**,** 1900194.

TAN, B.-H., NASON, E., STAEUBER, N., JIANG, W., MONASTRYRSKAYA, K. & ROY, P. 2001. RGD tripeptide of bluetongue virus VP7 protein is responsible for core attachment to Culicoides cells. *Journal of virology,* 75**,** 3937-3947.

THUENEMANN, E. C. & LOMONOSSOFF, G. P. 2018. Delivering Cargo: Plant-Based Production of Bluetongue Virus Core-Like and Virus-Like Particles Containing Fluorescent Proteins. *In:* WEGE, C. & LOMONOSSOFF, G. P. (eds.) *Virus-Derived Nanoparticles for Advanced Technologies: Methods and Protocols.* New York, NY: Springer New York.

THUENEMANN, E. C., MEYERS, A. E., VERWEY, J., RYBICKI, E. P. & LOMONOSSOFF, G. P. 2013. A method for rapid production of heteromultimeric protein complexes in plants: assembly of protective bluetongue virus-like particles. *Plant biotechnology journal,* 11**,** 839-846.

TREMBLAY, R., WANG, D., JEVNIKAR, A. M. & MA, S. 2010. Tobacco, a highly efficient green bioreactor for production of therapeutic proteins. *Biotechnology Advances,* 28**,** 214-221.

TSCHOFEN, M., KNOPP, D., HOOD, E. & STÖGER, E. 2016. Plant molecular farming: much more than medicines.

UCHIDA, M., KANG, S., REICHHARDT, C., HARLEN, K. & DOUGLAS, T. 2010. The ferritin superfamily: Supramolecular templates for materials synthesis. *Biochimica et Biophysica Acta (BBA) - General Subjects,* 1800**,** 834-845.

UNZUETA, U., CÉSPEDES, M. V., VÁZQUEZ, E., FERRER-MIRALLES, N., MANGUES, R. & VILLAVERDE, A. 2015. Towards protein-based viral mimetics for cancer therapies. *Trends in Biotechnology,* 33**,** 253-258.

VILLARREAL, L. P. 2004. Are viruses alive? *Scientific American,* 291**,** 100-105.

WU, M., BROWN, W. L. & STOCKLEY, P. G. 1995. Cell-specific delivery of bacteriophage-encapsidated ricin A chain. *Bioconjugate chemistry,* 6**,** 587-595.

WU, Y., YANG, H. & SHIN, H.-J. 2013. Viruses as self-assembled nanocontainers for encapsulation of functional cargoes. *Korean Journal of Chemical Engineering,* 30**,** 1359-1367.

YAN, D., WEI, Y.-Q., GUO, H.-C. & SUN, S.-Q. 2015. The application of virus-like particles as vaccines and biological vehicles. *Applied Microbiology and Biotechnology,* 99**,** 10415-10432.

YE, J., COULOURIS, G., ZARETSKAYA, I., CUTCUTACHE, I., ROZEN, S. & MADDEN, T. L. 2012. Primer-BLAST: a tool to design target-specific primers for polymerase chain reaction. *BMC bioinformatics,* 13**,** 1-11.

YILDIZ, I., SHUKLA, S. & STEINMETZ, N. F. 2011. Applications of viral nanoparticles in medicine. *Current Opinion in Biotechnology,* 22**,** 901-908.

ZANGABAD, P. S., KARIMI, M., MEHDIZADEH, F., MALEKZAD, H., GHASEMI, A., BAHRAMI, S., ZARE, H., MOGHOOFEI, M., HEKMATMANESH, A. & HAMBLIN, M. R. 2017. Nanocaged platforms: modification, drug delivery and nanotoxicity. Opening synthetic cages to release the tiger. *Nanoscale,* 9**,** 1356-1392.

ZDANOWICZ, M. & CHROBOCZEK, J. 2016. Virus-like particles as drug delivery vectors. *Acta Biochimica Polonica,* 63**,** 469-473.

ZELTINS, A. 2013. Construction and characterization of virus-like particles: a review. *Molecular biotechnology,* 53**,** 92-107.

ZHANG, Y., ARDEJANI, M. S. & ORNER, B. P. 2016. Design and Applications of Protein-Cage-Based Nanomaterials. *Chemistry – An Asian Journal,* 11**,** 2814-2828.

ZHU, B., CAI, G., HALL, E. O. & FREEMAN, G. J. 2007. In-Fusion™ assembly: seamless engineering of multidomain fusion proteins, modular vectors, and mutations. *Biotechniques,* 43**,** 354-359.

# Supplementary material

Supplementary table 1: Antibiotics required for the selection of plasmid constructs present in *E. coli* and *A. tumefaciens* cells.

| Plasmid | Bacterial strain | Antibiotics |
|---|---|---|
| pEGFP | DH5α *E. coli* | Ampicillin (100 ug/mL) |
| pEAQ-*HT* | DH5α *E. coli* | Kanamycin (50 ug/mL) |
| | AGL-1 | Kanamycin (50 ug/mL)<br>Carbenicillin (25 ug/mL) |
| pEAQ-*HT*-VP3 | DH5α *E. coli* | Kanamycin (50 ug/mL) |
| | AGL-1 | Kanamycin (50 ug/mL)<br>Carbenicillin (25 ug/mL) |
| pEAQ-*HT*-VP7 | AGL-1 | Kanamycin (50 ug/mL)<br>Carbenicillin (25 ug/mL) |
| pUC19 | DH5α *E. coli* | Ampicillin (100 ug/mL) |
| pEAQ-*HT*-EGFP-VP3 | DH5α *E. coli* | Kanamycin (50 ug/mL) |
| | AGL-1 | Kanamycin (50 ug/mL)<br>Carbenicillin (25 ug/mL) |
| pRIC4.0 | DH5α *E. coli* | Ampicillin (100 ug/mL) |
| | GV3101::pMP90RK | Rifampicin (50 µg/mL)<br>Kanamycin (30 µg/mL)<br>Carbenicillin (50 µg/mL) |
| pRIC4.0-EGFP-VP3 | DH5α *E. coli* | Ampicillin (100 ug/mL) |
| | GV3101::pMP90RK | Rifampicin (50 µg/mL)<br>Kanamycin (30 µg/mL)<br>Carbenicillin (50 µg/mL) |